Supporting Information

Synergistic Steric–Dipole Modulation via Stepwise Trifluoromethyl Substitution Enables Active-Layer Hierarchical Assembly and >20% Power Conversion Efficiency in Organic Photovoltaic Devices

Jie Wang [a] ‡, Xin Chen [a] ‡, Jingyi Huo, [a] Jiong Yang [a], Longyu Li [a], Wendi, Shi [a], Ruibin Bian [a], Wenkai Zhao [b], Guankui Long, [b] Zhaoyang Yao [a], Chenxi Li [a], Xiangjian Wan*[a] and Yongsheng Chen*[a]

[a] *State Key Laboratory of Elemento-Organic Chemistry, Frontiers Science Center for New Organic Matter, Key Laboratory of Functional Polymer Materials, Institute of Polymer Chemistry, Tianjin Key Laboratory of functional polymer materials Nankai University, Tianjin, 300071, China*.

[b] *School of Materials Science and Engineering, National Institute for Advanced Materials Nankai University, Tianjin, 300071, China*.

E-mail: xjwan@nankai.edu.cn； yschen99@nankai.edu.cn.

‡These authors contributed equally: Jie Wang, Xin Chen

Table of contents

1. Material synthesis

All reactions and manipulations were carried out under argon atmosphere with the use of standard Schlenk techniques. All starting materials were purchased from commercial suppliers and used without further purification unless indicated otherwise. Polymer donor PM6 (M_w around 40-50 kDa) and starting material **1** were purchased from Solarmer Energy, Inc.

Synthetic Section and Supporting Schemes：

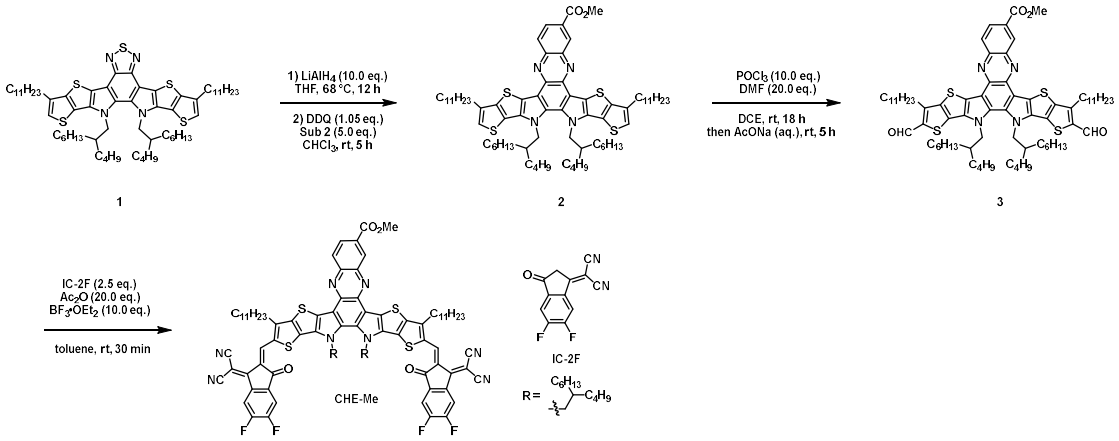

Scheme S1. The overall synthetic route for **CHE-Me**.

Synthesis of intermediate 2：

Under the protection of nitrogen, compound **1** (542 mg, 0.5 mmol, 1.0 eq.) was dissolved in anhydrous tetrahydrofuran (THF, 30.0 mL). After that, a solution of Lithium aluminum hydride ($LiAlH_4$, 1.0 M, 5.0 mL, 10.0 eq.) was slowly added to the mixed solution. The resulting mixture was stirred and heated overnight, then the mixture was gently added to the saturated ammonium chloride (NH_4Cl) solution on ice and extracted with dichloromethane (DCM, 50.0 mL×3). The organic phase was dried over anhydrous sodium sulfate (Na_2SO_4) and concentrated under reduced pressure. The crude product was dissolved in a chloroform ($CHCl_3$, 50.0 mL) without further purification. Then, 3-dichloro-5,6-dicyano-1,4-benzoquinone (DDQ, 125 mg, 0.55 mmol, 1.1 eq.) and methyl 3,4-diaminobenzoate (415 mg, 2.5 mmol, 5.0 eq.) are sequentially added to the solution. Stir the reactant at room temperature for 5 hours and remove the solvent under vacuum. The crude product was purified via silica gel column

chromatography with hexane/dichloromethane (2:1, v/v) as eluent to afford **intermediate 2** as a green solid (532 mg, 82% yield).

^{1}H NMR (400 MHz, Chloroform-*d*) δ = 9.19 (s, 1H), 8.49 (d, *J* = 8.9 Hz, 1H), 8.39 (d, *J* = 8.9 Hz, 1H), 7.01 (s, 2H), 4.64 (d, *J* = 7.8 Hz, 4H), 4.06 (s, 3H), 2.86 (t, *J* = 7.9 Hz, 4H), 2.14 (s, 2H), 1.88 (t, *J* = 7.8 Hz, 4H), 1.50–1.37 (m, 8H), 1.28 (d, *J* = 14.3 Hz, 26H), 1.09–0.82 (m, 36H), 0.60 (q, *J* = 8.2 Hz, 12H).

^{13}C NMR (101 MHz, $CDCl_3$) δ = 167.02, 143.32, 143.22, 142.98, 140.18, 139.23, 139.11, 137.13, 136.97, 132.40, 132.28, 131.51, 129.38, 129.21, 127.46, 123.55, 123.43, 119.15, 116.99, 116.71, 55.18, 52.43, 38.74, 38.70, 31.93, 31.57, 30.37, 30.28, 29.71, 29.66, 29.56, 29.52, 29.48, 29.36, 28.95, 28.92, 27.98, 27.85, 25.40, 25.27, 22.76, 22.73, 22.70, 22.41, 14.11.

HRMS (m/z) $[M+H]^+$ calcd. for ($C_{72}H_{105}N_4O_2S_4$): 1185.7115. Found: 1185.7118.

Synthesis of intermediate 3:

Under the protection of nitrogen, phosphorus oxychloride ($POCl_3$, 0.5 mL) was added dropwise to a solution of anhydrous *N*,*N*-dimethylformamide (DMF, 1.0 mL) at 0°C and stirred at room temperature for 30 min. **Intermediate 2** (260 mg, 0.2 mmol, 1.0 eq.) dissolved in anhydrous 1,2-dichloroethane (DCE, 20.0 mL) was add to the above solution and stirred at 85 °C for 12 h. Then, the reaction mixture is quenched by stirring with saturated sodium acetate (AcONa) solution and extracted with dichloromethane (DCM, 50 mL×3). The combined organic phase was washed with saturated saline solution (NaCl, aq.) for three times and dried over anhydrous with sodium sulfate (Na_2SO_4). After solvent was evaporated under reduced pressure, the residue was purified through a silica gel column with petroleum ether/dichloromethane (1:1, v/v) as eluent to give **intermediate 3** as an orange red solid (343 mg, 90% yield).

^{1}H NMR (400 MHz, Chloroform-*d*) δ = 10.08 (d, *J* = 5.0 Hz, 2H), 8.97 (s, 1H), 8.35–8.29 (m, 2H), 4.63 (d, *J* = 8.0 Hz, 4H), 3.95 (s, 3H), 3.15 (dt, *J* = 10.6, 7.7 Hz, 4H), 2.15–2.07 (m, 2H), 1.88 (q, *J* = 7.5 Hz, 4H), 1.42 (q, *J* = 7.5 Hz, 4H), 1.34 (d, *J* = 8.2 Hz, 4H), 1.28–1.14 (m, 26H), 1.11–0.95 (m, 14H), 0.94–0.82 (m, 14H), 0.78 (h, *J* = 3.1 Hz, 8H), 0.56 (ddt, *J* = 13.7, 11.5, 7.2 Hz, 12H).

^{13}C NMR (101 MHz, $CDCl_3$) δ = 181.75, 166.63, 146.93, 144.34, 144.26, 143.32, 140.50, 139.23, 138.92, 136.86, 136.77, 136.71, 133.20, 133.18, 132.65, 132.63, 132.20, 129.86, 129.46, 129.41, 128.23, 128.21, 128.17, 128.15, 128.06, 117.86, 117.70, 55.44, 52.47, 39.02, 31.90, 31.52, 30.57, 30.50, 30.39, 30.36, 30.31, 30.27, 29.74, 29.67, 29.65, 29.62, 29.58, 29.56, 29.46, 29.42, 29.37, 29.34, 29.32, 28.22, 28.18, 27.98, 27.88, 25.45, 25.42, 25.33, 22.78, 22.76, 22.67, 22.41, 14.10, 13.89, 13.74, 13.72.

HRMS (m/z) $[M+H]^+$ calcd. for ($C_{74}H_{105}N_4O_4S_4$): 1241.7014. Found: 1241.6951.

Synthesis of CHE-Me:

Intermediate 3 (204 mg, 0.15 mmol, 1.0 eq.) and **IC-2F** (86 mg, 0.38 mmol, 2.5 eq.) were dissolved in toluene (20.0 mL), then 1.0 mL acetic anhydride (Ac_2O) and 0.2 ml boron trifluoride diethyl etherate ($BF_3{\cdot}OEt_2$) added separately. The resulting mixture was stirred 15 minutes at room temperature. Subsequently, 1.5 mL of methanol (MeOH) was added to the reaction system to quench the reaction. The reaction mixture concentrated under reduced pressure. The crude product was purified via silica gel column chromatography with petroleum ether/chloroform (1:1, v/v) as eluent to afford **CHE-Me** as a black solid (232 mg, 87%).

^{1}H NMR (400 MHz, Chloroform-*d*) δ = 9.14 (s, 1H), 9.09 (s, 1H), 8.95 (s, 1H), 8.51 (td, *J* = 10.7, 6.3 Hz, 2H), 8.41 – 8.32 (m, 2H), 7.70 (q, *J* = 6.8 Hz, 2H), 4.83 (s, 4H), 3.99 (s, 3H), 3.24 (q, *J* = 7.6 Hz, 4H), 2.25 (s, 2H), 1.92 – 1.82 (m, 4H), 1.53 (t, *J* = 7.8 Hz, 4H), 1.39 (d, *J* = 11.2 Hz, 4H), 1.33 – 1.09 (m, 42H), 0.99 (s, 12H), 0.84 (dd, *J* = 10.3, 5.4 Hz, 8H), 0.66 (dq, *J* = 31.7, 7.3 Hz, 12H).

^{13}C NMR (101 MHz, $CDCl_3$) δ = 183.94, 164.19, 156.47, 153.56, 151.85, 150.83, 144.20, 141.24, 138.49, 137.08, 136.74, 135.57, 135.50, 134.43, 133.78, 132.98, 132.29, 132.08, 131.66, 131.02, 129.87, 129.58, 128.24, 127.33, 126.46, 117.59, 117.51, 116.88, 116.73, 112.81, 112.62, 112.35, 110.32, 110.15, 66.34, 66.21, 53.73, 50.35, 37.25, 29.72, 29.42, 29.28, 29.20, 28.41, 28.36, 27.79, 27.68, 27.52, 27.46, 27.36, 27.18, 25.94, 23.41, 20.74, 20.49, 20.28, 11.91, 11.78, 11.63.

^{19}F NMR (376 MHz, $CDCl_3$) δ = -122.95, -123.00, -123.06, -123.11, -124.23, -124.28, -124.38, -124.43.

HRMS (m/z) $[M]^+$ calcd. for ($C_{98}H_{108}F_4N_8O_4S_4$): 1665.7346. Found: 1665.7348.

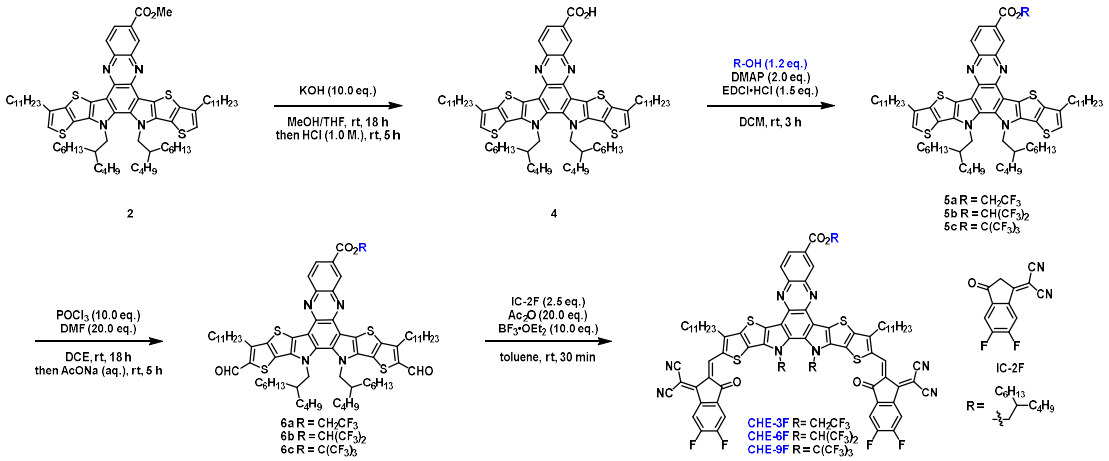

Scheme S2. The overall synthetic route for **CHE-3F, CHE-6F and CHE-9F**.

Synthesis of intermediate 4:

Intermediate 2 (593 mg, 0.5 mmol, 1.0 eq.) was dissolved in tetrahydrofuran (30.0 mL), then 10.0 mL of a methanol (MeOH) solution containing 1.0 M KOH was slowly added to the reaction system. After the addition was completed, the reaction system was stirred at room temperature for approximately 12 h. Subsequently, 20 mL of 1.0 M hydrochloric acid (HCl, aq.) was dropwise to the reaction system to quench the reaction. The reaction system was extracted with dichloromethane (DCM, 50 mL×3), then the organic phase was separated and concentrated under reduced pressure. Finally, the crude product was purified via silica gel column chromatography with dichloromethane/acetone (10:1, v/v) as eluent to afford **intermediate 4** as a green solid (551 mg, 94%).

^{1}H NMR (400 MHz, Chloroform-*d*) δ = 9.36 (s, 1H), 8.54 (q, *J* = 8.9 Hz, 2H), 7.07 (d, *J* = 3.9 Hz, 2H), 4.71 (d, *J* = 7.8 Hz, 4H), 2.92 (q, *J* = 6.7, 6.2 Hz, 4H), 2.22 (d, *J* = 6.5 Hz, 2H), 1.95 (q, *J* = 7.5 Hz, 4H), 1.50 (dq, *J* = 21.2, 7.2 Hz, 10H), 1.33 (d, *J* = 8.5 Hz, 24H), 1.13 – 0.87 (m, 36H), 0.67 (p, *J* = 7.1 Hz, 12H).

^{13}C NMR (101 MHz, $CDCl_3$) δ = 171.81, 143.52, 143.41, 143.23, 140.15, 139.53, 139.26, 137.16, 137.02, 136.95, 133.63, 132.38, 131.50, 129.64, 128.26, 127.51, 123.62, 123.46, 123.40, 119.14, 117.08, 116.76, 55.20, 38.77, 38.74, 31.96, 31.61, 30.39, 30.30, 29.75, 29.70, 29.60, 29.56, 29.52, 29.40, 28.97, 28.95, 28.01, 27.88, 25.43,

25.30, 22.80, 22.77, 22.73, 22.45, 14.16, 13.94, 13.78, 13.76.

HRMS (m/z) $[M+H]^+$ calcd. for ($C_{71}H_{102}N_4O_2S_4$): 1171.6959. Found: 1171.6906.

Synthesis of intermediate 5a：

Under the protection of nitrogen, **Intermediate 4** (118 mg, 0.1 mmol, 1.0 eq.), 4-Dimethylaminopyridine (DMAP, 25mg, 0.2 mmol, 2.0 eq.), *n*-(3-dimethylaminopropyl) -*n*'-ethylcarbodiimide hydrochloride (EDCI, 29 mg, 0.15 mmol, 1.5 eq.) and 2,2,2-trifluoroethanol (12 mg, 0.12 mmol, 1.2 eq.) dissolved in anhydrous dichloromethane (DCM, 20.0 mL) and stirred at room temperature for 12 h. Then, the reaction mixture is quenched by dropwise with saturated ammonium chloride solution (NH_4Cl, aq.) and extracted with dichloromethane (DCM, 50 mL×3). The combined organic phase was washed with saturated saline solution for three times and dried over anhydrous with sodium sulfate (Na_2SO_4). After solvent was evaporated under reduced pressure, the residue was purified through a silica gel column with petroleum ether/dichloromethane (1:1, v/v) as eluent to give compound **5a** as an green solid (110 mg, 88% yield).

^{1}H NMR (400 MHz, Chloroform-*d*) δ = 9.42 (s, 1H), 8.70 (d, *J* = 8.9 Hz, 1H), 8.60 (d, *J* = 8.8 Hz, 1H), 5.06 (q, *J* = 8.4 Hz, 2H), 4.89 (d, *J* = 7.8 Hz, 4H), 3.08 (t, *J* = 7.8 Hz, 4H), 2.45–2.37 (m, 2H), 2.11 (t, *J* = 7.7 Hz, 4H), 1.72–1.60 (m, 8H), 1.50 (d, *J* = 9.3 Hz, 26H), 1.30–1.08 (m, 32H), 0.83 (q, *J* = 7.5, 6.4 Hz, 12H).

^{13}C NMR (101 MHz, $CDCl_3$) δ = 164.96, 143.48, 143.37, 143.25, 140.04, 139.66, 139.33, 137.17, 137.00, 136.94, 133.31, 132.36, 131.59, 129.83, 129.73, 127.37, 127.16, 127.12, 125.05, 124.61, 123.61, 123.58, 123.55, 123.43, 121.86, 119.17, 119.10, 116.99, 116.77, 61.29, 60.92, 55.22, 38.78, 38.74, 31.95, 31.60, 31.57, 30.41, 30.37, 30.31, 30.26, 29.74, 29.68, 29.57, 29.54, 29.51, 29.39, 28.95, 28.03, 28.00, 27.91, 27.87, 25.46, 25.41, 25.33, 25.27, 22.79, 22.76, 22.72, 22.44, 14.13, 13.92, 13.76.

^{19}F NMR (376 MHz, $CDCl_3$) δ = -73.34.

HRMS (m/z) $[M+H]^+$ calcd. for ($C_{73}H_{104}F_3N_4O_2S_4$): 1253.6989. Found: 1253.6989.

Synthesis of intermediate 5b：

Intermediate 5b was obtained by a similar method with a yield of 86% yield and is a green solid.

^{1}H NMR (400 MHz, Chloroform-*d*) δ = 9.21 (d, *J* = 1.9 Hz, 1H), 8.48 (d, *J* = 8.9 Hz, 1H), 8.34 (dd, *J* = 8.9, 2.0 Hz, 1H), 6.98 (s, 2H), 6.11 (d, *J* = 6.1 Hz, 1H), 4.59 (d, *J* = 7.8 Hz, 4H), 2.81 (q, *J* = 7.0 Hz, 4H), 2.10 (s, 2H), 1.84 (dq, *J* = 7.9, 4.4, 3.7 Hz, 4H), 1.44–1.32 (m, 8H), 1.28 – 1.16 (m, 26H), 0.99 – 0.78 (m, 32H), 0.58–0.51 (m, 12H).

^{13}C NMR (101 MHz, $CDCl_3$) δ = 163.39, 143.75, 139.85, 134.13, 130.14, 127.09, 125.39, 123.54, 119.30, 55.22, 38.71, 31.94, 31.92, 31.57, 30.34, 30.28, 30.23, 29.72, 29.70, 29.67, 29.65, 29.52, 29.49, 29.38, 29.36, 28.92, 27.95, 27.84, 25.37, 25.23, 22.70, 22.42, 14.13, 14.10, 13.92, 13.74, 13.71.

^{19}F NMR (376 MHz, $CDCl_3$) δ = -72.87

HRMS (m/z) $[M+H]^+$ calcd. for ($C_{74}H_{103}F_6N_4O_2S_4$): 1321.6863. Found: 1321.6821.

Synthesis of intermediate 5c：

Intermediate 5c was obtained by a similar method with a yield of 86 % yield and is a green solid.

^{1}H NMR (400 MHz, Chloroform-*d*) δ = 9.22 (s, 1H), 8.55 (d, *J* = 8.9 Hz, 1H), 8.35 (d, *J* = 8.8 Hz, 1H), 7.07 (s, 2H), 4.69 (d, *J* = 7.8 Hz, 4H), 2.91 (td, *J* = 7.7, 4.4 Hz, 4H), 2.23–2.16 (m, 2H), 1.93 (t, *J* = 7.6 Hz, 4H), 1.53–1.43 (m, 8H), 1.38–1.29 (m, 26H), 1.07–0.89 (m, 32H), 0.65 (q, *J* = 6.3, 5.5 Hz, 12H).

^{13}C NMR (101 MHz, $CDCl_3$) δ = 159.99, 143.82, 143.44, 143.29, 139.98, 139.79, 139.55, 137.26, 137.05, 136.94, 134.40, 132.59, 131.68, 130.27, 126.91, 125.51, 123.61, 123.44, 123.38, 121.38, 119.31, 118.47, 116.89, 116.64, 55.22, 38.76, 38.73, 31.92, 31.57, 30.35, 30.28, 29.72, 29.70, 29.65, 29.51, 29.48, 29.36, 28.91, 27.96, 27.85, 25.41, 25.28, 22.75, 22.73, 22.70, 22.41, 14.12, 14.09, 13.90, 13.73, 13.70.

^{19}F NMR (376 MHz, $CDCl_3$) δ = -68.98.

HRMS (m/z) $[M+H]^+$ calcd. for ($C_{75}H_{101}F_9N_4O_2S_4$): 1388.6664. Found: 1388.6634.

Synthesis of intermediate 6a：

Intermediate 6a was obtained by a similar method with a yield of 84% yield and is a orange red solid.

^{1}H NMR (400 MHz, Chloroform-*d*) δ = 10.10 (d, *J* = 1.5 Hz, 2H), 9.16 (d, *J* = 1.8 Hz, 1H), 8.45 (d, *J* = 8.9 Hz, 1H), 8.37 (dd, *J* = 8.9, 1.9 Hz, 1H), 4.85–4.77 (m, 2H), 4.62

(d, J = 7.9 Hz, 4H), 3.19 (td, J = 7.6, 3.7 Hz, 4H), 2.06 (d, J = 8.4 Hz, 2H), 1.91 (s, 4H), 1.51 (s, 2H), 1.47–1.40 (m, 4H), 1.35 (d, J = 6.8 Hz, 4H), 1.26–1.17 (m, 24H), 1.02–0.78 (m, 32H), 0.60–0.52 (m, 12H).

^{13}C NMR (101 MHz, $CDCl_3$) δ = 181.83, 164.71, 147.03, 146.94, 144.39, 144.28, 143.76, 140.44, 139.68, 139.26, 137.01, 136.89, 136.78, 133.45, 133.25, 132.81, 129.94, 129.45, 128.17, 128.00, 127.88, 117.74, 117.58, 61.04, 55.42, 38.97, 31.90, 31.50, 30.56, 30.50, 30.32, 29.66, 29.62, 29.60, 29.56, 29.45, 29.41, 29.34, 29.31, 28.20, 27.90, 27.79, 25.34, 22.71, 22.67, 22.41, 14.10, 13.90, 13.71, 13.68.

^{19}F NMR (376 MHz, $CDCl_3$) δ = -73.38.

HRMS (m/z) $[M+H]^+$ calcd. for ($C_{75}H_{104}F_3N_4O_4S_4$): 1309.6888. Found: 1309.6857.

Synthesis of intermediate 6b：

Intermediate 6b was obtained by a similar method with a yield of 85% yield and is a orange red solid solid.

^{1}H NMR (400 MHz, Chloroform-*d*) δ = 10.10 (s, 2H), 9.20 (s, 1H), 8.47 (d, J = 8.9 Hz, 1H), 8.38 (d, J = 9.0 Hz, 1H), 6.17–6.09 (m, 1H), 4.63 (d, J = 7.9 Hz, 4H), 3.19 (q, J = 7.2 Hz, 4H), 2.11–2.04 (m, 2H), 1.91 (q, J = 7.1 Hz, 4H), 1.44 (t, J = 7.8 Hz, 4H), 1.34 (t, J = 7.1 Hz, 4H), 1.20 (t, J = 8.9 Hz, 26H), 1.04–0.81 (m, 32H), 0.59–0.52 (m, 12H).

^{13}C NMR (101 MHz, $CDCl_3$) δ = 182.75, 182.71, 180.99, 180.95, 163.23, 163.18, 163.14, 147.03, 146.93, 144.41, 144.36, 144.31, 144.14, 144.08, 144.04, 143.99, 140.28, 140.23, 139.95, 139.44, 137.26, 137.21, 136.95, 136.82, 134.91, 134.85, 133.61, 133.25, 132.90, 131.09, 129.46, 129.42, 128.63, 128.56, 128.33, 128.30, 128.18, 128.16, 126.98, 126.90, 126.28, 126.19, 124.87, 122.07, 119.27, 119.22, 117.66, 117.49, 116.46, 68.40, 68.06, 67.72, 66.91, 66.57, 66.22, 56.82, 55.44, 54.07, 39.61, 38.34, 32.75, 31.87, 31.51, 30.88, 30.58, 30.26, 29.64, 29.37, 29.02, 28.40, 28.18, 26.92, 26.57, 25.30, 23.98, 23.66, 22.72, 22.43, 21.47, 21.19, 15.76, 15.56, 14.72, 14.53, 14.32, 13.49, 13.29, 13.08, 12.06.

^{19}F NMR (376 MHz, $CDCl_3$) δ = -72.89.

HRMS (m/z) $[M+H]^+$ calcd. for ($C_{76}H_{102}F_6N_4O_4S_4$): 1377.6761. Found: 1377.6656.

Synthesis of intermediate 6c：

Intermediate 6c was obtained by a similar method with a yield of 75% yield and is a orange red solid solid.

^{1}H NMR (400 MHz, Chloroform-*d*) δ = 10.09 (s, 2H), 9.09 (d, *J* = 1.9 Hz, 1H), 8.44 (d, *J* = 8.9 Hz, 1H), 8.27 (dd, *J* = 9.0, 2.0 Hz, 1H), 4.69–4.56 (m, 4H), 3.18 (t, *J* = 7.7 Hz, 4H), 2.08 (d, *J* = 7.4 Hz, 2H), 1.93–1.84 (m, 4H), 1.47–1.39 (m, 4H), 1.33 (t, *J* = 7.4 Hz, 4H), 1.20 (dp, *J* = 15.2, 6.0, 4.6 Hz, 26H), 1.08–0.81 (m, 28H), 0.77 (td, *J* = 6.8, 3.7 Hz, 8H), 0.60–0.51 (m, 12H).

^{13}C NMR (101 MHz, $CDCl_3$) δ = 181.80, 181.77, 159.75, 146.95, 146.86, 144.43, 144.32, 144.02, 140.16, 140.02, 139.50, 137.11, 137.08, 136.96, 136.80, 134.30, 133.68, 133.67, 132.90, 132.88, 130.32, 129.44, 129.36, 128.34, 128.31, 128.20, 128.17, 127.55, 126.37, 121.34, 118.44, 117.67, 117.45, 55.48, 39.00, 31.91, 31.88, 31.50, 30.51, 30.35, 30.28, 30.25, 29.67, 29.64, 29.60, 29.55, 29.49, 29.41, 29.34, 29.30, 28.17, 27.92, 27.82, 25.38, 25.26, 22.76, 22.73, 22.71, 22.68, 22.65, 22.41, 14.08, 14.05, 13.89, 13.71, 13.68, 13.66.

^{19}F NMR (376 MHz, $CDCl_3$) δ = -68.99.

HRMS (m/z) $[M]^+$ calcd. for ($C_{77}H_{101}F_9N_4O_4S_4$): 1444.6562. Found: 1444.6599.

Synthesis of CHE-3F：

CHE-3F was obtained by a similar method with a yield of 86% yield and is a black solid.

^{1}H NMR (400 MHz, Chloroform-*d*) δ = 9.19 (t, *J* = 2.2 Hz, 3H), 8.58 (ddd, *J* = 9.9, 6.7, 1.9 Hz, 2H), 8.51–8.46 (m, 2H), 7.74 (t, *J* = 7.4 Hz, 2H), 4.87 (dd, *J* = 12.0, 7.8 Hz, 6H), 3.31 (s, 4H), 2.26 (s, 2H), 1.94 (s, 4H), 1.58 (s, 4H), 1.43 (s, 4H), 1.35–1.24 (m, 26H), 1.20–0.97 (m, 24H), 0.87 (td, *J* = 6.8, 4.3 Hz, 8H), 0.75–0.62 (m, 12H).

^{13}C NMR (101 MHz, $CDCl_3$) δ = 186.15, 164.47, 158.77, 155.75, 154.09, 154.01, 146.30, 143.82, 140.58, 139.71, 139.25, 137.80, 137.71, 135.89, 135.25, 134.47, 133.95, 133.25, 133.21, 133.06, 131.81, 131.70, 129.94, 128.51, 128.38, 121.75, 119.85, 118.89, 118.76, 115.07, 114.98, 114.85, 114.56, 112.34, 55.89, 39.36, 31.92, 31.90, 31.61, 31.50, 31.40, 30.49, 29.91, 29.85, 29.71, 29.68, 29.65, 29.63, 29.59, 29.56, 29.53, 29.51, 29.49, 29.36, 29.33, 28.11, 28.00, 25.58, 22.91, 22.88, 22.69, 22.66, 22.47, 14.10,

14.08, 13.98, 13.81, 13.79.

^{19}F NMR (376 MHz, $CDCl_3$) δ = -73.35, -122.98, -123.03, -123.08, -124.27, -124.32, -124.35, -124.40.

HRMS (m/z) $[M]^+$ calcd. for ($C_{99}H_{107}F_7N_8O_4S_4$): 1733.7220. Found: 1733.7225.

Synthesis of CHE-6F：

CHE-6F was obtained by a similar method with a yield of 85% yield and is a black solid.

^{1}H NMR (400 MHz, Chloroform-*d*) δ = 9.22 (s, 1H), 9.15 (d, *J* = 4.2 Hz, 2H), 8.55–8.45 (m, 4H), 7.74 (t, *J* = 7.4 Hz, 2H), 6.22 (d, *J* = 6.0 Hz, 1H), 4.89 (d, *J* = 8.0 Hz, 4H), 3.30 (q, *J* = 9.4, 8.7 Hz, 4H), 2.34–2.25 (m, 2H), 1.92 (q, *J* = 7.8 Hz, 4H), 1.58 (q, *J* = 7.7 Hz, 4H), 1.46–1.39 (m, 4H), 1.35–1.23 (m, 28H), 1.21–1.11 (m, 10H), 1.02 (qt, *J* = 12.8, 6.3 Hz, 16H), 0.87 (q, *J* = 6.7, 6.0 Hz, 8H), 0.77–0.65 (m, 12H).

^{13}C NMR (101 MHz, $CDCl_3$) δ = 186.13, 162.98, 158.70, 155.72, 154.08, 153.95, 146.39, 146.28, 144.13, 140.45, 140.05, 139.50, 137.86, 137.73, 136.59, 135.85, 135.22, 134.62, 134.01, 133.29, 133.23, 131.84, 131.65, 130.25, 128.23, 126.80, 119.92, 118.81, 118.66, 114.94, 114.50, 112.31, 68.64, 55.92, 39.38, 31.92, 31.89, 31.60, 31.48, 31.39, 30.50, 29.85, 29.70, 29.65, 29.62, 29.56, 29.54, 29.49, 29.36, 29.31, 28.08, 25.49, 22.89, 22.68, 22.65, 22.47, 14.09, 14.06, 13.99, 13.78.

^{19}F NMR (376 MHz, $CDCl_3$) δ = -72.90, -122.98, -123.03, -123.08, -124.27, -124.32, -124.35, -124.40.

HRMS (m/z) $[M]^+$ calcd. for ($C_{100}H_{106}F_{10}N_8O_4S_4$): 1801.7094. Found: 1801.7089.

Synthesis of CHE-9F：

CHE-9F was obtained by a similar method with a yield of 82% yield and is a black solid.

^{1}H NMR (400 MHz, Chloroform-*d*) δ = 9.14 (d, *J* = 7.3 Hz, 3H), 8.50 (dd, *J* = 9.7, 5.5 Hz, 3H), 8.36 (d, *J* = 8.9 Hz, 1H), 7.69 (t, *J* = 7.5 Hz, 2H), 4.83 (d, *J* = 8.0 Hz, 4H), 3.27 (q, *J* = 6.6 Hz, 4H), 2.23 (q, *J* = 6.8 Hz, 2H), 1.89 (t, *J* = 8.0 Hz, 4H), 1.56–1.51 (m, 4H), 1.39 (t, *J* = 7.0 Hz, 4H), 1.26 (d, *J* = 18.1 Hz, 28H), 1.12 (s, 10H), 0.99 (p, *J* = 10.0, 9.3 Hz, 16H), 0.83 (q, *J* = 6.3 Hz, 8H), 0.71–0.60 (m, 12H).

^{13}C NMR (101 MHz, $CDCl_3$) δ = 186.13, 159.57, 158.76, 155.73, 153.98, 153.11, 146.27, 144.17, 140.42, 140.15, 139.58, 137.86, 135.80, 135.28, 134.68, 134.52, 134.26, 134.03, 133.29, 131.85, 131.67, 130.43, 128.08, 126.97, 121.31, 119.96, 118.76, 118.42, 115.06, 114.94, 114.51, 112.49, 112.32, 68.71, 55.91, 39.34, 31.88, 31.58, 31.38, 30.50, 29.82, 29.69, 29.64, 29.53, 29.50, 29.46, 29.35, 29.30, 28.05, 27.95, 25.55, 25.43, 22.85, 22.67, 22.63, 22.45, 14.07, 14.03, 13.96, 13.75.

^{19}F NMR (376 MHz, $CDCl_3$) δ = -69.02, -122.99, -123.02, -123.04, -123.08, -124.31, -124.37, -124.42.

HRMS (m/z) $[M]^+$ calcd. for ($C_{101}H_{105}F_{13}N_8O_4S_4$): 1869.6968. Found: 1869.6971.

2. Device Fabrication and Characterization

2.1 Device fabrication

The conventional devices were fabricated with the architecture of ITO/ 2PACz/active layer/PNDIT-F3N/Ag. In detail, ITO coated glass substrates were cleaned in turn with detergent water, deionized water, acetone and isopropyl alcohol in an ultrasonic bath sequentially for 15 mins and dried by nitrogen purge. Before use, the cleaned ITO substrates were treated with UV exposure for 15 mins in a UV-ozone chamber (Jelight Company). Then a thin layer of 2PACz was first spin-coated on the ITO substrates with 3000 rpm for 20 s with thermal annealed for 5 minutes at 100 °C. The PM6: CHE-9F/6F/3F/Me (1:1.3 w/w) was dissolved in chloroform at the total blend concentration of 13.8 mg/mL with 140 wt% TCB. The PM6:BO-4Cl:CHE-9F,PM6:btp-eC9:CHE-F (1:1.1:0.2) and D18:L8-Bo:CHE-9F (1:1.2:0.1) were dissolved in chloroform at the total blend concentration of 14.4 mg/mL with 140 wt% TCB (mass of A). All the solutions need to be stirred at room temperature overnight. Subsequently, the active layer was spin-coated onto the hole transport layer at 1800 rpm for 30 s, yielding a film with a target thickness of 105 nm. After spin coating, the blend films were annealed at 90 °C for 5 mins. PNDIT-F3N (dissolved 2 in methanol with 0.5% v/v glacial acetic acid at the concentration of 1 mg mL^{-1}) layer was spin-coated on the top of the active layers at 3000 rpm for 20 s. Finally, 150 nm Ag was deposited under 2×10^{-6} Pa. The active area of the device was 4 mm^2. The area of the mask was

about 3.24 mm^2 for device in our laboratory.

2.2 Characterization of the OSC

The *J-V* measurements were performed by using the solar simulator (SS-F5-3A, Enli Technology, xenon lamp, filter model AMFG2.0) along with AM 1.5G spectra (100 mW cm^{-2}), Which was calibrated by a standard Si solar cell (made by Enli Technology Co., Ltd., Taiwan, and calibrated report can be traced to NREL. The spectral between reference cell and devices could match well during the test (within 3% errors). The current-voltage scan speed and delay time are 0.02 V/s and 1 ms respectively. No pretreatments (light soaking or holding cell at a bias) were required before *J-V* testing, and all the measurements were conducted in a nitrogen-filled glovebox at room temperature (ca. 25° C) without attaching any antireflection coating on the incident plane of solar cells. Note that there is no hysteresis or other unusual behaviors during the measurements of solar cells. The EQE spectra were measured by using a QE-R Solar Cell Spectral Response Measurement System (Enli Technology Co., Ltd., Taiwan).

3. Supplementary Note

3.1 Supplementary Note 1

The ground-state (S_0) geometries and frontier molecular orbital energy levels of the studied molecules were optimized using density functional theory (DFT) with the Becke three-parameter Lee-Yang-Parr (B3LYP) hybrid functional [1]. Among them, the 6-31G(d) basis set was employed for light atoms (C, H, O, N, S, F) [2]. To reduce computational costs, all alkyl chains were replaced with methyl groups (-CH_3). Vibrational frequencies were calculated after geometry optimization, and no imaginary frequencies were found. All calculations were performed using the Gaussian 16 package [3].

3.2. Supplementary Note 2

Single-crystal Growth Single crystals of CHE-Me, CHE-3F and CHE-6F were grown by the liquid diffusion method at room temperature. In detail, 1.5 mL of methanol was transferred to 0.15 mL of concentrated chloroform solution of CHE-Me slowly, and the beautiful cuboid-shape dark purple crystals were formed on the inner glassy tube after

about 10 days. The X-ray diffraction signals of single crystal were collected on Bruker D8 Venture diffractometer. The crystal was kept at 193.0 K during data collection. The single crystals growth methods of CHE-3F and CHE-6F were the same as CHE-Me. Although a Bruker D8 Venture diffractometer was used with the exposure time maximized, the high-angle diffraction signals were inevitably weak due to the intrinsic disorder of the structures. The final structural solution and refinement were thus conducted using truncated data with $I/\sigma > 2$. The current data are sufficient to unambiguously establish the molecular connectivity and conformation."

3.3 Supplementary Note 3

UV-Visible (UV-vis) Absorption. The UV-vis spectra were obtained by a Cary 5000 UV-vis spectrophotometer.

Thermogravimetric Analysis (TGA) and Differential Scanning Calorimetry (DSC) analysis.

The TGA analysis and the DSC were carried out on a TG209 DSC204DMA242 TMA202 (NETZSCH) instrument with a heating rate of 10 K min^{-1} under a nitrogen atmosphere.

Cyclic Voltammetry (CV).

The CV experiments were performed with a LK98B II Microcomputer-based Electrochemical Analyzer. All measurements were conducted at room temperature with a three-electrode configuration. Among them, a glassy carbon electrode was employed as the working electrode, a saturated calomel electrode (SCE) was used as the reference electrode, and a Pt wire was used as the counter electrode. Tetrabutylammonium phosphorus hexafluoride (nBu$_4$NPF$_6$, 0.1 M) in acetonitrile was employed as the supporting electrolyte, and the scan rate was kept at 100 mV s^{-1}. Electrochemically reversible ferrocene was employed as internal reference. The HOMO and LUMO energy levels were calculated from the onset oxidation and the onset reduction potentials, respectively, by following the Supplementary **Equation 1–2**:

$$E_{HOMO} = -(4.80+E_{ox}^{onest}) \text{ eV (S1)}$$

$$E_{LUMO} = -(4.80+E_{re}^{onest}) \text{ eV (S2)}$$

Photoluminescent (PL) Steady-state photoluminescence measurements were

performed using a FLS1000 spectrometer. The emission spectra of the four non-fullerene acceptors (SMAs) were recorded with a near-infrared (NIR) 5509 photomultiplier tube (PMT). For four SMAs (CHE-Me to CHE-9F), the excitation wavelength for their solutions was 640 nm, while the excitation wavelengths for their thin films were 765 nm, 762 nm, 760 nm, and 760 nm in sequence.

Space-Charge-Limited Current (SCLC) Measurement. The SCLC method was used to measure the hole and electron mobilities, by using a diode configuration of ITO/2PACZ/active layer/MoO_3/Ag for hole and ITO/ZnO/active layer/PNDIT-F3N/Ag for electron. The SMAs were fully dissolved (D:A ratio = 1:1.3; 13.8 mg mL^{-1}) and then the solutions were stirred 3 hours at RT and spin-casted at 1800 rpm for 30 s. After spin-coating, the neat films were annealed at 90 °C for 5 mins. The fabrication method of blended films was consistent with that of active layer of device. The dark current density curves were recorded with a bias voltage in the range of 0~8 V. The mobilities were estimated by taking current-voltage curves and fitting the results based on the Supplementary **Equation 3** listed below:

$$J = \frac{9\varepsilon_0\varepsilon_r\mu V^2}{8L^3} \quad \text{(S3)}$$

Where J is the current density, ε_0 is the vacuum permittivity, ε_r is the relative dielectric constant, μ is the mobility, and L is the film thickness. $V = (V_{app}–V_{bi})$ is the internal voltage in the device, where V_{app} is the applied voltage to the device and V_{bi} is the built-in voltage due to the relative work function difference between the two electrodes.

Atomic Force Microscopy Based Infrared Spectroscopy (AFM-IR)

The AFM-IR images were performed using in tapping mode on a Bruker nano IR 3. AFM-IR images of the corresponding blend films measured at a wavenumber of 2216 cm^{-1}, which is a characteristic absorption peak of the C≡N bond in SMAs, compared with PM6. All film samples were spin–cast on ITO/2PACZ substrates under the same conditions as those used for device fabrication.

Grazing Incidence Wide Angle X-ray Scattering (GIWAXS). The GIWAXS samples were prepared on Si substrates by use of the same preparation conditions with devices and were carried out at XEUSS SAXS/WAXS equipment.

Film-depth-dependent light absorption spectroscopy (FLAS). FLAS was conducted by Shaanxi Puguangweishi Technology Co., Ltd. Low-pressure (less than 20 Pa) oxygen plasma was used for the incremental etching of the film. The UV–Vis absorption spectrum after each etching was monitored by an optical spectrometer. Beer-Lambert's law was utilized to fit the film-depth-dependent light absorption spectra.

The Calculation of Energy Loss. The following equation was used to quantify the E_{loss} of OSCs: $E_{\text{loss}} = E_g^{pv} - q\ V_{oc} = \left(E_g^{pv} - qV_{oc}^{SQ}\right) + \left(qV_{oc}^{SQ} - qV_{oc}^{rad}\right) + (qV_{oc}^{rad} - qV_{oc}) = \Delta E_1 + \Delta E_2 + \Delta E_3$. E_g^{pv} represents the bandgap of the blend film and q is the elementary charge. E_g^{pv} is estimated by the cross-point of normalized ultraviolet absorption (UV) and photoluminescence (PL) spectra:

(1) $\Delta E_1 = E_g - V_{oc}^{SQ}$, represents the unavoidable radiative loss originating from absorption above the bandgap. The V_{oc}^{SQ} is the maximum voltage based on the Shockley–Queisser (SQ) limit (**Equation 4):**

$$V_{oc}^{SQ} = \frac{kT}{q}\ln\left(\frac{J_{sc}^{SQ}}{J_0^{SQ}} + 1\right) \cong \frac{kT}{q}\ln\left(\frac{q\bullet\int_{E_g}^{+\infty}\phi_{AM\ 1.5G}\,(E)dE}{q\bullet\int_{E_g}^{+\infty}\phi_{BB}\,(E)dE}\right) \quad \text{(S4)}$$

(2) $\Delta E_2 = E_{\text{loss}} - \Delta E_1 - \Delta E_2$.

(3) $\Delta E_3 = -k\text{Tln}(\text{EQE}_{\text{EL}})$. For the EQE_{EL} measurements, a digital source meter (Keithley 2400) was 80 employed to inject electric current into the solar cells, and the emitted photons were collected by a Si diode (Hamamatsu s1337-1010BQ) and indicated by a picoammeter (Keithley 6482).

Photoluminescence Quantum Yield (PLQY). The PLQY was estimated by using an Edinburgh FLS1000 spectrometer which is equipped with an integrating sphere (HORIBA, Japan). The excitation wavelength and emission wavelength are 762 nm. The signal of four SMAs were recorded by an NIR photomultiplier (PMT-1700 nm) cooled to −80 ℃ with liquid N_2 and the wavelength detection range is between 800 nm and 1200 nm.

Electroluminescence External Quantum Efficiency (EQE_{EL}). For the EQE_{EL} measurements, a digital source meter (Keithley 2400) was employed to inject electric

current into the solar cells, and the emitted photons were collected by a Si diode 10 (Hamamatsu s1337-1010BQ) and indicated by a picometer (Keithley 6482). The injection current to the OSCs was kept at 1 mA by the direct current meter (PWS2326Tectronix). The Calculation of Non-Radiative Energy Loss: ΔE_3 is confirmed by directly measuring the external quantum efficiency of electroluminescence (EQE_{EL}) of the solar cell through the **Equation 6**:

$$\Delta E_3 = kTln(\frac{1}{EQE_{EL}}) \text{ (S5)}$$

Measurements of Transient Photocurrent (TPC) and Transient photovoltage (TPV). A white light bias was generated from an array of diodes (Molex 180081-4320) with light intensity about 0.5 sun. The light intensity of the diode pumped laser passing through an attenuator is about 1132.5 μW cm^{-2}. A diode pumped laser (Lapa-80) was used as the perturbation source, with a pulse duration of 10 ns and a repetition frequency of 20 Hz. The perturbation light intensity was attenuated to keep the amplitude of transient V_{OC} (ΔV_{OC}) below 10 mV so that $\Delta V_{OC} << V_{OC}$. Current dynamics were recorded on a digital oscilloscope (Tektronix MDO4104C), and currents under short circuit conditions were measured over a 50 Ω resistor.

Capacitance spectra. An impedance analyzer (Zennium E41081) was used to obtain capacitance voltage (C-V) characteristics in dark room temperature conditions. For the C-V measurement, the applied AC voltage was 100 mV and a frequency of 10 kHz was used. Based on Mott-Shockley analysis, the trap density (NA) was calculated using **Equation 7**.

$$N_A = \frac{-2}{q\varepsilon_r\varepsilon_0 A^2}\left(\frac{dV}{dC^{-2}}\right) \text{ (S6)}$$

Where q is the charge of an electron, ε_r is the relative dielectric constant of the active layer, ε_0 is the vacuum permittivity, A is the device area.

4. Supporting Tables and Figures.

4.1 Supporting Tables.

Table S1. Photoelectric properties of four SMAs as solution and neat films.

Materials	λ_{sol}^{max} [nm]	λ_{film}^{max} [nm]	Δ_{λ}[nm] [a]	α_{max} [M^{-1} cm^{-1}]	λ_{onset} [nm]
CHE-Me	743	818	75	2.08×10^5	908
CHE-3F	740	806	66	2.14×10^5	893
CHE-6F	737	801	64	2.22×10^5	881
CHE-9F	736	798	62	2.30×10^5	860

[a]$\Delta\lambda = \lambda_{max}^{film} - \lambda_{max}^{sol}$.

Table S2. Summary of energy levels of four SMAs in neat film.

Materials	E_g^{opt} [eV] [a]	E_{HOMO}^{CV} [eV]	E_{LUMO}^{CV} [eV]	E_g^{CV} [eV]
CHE-Me	1.37	-5.64	-3.86	1.78
CHE-3F	1.39	-5.68	-3.86	1.86
CHE-6F	1.41	-5.69	-3.86	1.83
CHE-9F	1.44	-5.71	-3.86	1.85

[b] $E_g^{onest} = 1240/\lambda_{edg}^{film}$.

Table S3. Detailed parameters of 2D grazing incidence wide-angle x-ray scattering (2D GIWAXs) for **CHE-Me** and **CHE-*n*F** in neat film.

Materials	(010) Diffraction Peak				(100) Diffraction Peak			
	q ($Å^{-1}$)	d[a] (Å)	FWHM ($Å^{-1}$)	CCL[b] (Å)	q ($Å^{-1}$)	d[a] (Å)	FWHM ($Å^{-1}$)	CCL[b] (Å)
CHE-Me	1.770	3.55	0.293	19.23	0.344	18.27	0.607	9.31
CHE-3F	1.734	3.62	0.326	17.34	0.356	17.64	0.867	6.52

CHE-6F	1.731	3.63	0.347	16.29	0.368	17.07	0.957	5.90
CHE-9F	0.584	10.75	0.105	66.48	0.685	9.172	0.132	42.64
	1.728	3.64	0.376	15.04	0.376	16.71	0.089	63.53

[a] Calculated from the equation: *d*-spacing=2π/q. [b] Obtained from the Scherrer equation: CCL= 2πK/FWHM, where FWHM is the full-width at half-maximum and K is a shape factor (K= 0.9 here).

Table S4. Crystal data and structure refinement for **CHE-Me**, **CHE-3F** and **CHE-6F**.

Compound	**CHE-Me**	**CHE-3F**	**CHE-6F**
Empirical formula	$C_{99}H_{109}Cl_3F_4N_8O_4S_4$	$C_{199}H_{215}Cl_3F_{14}N_{16}O_6S_8$	$C_{101}H_{107}Cl_3F_{10}N_8O_4S_4$
Formula weight	1785.53	3587.69	1921.53
Temperature/K	180	170	170
Crystal system	triclinic	triclinic	triclinic
Space group	P-1	P-1	P-1
a/Å	12.9602(6)	12.9860(6)	12.8673(9)
b/Å	17.7674(12)	17.7668(11)	16.3829(12)
c/Å	23.0842(11)	23.1063(12)	23.2488(16)
α/°	68.881(4)	68.582(4)	99.692(4)
β/°	81.564(3)	81.345(3)	98.243(3)
γ/°	71.711(4)	71.646(3)	94.310(4)
Volume/Å^3	4704.7(5)	4706.7(5)	4756.2(6)
Z	2	1	2
ρ_{calc}g/cm^{-3}	1.260	1.221	1.258
μ/mm^{-1}	2.218	1.834	1.536
F(000)	1884.0	1827.0	1896.0
Crystal size/mm^3	0.16×0.13×0.12	0.16×0.12×0.11	0.17×0.11×0.1
Radiation	CuKα(λ=1.54178)	CuKα(λ=1.54178)	CuKα (λ=1.54178)

2Θ range for data collection/°	4.106 to 100.868	5.57 to 94.474	3.904 to 94.844
Index ranges	-12≤h≤12, -17≤k ≤17, -23≤l≤ 22	-12≤h≤12, -16≤k≤16, -21≤l ≤ 22	-12≤h≤12, -15≤k≤15, -19≤l≤22
Reflections collected	36351	43250	25866
Independent reflections	9834[R_{int}=0.1374, R_{sigma}=0.1773]	8519 [R_{int} = 0.1270, R_{sigma} = 0.1134]	8624[R_{int}=0.0645, R_{sigma}=0.0798]
Data/restraints/parameters	9834/2349/1078	8519/858/1113	8624/1032/1102
Goodness-of-fit on F^2	1.185	1.124	1.205
Final R indexes [I>=2σ (I)]	R_1 = 0.2049, wR_2 = 0.4540	R_1 = 0.1795, wR_2 = 0.4104	R_1=0.1740, wR_2=0.3957
Final R indexes [all data]	R_1=0.2773, wR_2=0.5046	R_1 = 0.2499, wR_2 = 0.4582	R_1=0.2196, wR_2=0.4234
Largest diff. peak/hole/e Å^3	1.15/-0.91	0.79/-0.75	1.17/-0.68

Table S5. Crystallographic and π-π interaction parameters of **CHE-Me**, **CHE-3F** and **CHE-6F.**

SMAs	**Void sizes (shapes)**	**Packing modes**	**$d_{\pi-\pi}$ [a] (Å)**	**Intermolecular potentials(kJ/mol)**
CHE-Me	11.436×22.272 Å	Mode 1 (E/C)	3.773 Å	322.7
		Mode 2 (E/B)	3.378 Å	328.1

		Mode 3 (E/E)	3.370 Å	133.3
CHE-3F	11.891×23.106 Å	Mode 1 (E/C)	3.816 Å	323.7
		Mode 2 (E/B)	3.344 Å	332.5
		Mode 3 (E/E)	3.366 Å	134.5
CHE-6F	---	Mode 1 (E/C)	3.978 Å	314.7
		Mode 2 (E/B)	3.080 Å	325.6
		Mode 3 (E/E)	3.373 Å	124.0

Table S6. Total energy loss values and different contributions in solar cells based on the SQ limit theory.

Active Layer	E_g	V_{oc}^{SQ} **(V)**	ΔE_1 **(eV)**	ΔE_2[a] **(eV)**	ΔE_3[b] **(eV)**	EQE_{EL} **(10^{-2})**	V_{oc} **(V)**	E_{loss} **(eV)**
PM6: CHE-Me	1.411	1.145	0.265	0.049	0.226	0.016	0.885	0.526
PM6: CHE-3F	1.423	1.175	0.268	0.027	0.236	0.011	0.892	0.516
PM6: CHE-6F	1.425	1.175	0.267	0.036	0.224	0.017	0.898	0.527
PM6:	1.428	1.191	0.268	0.041	0.221	0.020	0.898	0.530

CHE-9F								

[a]$\Delta E_2 = E_{loss}$-ΔE_1-ΔE_3.

[b]$\Delta E_3 = -k\mathrm{T}\ln(\mathrm{EQE_{EL}})$.

Table S7. Detailed parameters of 2D grazing incidence wide-angle x-ray scattering (2D GIWAXs) for **PM6:CHE-Me** and **PM6:CHE-*n*F** blend film.

Materials	(010) Diffraction Peak				(100) Diffraction Peak			
	q ($Å^{-1}$)	d[a] (Å)	FWHM ($Å^{-1}$)	CCL[b] (Å)	q ($Å^{-1}$)	d[a] (Å)	FWHM ($Å^{-1}$)	CCL[b] (Å)
PM6: CHE-Me	1.814	3.46	0.208	27.18	0.325	19.333	0.073	77.46
PM6: CHE-3F	1.853	3.39	0.198	28.56	0.329	19.098	0.068	83.30
PM6: CHE-6F	1.877	3.34	0.187	30.23	0.332	18.925	0.061	92.70
PM6: CHE-9F	1.863	3.37	0.194	29.14	0.324	19.392	0.065	86.99

[a] Calculated from the equation: *d*-spacing=2π/q. [b] Obtained from the Scherrer equation: CCL= 2πK/FWHM, where FWHM is the full-width at half-maximum and K is a shape factor (K= 0.9 here).

Table S8. Information about surface energies of PM6, CHE-Me, CHE-3F, CHE-6F and CHE-9F neat films calculated by water and glycerol contact angle.

Materials	θ_{water} (°)	$\theta_{glycerol}$ (°)	γ_d (mN m^{-1})	γ_p (mN m^{-1})	γ (mN m^{-1})	$\chi_{D:A}$ [a] (K)
PM6	108.61	98.10	0.12	22.78	22.9	–
CHE-Me	98.23	94.43	0.62	29.97	30.59	0.55
CHE-3F	100.05	94.90	0.49	28.73	29.22	0.38
CHE-6F	101.23	95.45	0.43	27.79	28.22	0.27

CHE-9F	104.78	98.50	0.33	24.07	24.82	0.04

[a] The molecular miscibility can be evaluated by Flory–Huggins interaction parameter χ, which is calculated by using the equation of: $\chi_{D:A}=K(\sqrt{\gamma D}-\sqrt{\gamma A})^2$.

Table S9. The lifetime of the hole transfer process in blended films. The data was achieved through the biexponential fitting.

Materials	τ_1 (ps)	τ_2 (ps)
PM6:CHE-Me	0.343	12.07
PM6:CHE-3F	0.406	7.19
PM6:CHE-6F	0.426	7.06
PM6:CHE-9F	0.457	5.58

Table S10. Champion device efficiencies of the binary systems and the corresponding ternary systems blended with CHE-9F for PM6:BO-4Cl, PM6:eC9, and D18:L8BO.

Active layer	V_{oc} (V)	J_{sc} (mA/cm^2)	Cal. J_{sc} (mA/cm^2)	FF	PCE [%]
PM6:BO-4Cl	0.843	27.72	27.08	0.864	18.43
PM6:BO-4Cl: CHE-9F	0.864	28.87	27.58	80.22	20.01
PM6:eC9	0.849	28.39	27.25	79.08	19.23
PM6:eC9: CHE-9F	0.860	28.95	27.68	80.73	20.10
D18:L8-BO	0.910	26.34	25.26	80.84	19.37
D18:L8-BO: CHE-9F	0.909	27.09	25.88	82.40	20.30

Table S11. Statistical analysis of device parameters for eight independent devices based on PM6:Bo4Cl:CHE-9F, PM6:eC9:CHE-9F and D18:L8BO:CHE-9F.

Active layer	V_{oc} (V)	J_{sc} (mA/cm^2)	FF	PCE [%]
PM6:Bo-4Cl:CHE-9F	0.862	28.32	80.14	19.55
	0.864	28.87	80.22	20.01
	0.862	28.78	80.18	19.89
	0.862	28.72	79.80	19.74
	0.862	27.96	80.75	19.46
	0.866	28.16	80.68	19.68
	0.862	28.11	80.83	19.57
	0.859	28.74	79.27	19.57
	0.862±0.002	28.46±0.33	80.23±0.49	19.81±0.47
PM6:btp-eC9:CHE-9F	0.857	29.12	80.49	20.09
	0.860	28.95	80.73	20.10
	0.852	29.22	79.42	19.78
	0.861	28.62	80.30	19.78
	0.852	29.18	79.30	19.72
	0.857	29.13	79.62	19.88
	0.854	29.08	79.80	19.82
	0.855	28.24	81.53	19.69
	0.856±0.003	28.94±0.32	80.15±0.71	19.86±0.15
D18:L8-BO:CHE-9F	0.909	27.09	82.4	20.3
	0.912	26.86	82.57	20.23
	0.91	26.76	82.41	20.08

	0.915	26.99	81.64	20.16
	0.913	26.77	82.17	20.08
	0.912	27.08	82.08	20.27
	0.911	27.25	81.16	20.13
	0.912±0.002	27.01±0.19	81.95±0.53	20.18±0.08

4.2 Supporting Figures.

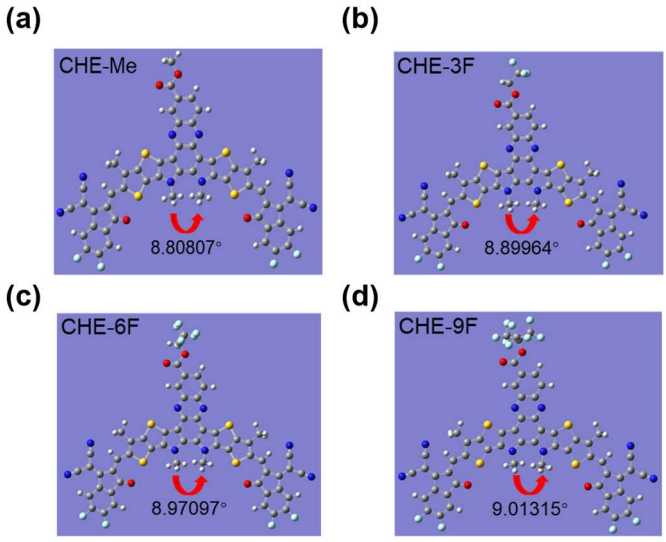

Figure S1. The N–C–C–N dihedral angle for four SMAs.

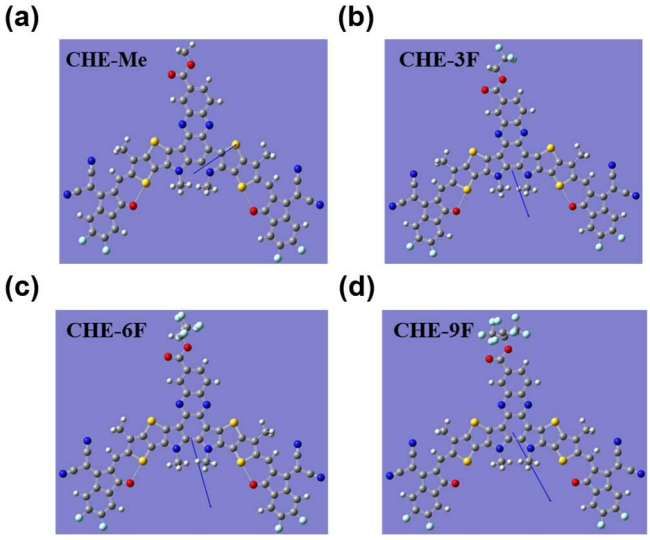

Figure S2. DFT calculated dipole moments and orientation of four SMAs.

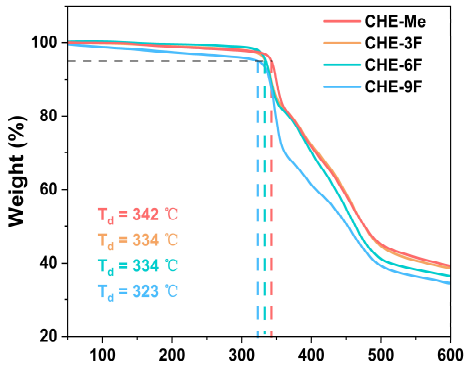

Figure S3. Thermogravimetric analysis of four SMAs. The heating rate is a heating rate of 10°C/min under nitrogen atmosphere**.**

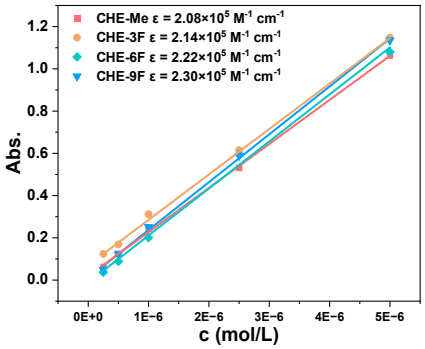

Figure S4. The molar extinction coefficients (ε) of four SMAs in chloroform solutions.

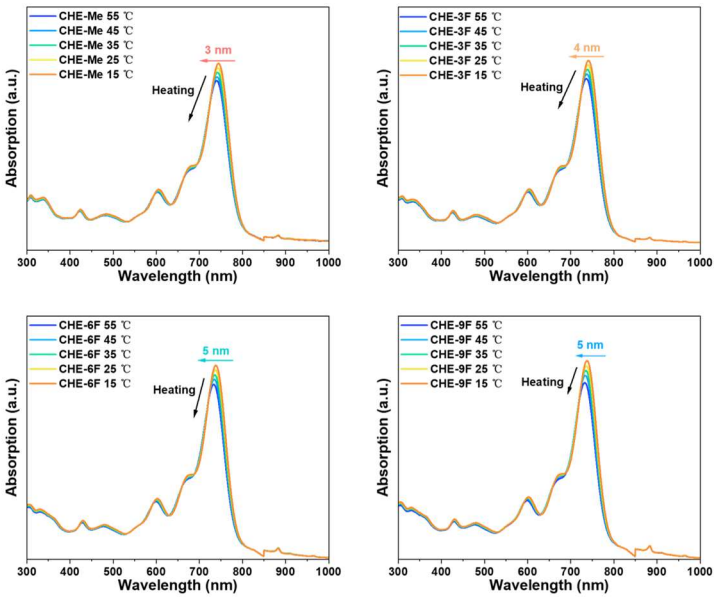

Figure S5. The temperature-dependent absorption spectra in $CHCl_3$ solution for four SMAs.

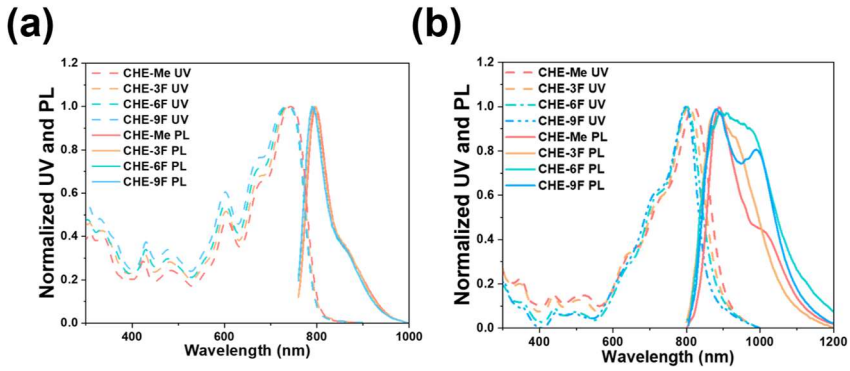

Figure S6. The UV absorption spectra and PL spectra of four SMAs. (a) in chloroform solutions, (b) in neat film.

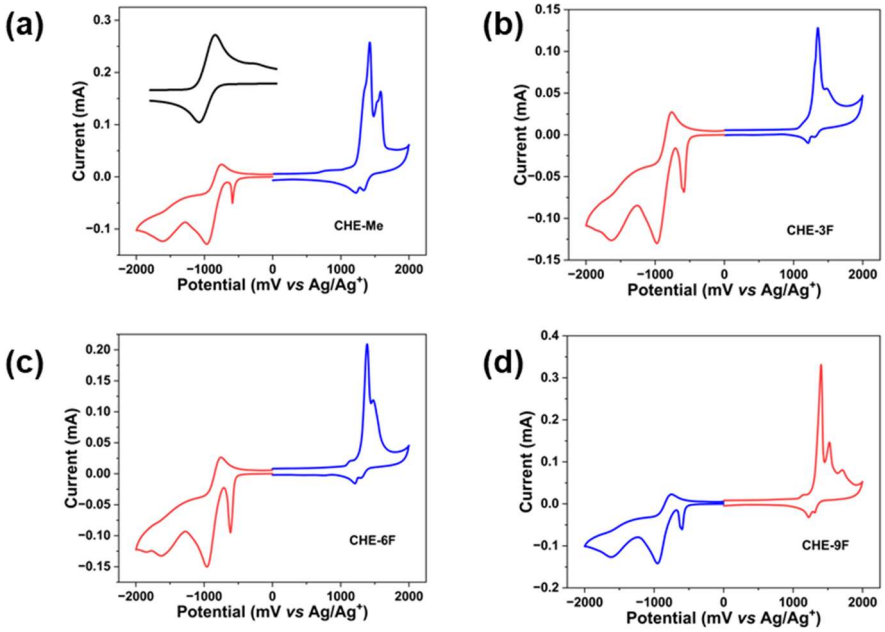

Figure S7. (a–d) Cyclic voltammograms of **CHE-Me**, **CHE-3F**, **CHE-6F** and **CHE-9F** neat films. Red line: oxidation cycle, blue line: reduction cycle.

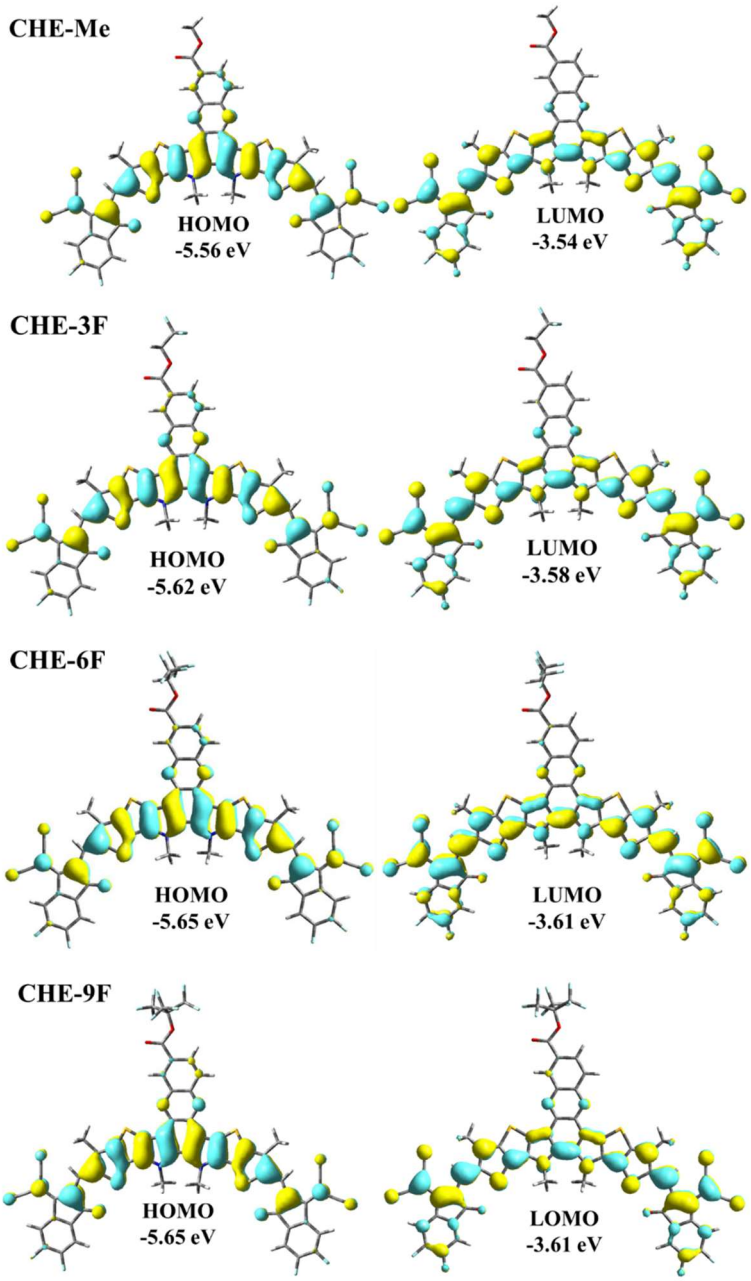

Figure S8. DFT theoretical density distribution for the frontier molecular orbits of four SMAs.

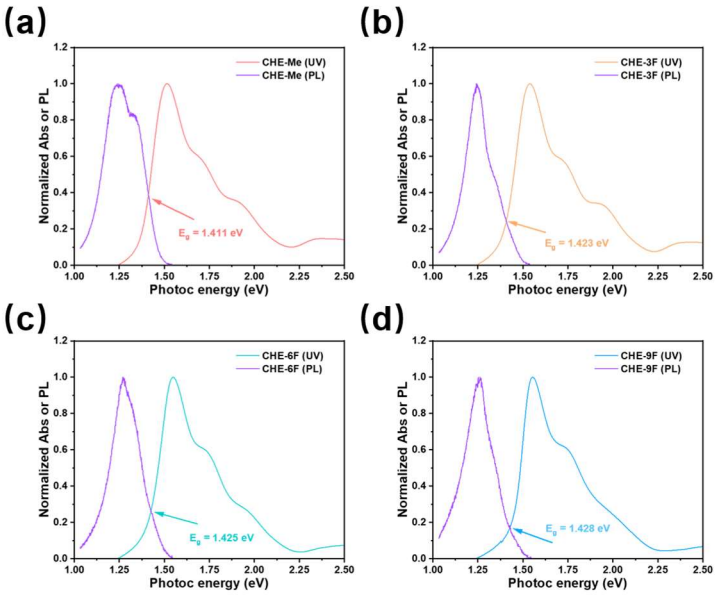

Figure S9. E_g is estimated by the cross-point of normalized absorption and photoluminescence (PL) spectra of the four SMAs neat films.

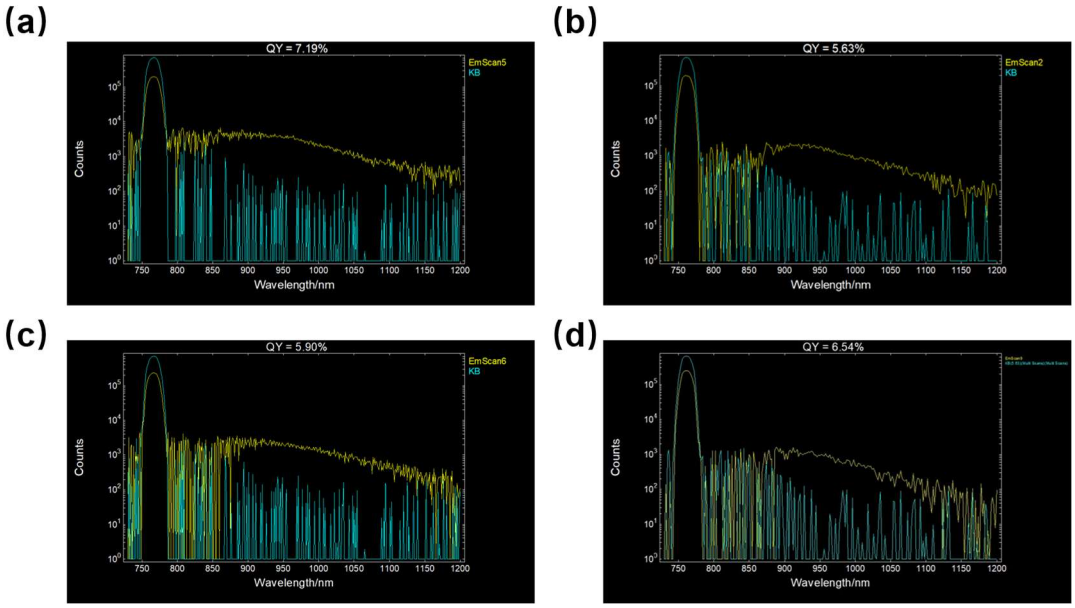

Figure S10. The photoluminescence quantum yield (PLQY) profiles of the four SMAs; from (a) to (d), they are CHE-Me, CHE-3F, CHE-6F, and CHE-9F, respectively.

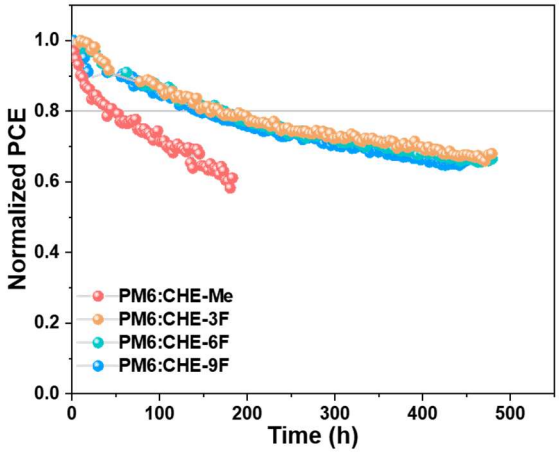

Figure S11： Operational stability test at MPP tracking with continuous illumination (AM 1.5G, 100 mW cm^{-2}) at 25°C in N_2 atmosphere.

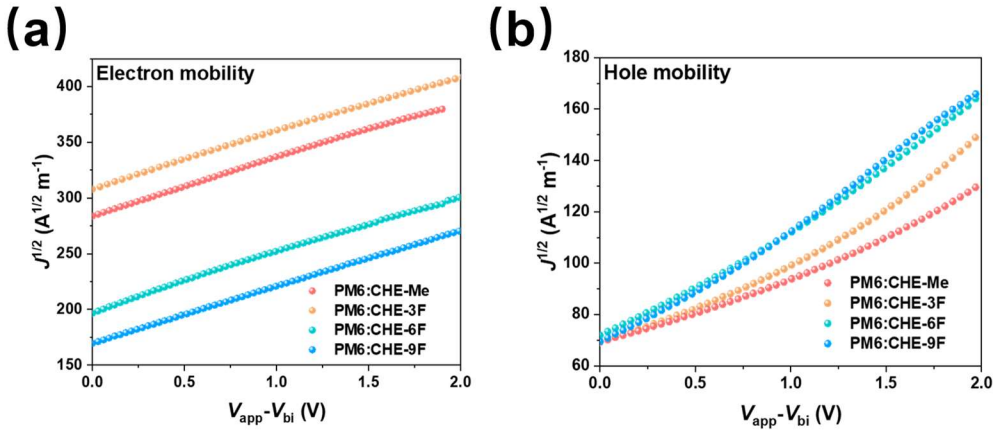

Figure S12. Electron mobilities(a) and hole mobilities(b) of the **PM6:CHE-Me**, **PM6: CHE-3F**, **PM6:CHE-6F** and **PM6: CHE-9F** blended films.

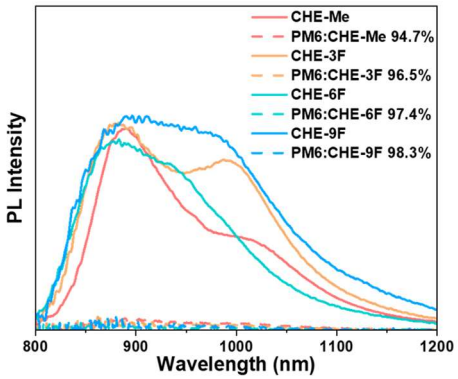

Figure S13. PL spectra of neat and blend films indicating efficiencies of PL quenching of four SMAs.

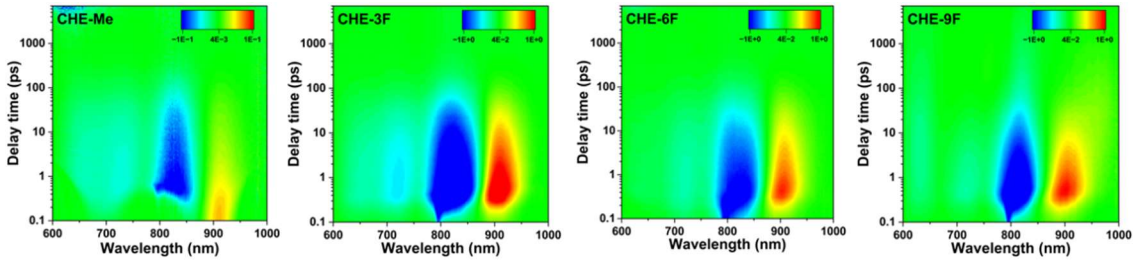

Figure S14. Femtosecond transient absorption spectroscopy (fs-tas) maps of the four SMAs in neat films.

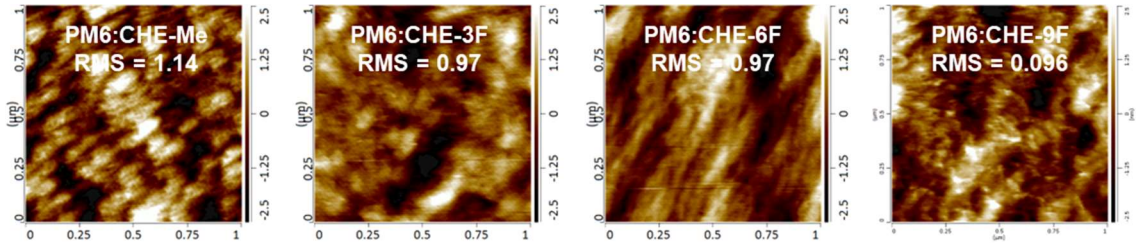

Figure S15. AFM height images the **PM6:CHE-Me**, **PM6: CHE-3F**, **PM6:CHE-6F** and **PM6: CHE-9F** blended films.

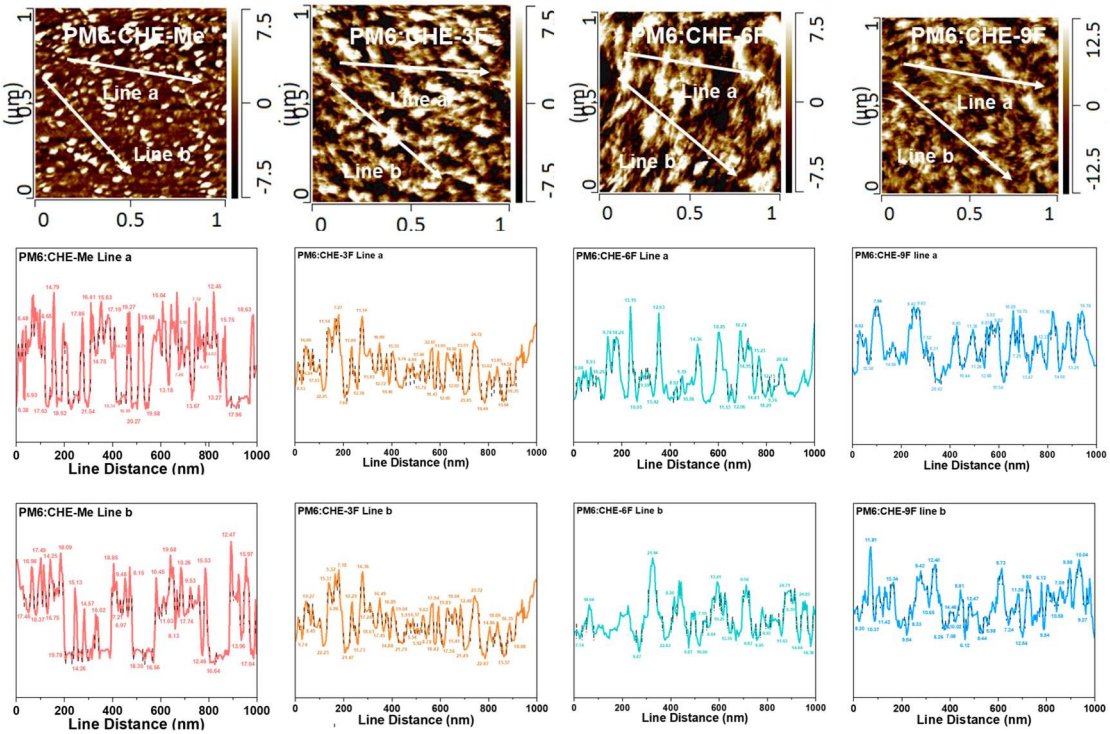

Figure S16. AFM phase images and the line profile to obtain the fibril width form the AFM phase images of the **PM6:CHE-Me**, **PM6: CHE-3F**, **PM6:CHE-6F** and **PM6: CHE-9F** blended films.

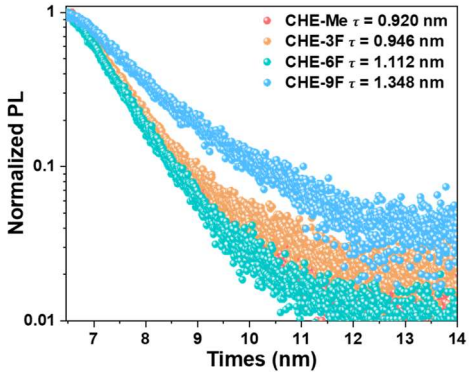

Figure S17. Time-resolved photoluminescence (PL) decay traces of four SMAs in neat films.

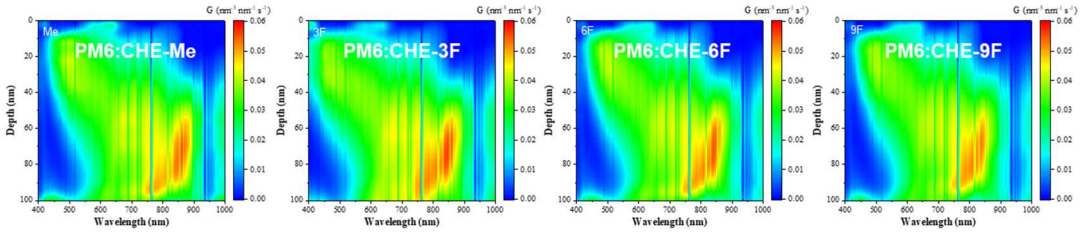

Figure S18. Exciton distribution cloud map of the **PM6:CHE-Me**, **PM6: CHE-3F**, **PM6:CHE-6F** and **PM6: CHE-9F** blended films.

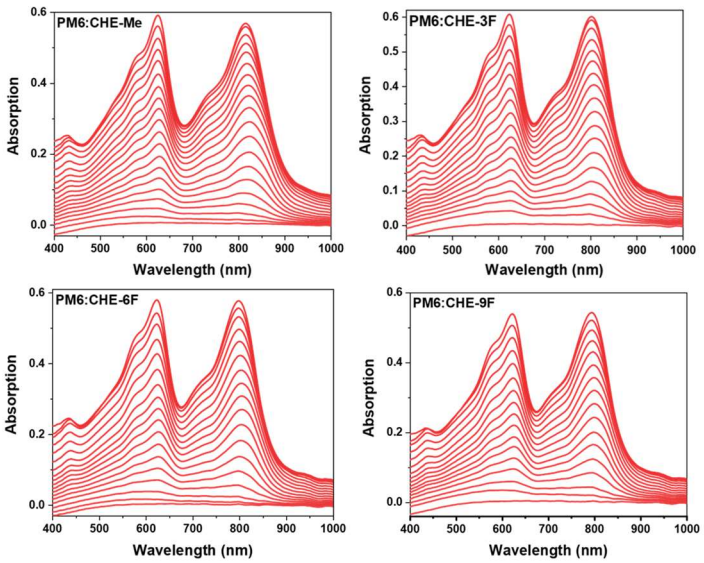

Figure S19. In-situ Etching Spectra of the **PM6:CHE-Me**, **PM6: CHE-3F**, **PM6:CHE-6F** and **PM6: CHE-9F** blended films.

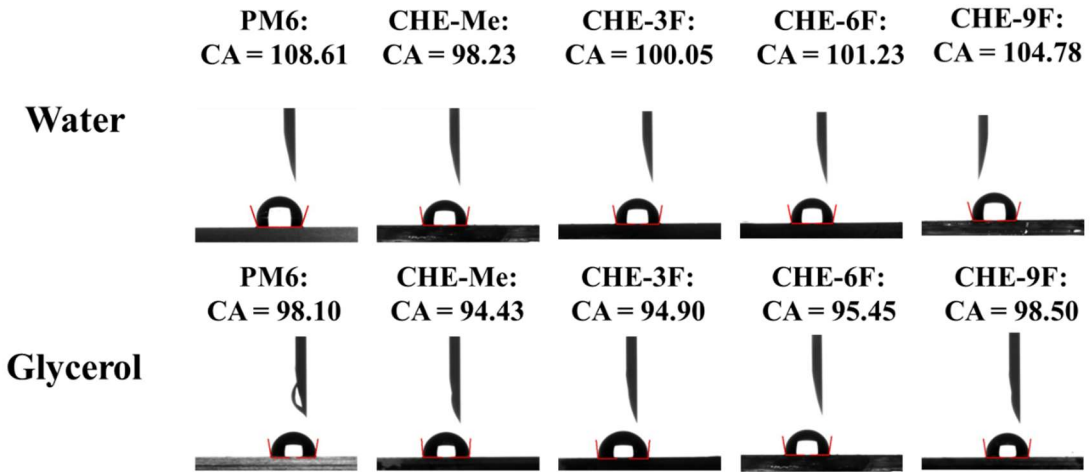

Figure S20. Contact angle images of **PM6**, **CHE-Me**, **CHE-3F**, **CHE-6F** and **CHE-9F** neat films with water and glycerol.

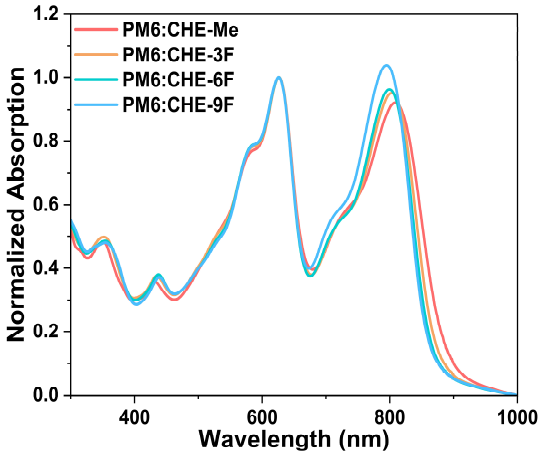

Figure S21. The UV absorption spectra of the blend films of **PM6**, **CHE-Me**, **CHE-3F**, **CHE-6F** and **CHE-9F**.

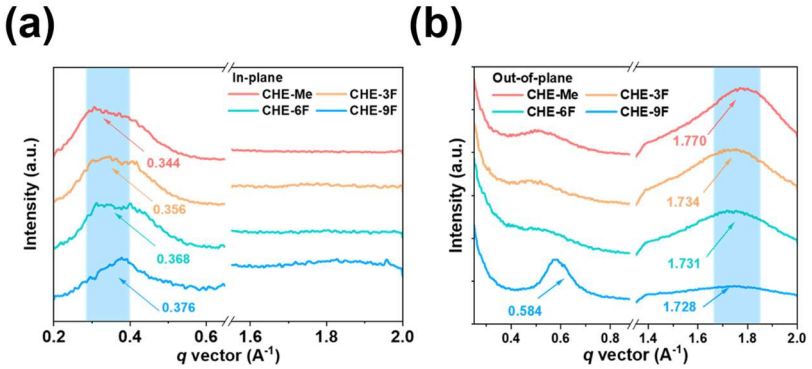

Figure S22. Line-cut profiles of 2D In GIWAXS patterns of four SMAs in neat films. (a) In-plane; (b) Out-of-plane.

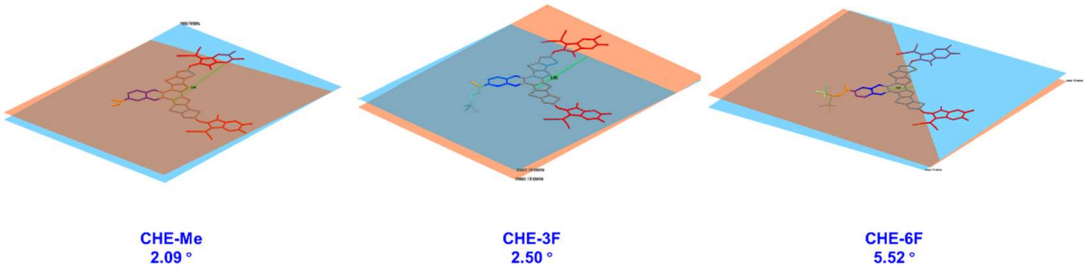

Figure S23. Side-view of the monomolecular single crystallographic structures of CHE-Me, CHE-3F, and CHE-6F (alkyl chains omitted for clarity)

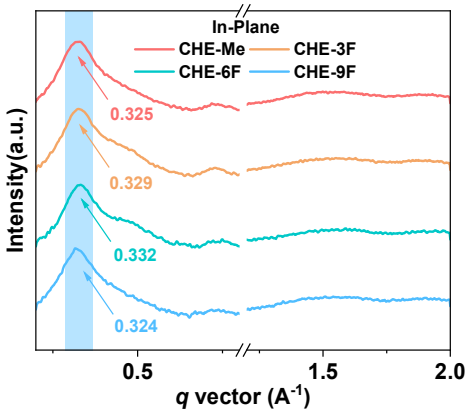

Figure S24. Line-cut profiles of 2D In GIWAXS patterns of **PM6:CHE-Me**, **PM6: CHE-3F**, **PM6:CHE-6F** and **PM6: CHE-9F** blended films in the in-plane direction.

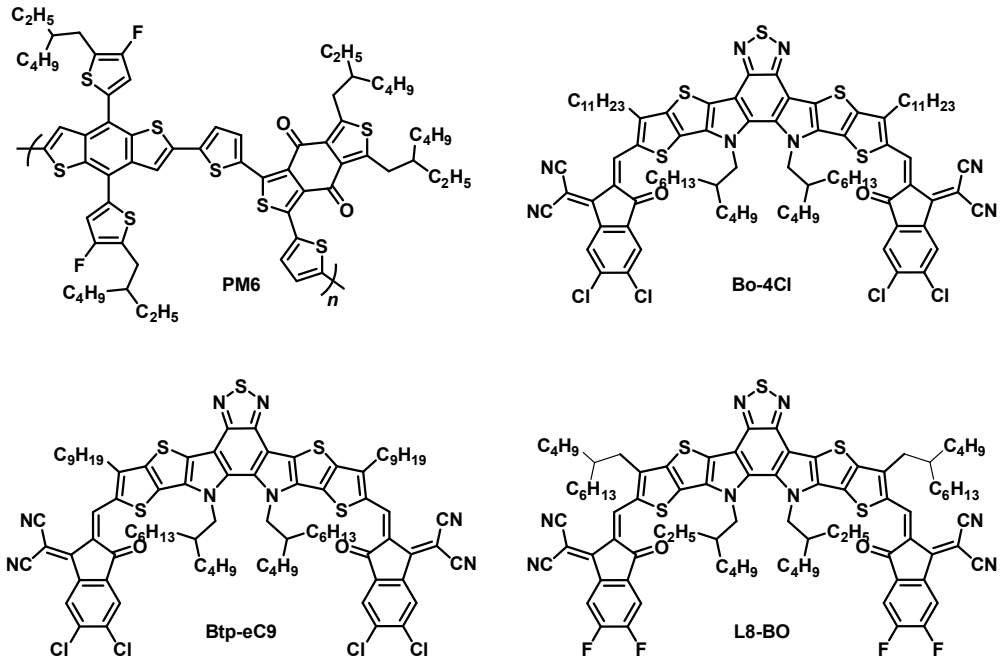

Figure S25. The chemical structure of **PM6** and **Bo-4Cl**, **Btp-eC9** and **L8-Bo**.

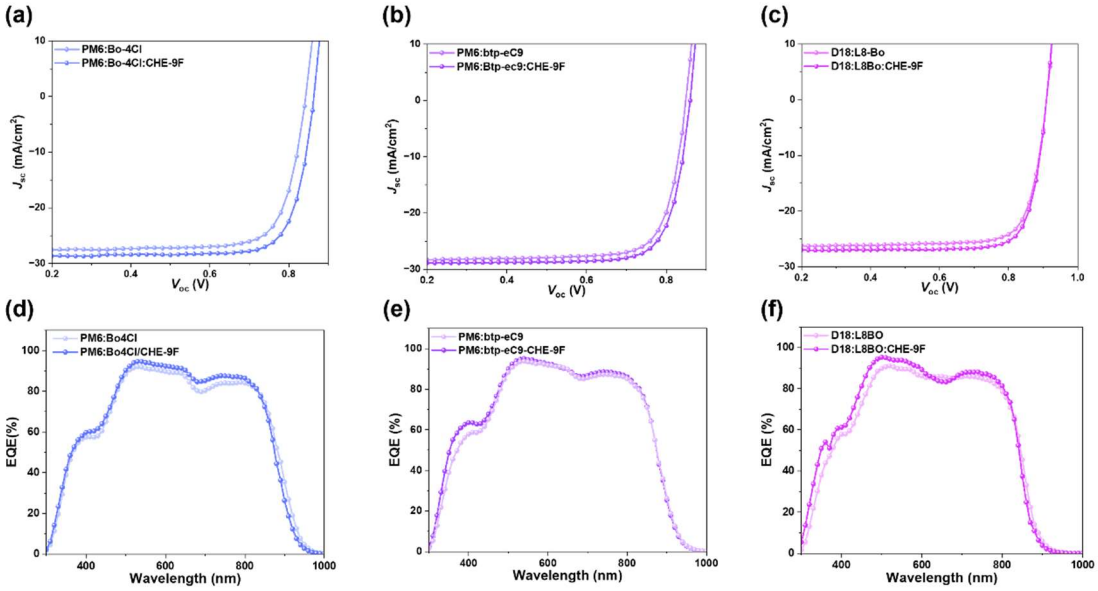

Figure S26. The *J-V* characteristics and external quantum efficiency (EQE) spectra of the binary devices based on **PM6:Bo4Cl**, **PM6:Btp-eC9**, and **D18:L8-BO**, as well as the corresponding ternary devices blended with **CHE-9F.**

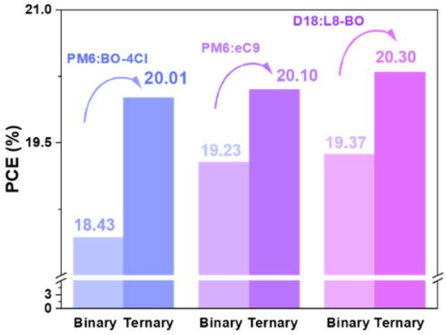

Figure S27. The champion efficiencies between the corresponding binary devices and the ternary devices blended with **CHE-9F** for the **PM6:BO-4Cl**, **PM6:eC9**, and **D18:L8-BO** systems**.**

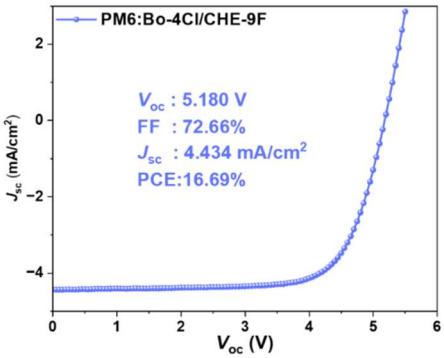

Figure S28. The *J-V* characteristics of **PM6:BO-4Cl:CHE-9F** module OSC**.**

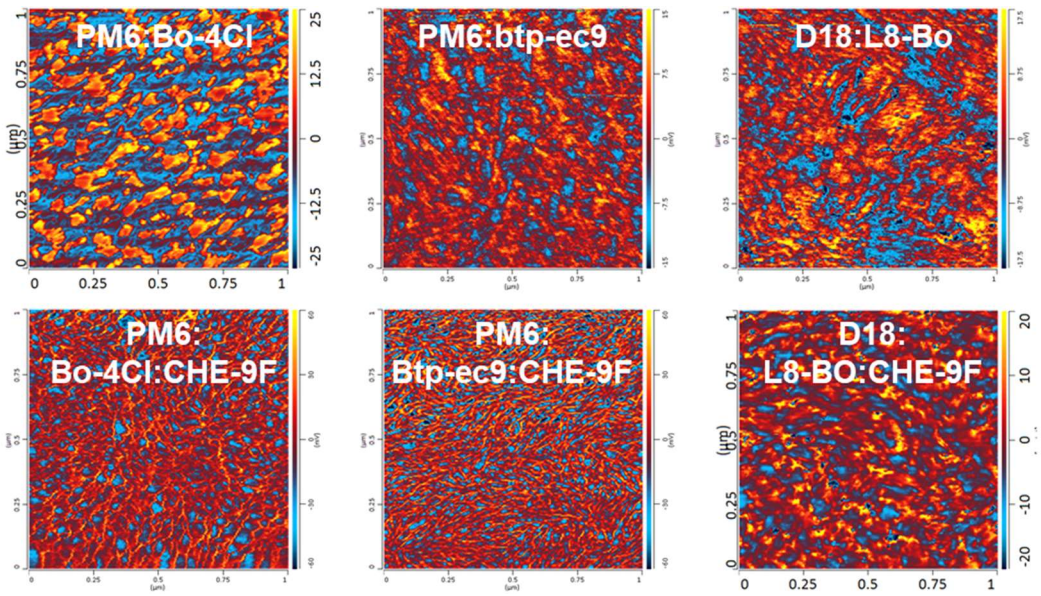

Figure S29. AFM-IR images the **PM6:Bo-4Cl**, **PM6:btp-ec9**, **D18:L8-Bo**, **PM6:Bo4-Cl:CHE-9F**, **PM6:btp-ec9:CHE-9F**, **D18:L8-Bo:CHE-9F** blended films.

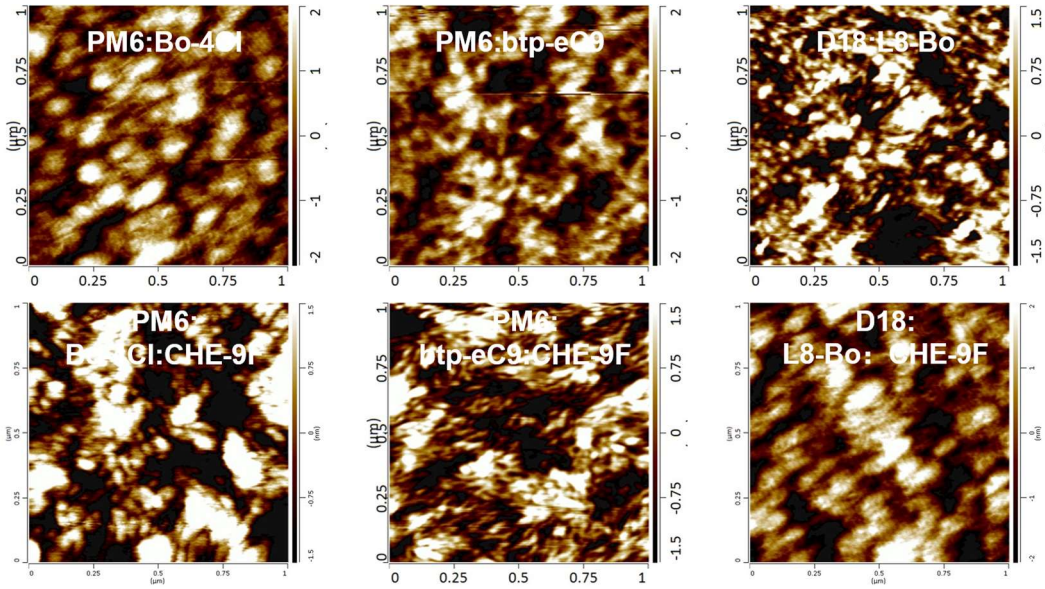

Figure S30. AFM height images the **PM6:Bo-4Cl**, **PM6:btp-ec9**, **D18:L8-Bo**, **PM6:Bo4-Cl:CHE-9F**, **PM6:btp-ec9:CHE-9F**, **D18:L8-Bo:CHE-9F** blended films.

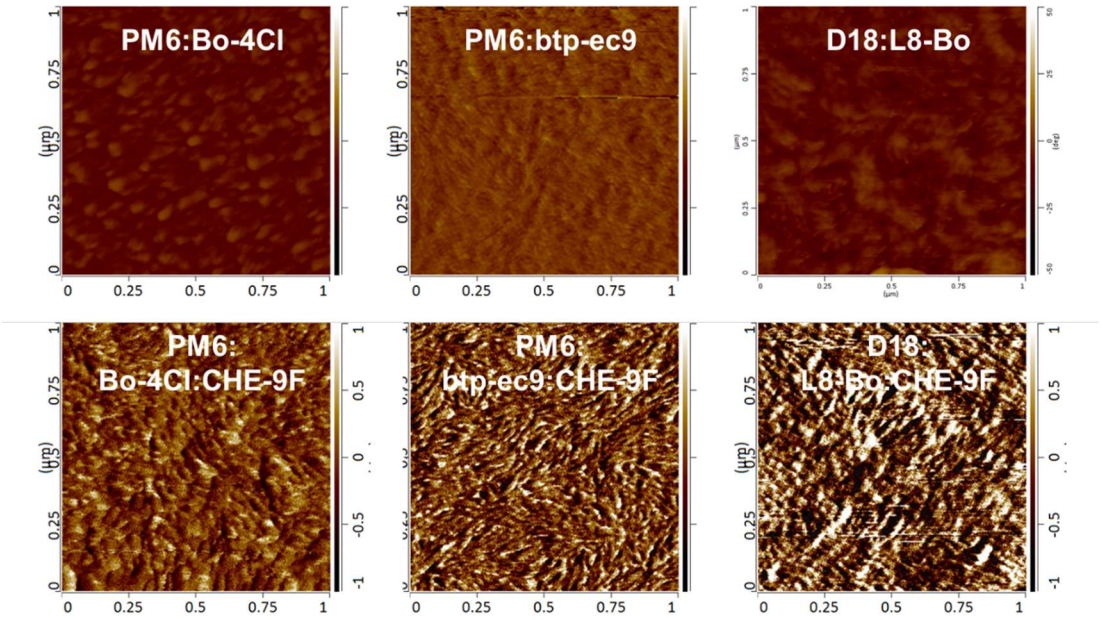

Figure S31. AFM height images the **PM6:Bo-4Cl**, **PM6:btp-ec9**, **D18:L8-Bo**, **PM6:Bo4-Cl:CHE-9F**, **PM6:btp-ec9:CHE-9F**, **D18:L8-Bo:CHE-9F** blended films.

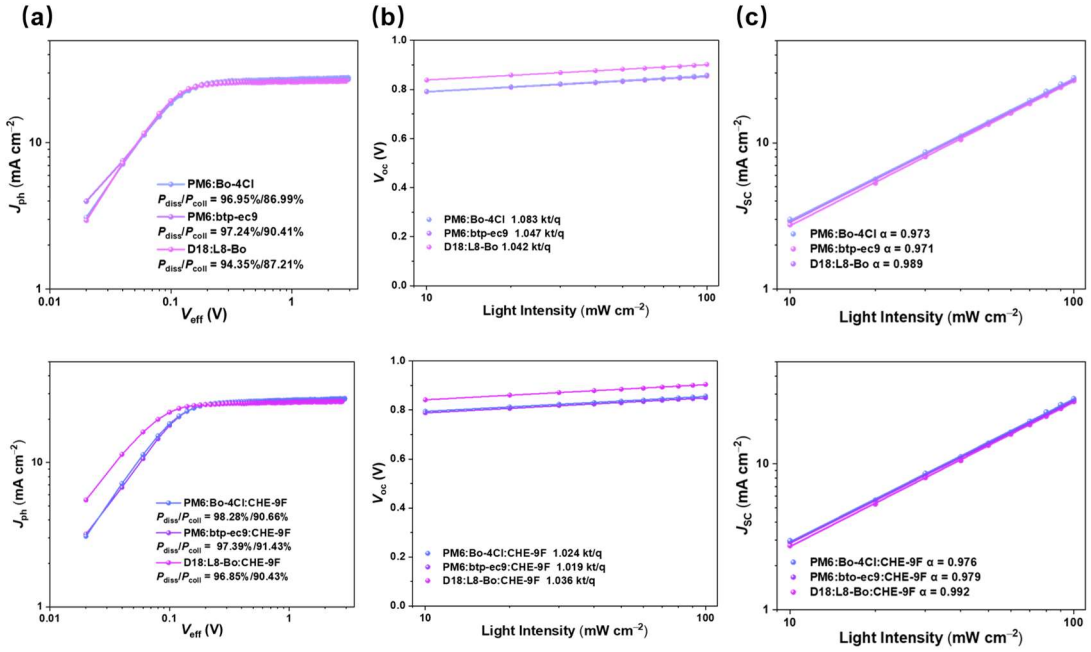

Figure S32. (a) J_{ph} versus V_{eff} curves indicating P_{diss} and P_{coll}, (b) Plight dependence of V_{oc}, and (c) Plight dependence of J_{sc} for the binary blend systems of **PM6:BO-4Cl**, **PM6:btp-eC9**, **D18:L8-BO** and their corresponding ternary blend devices with **CHE-9F** incorporation

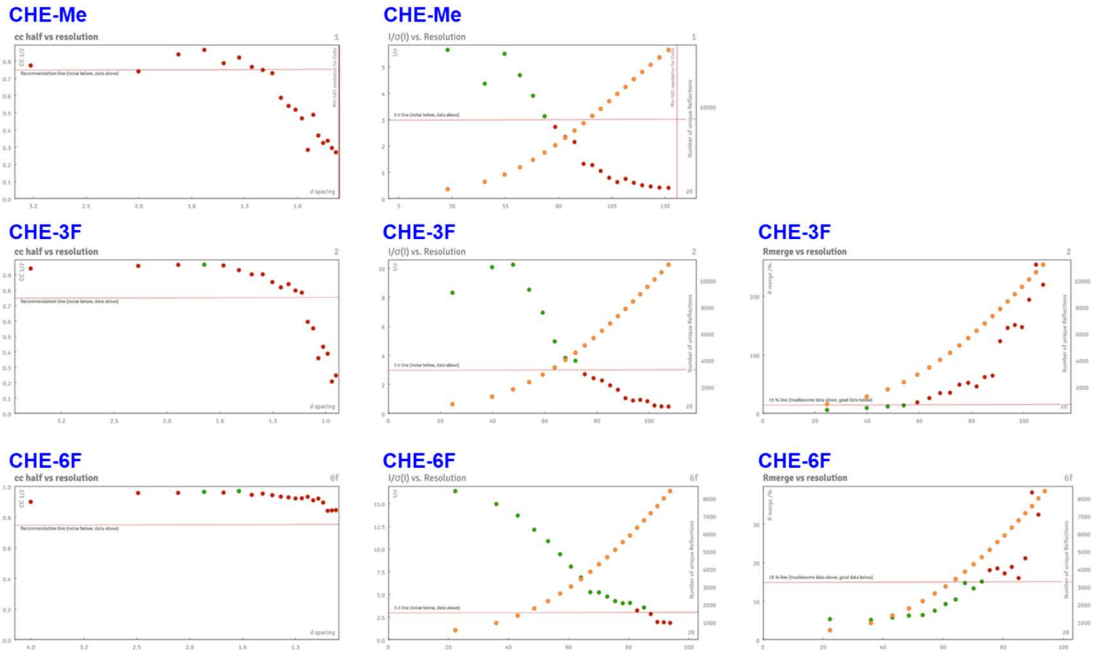

Figure S33. CC half vs. Resolution, 1/σ(I) vs. Resolution, and Rmerge vs. Resolution for **CHE-Me**, **CHE-3F**, and **CHE-6F**.

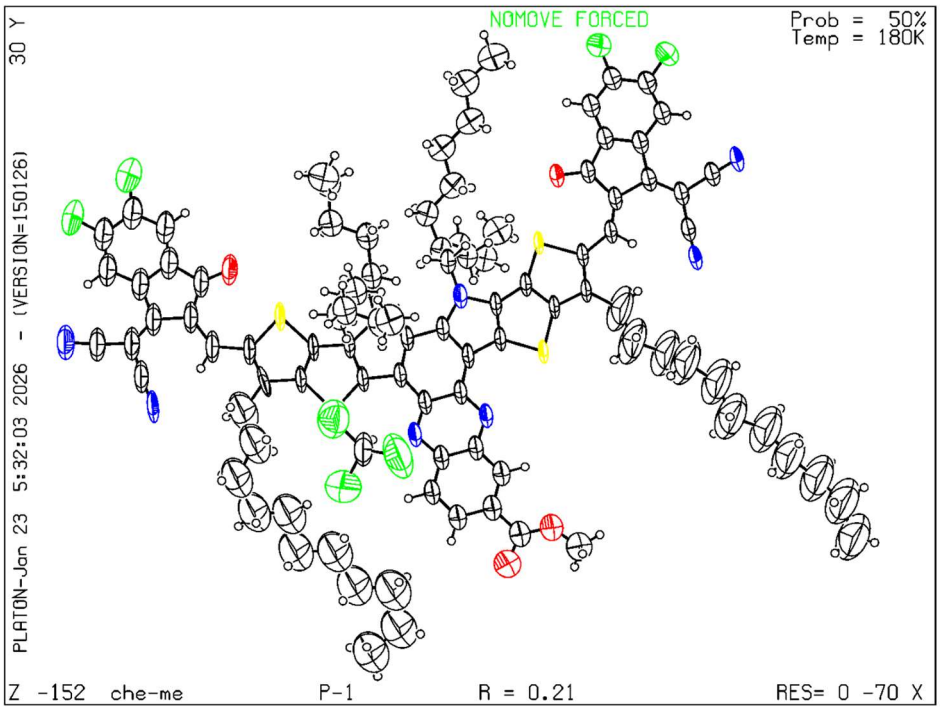

Figure S34. The ORTEP-style illustration with probability ellipsoids of **CHE-Me** (CCDC: 2502135).

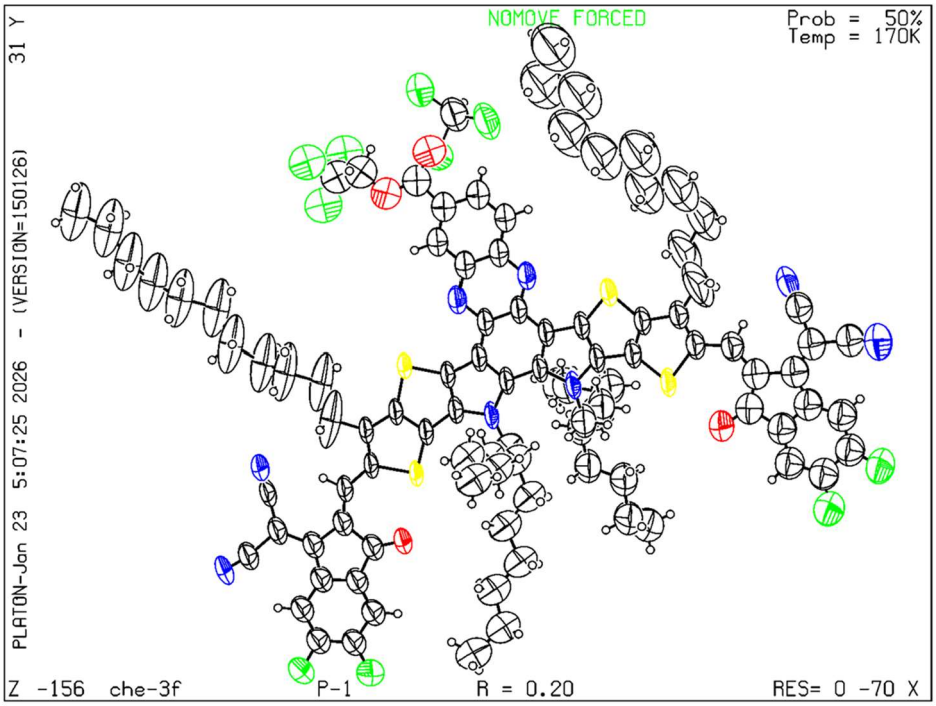

Figure S35. The ORTEP-style illustration with probability ellipsoids of **CHE-3F** (CCDC: 2502137).

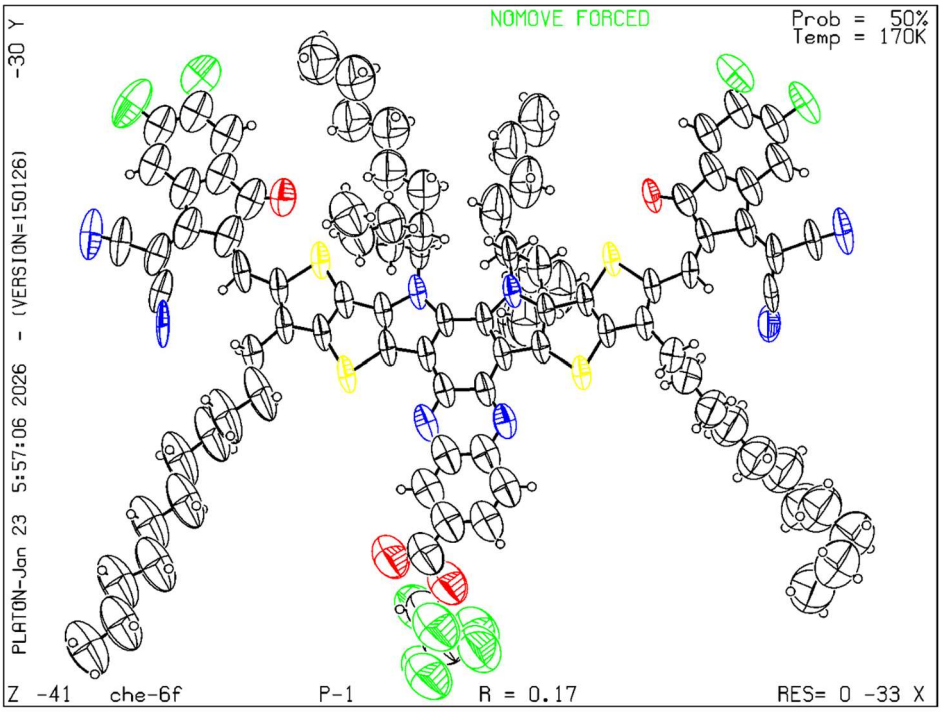

Figure S36. The ORTEP-style illustration with probability ellipsoids of **CHE-6F** (CCDC: 2502136).

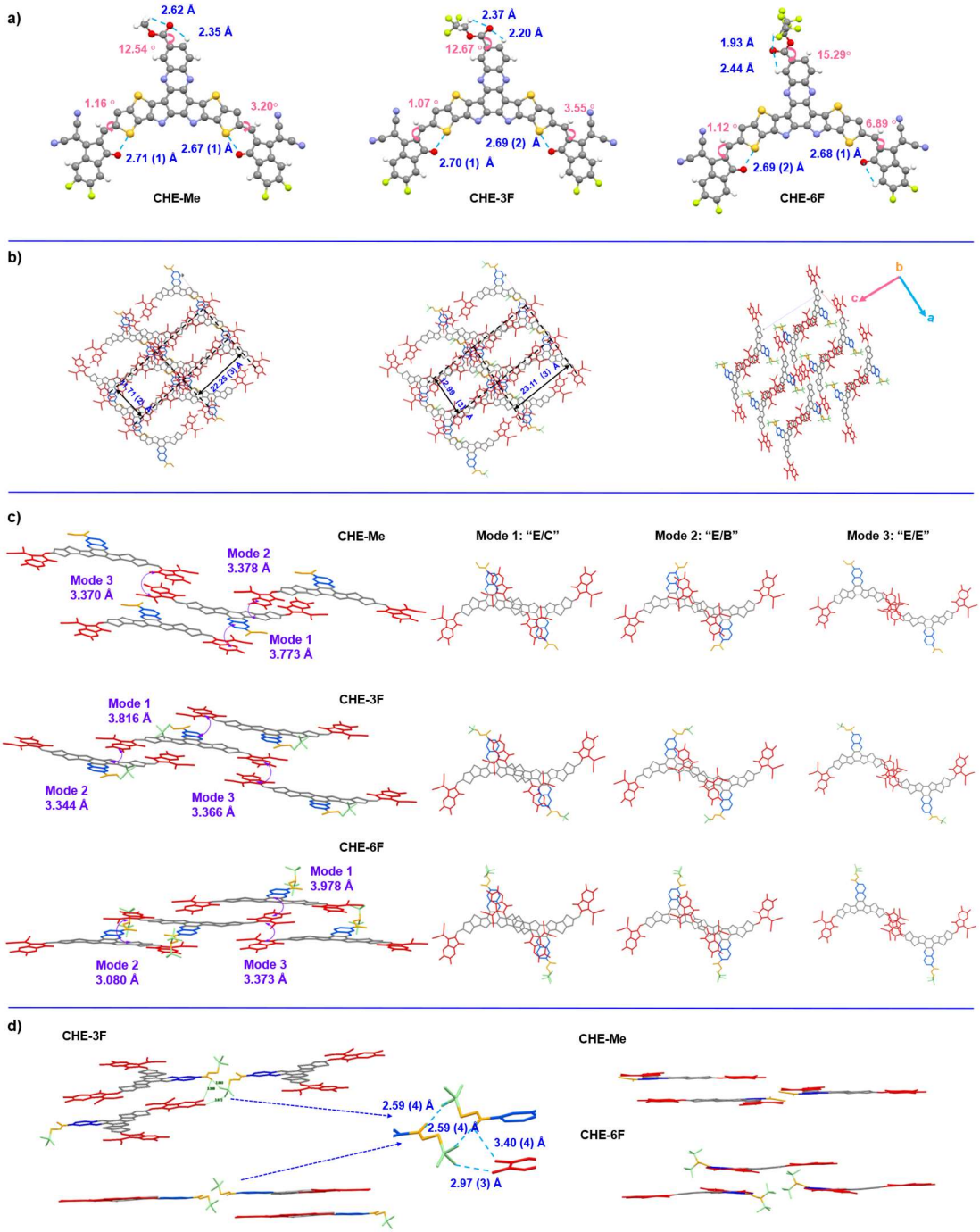

Figure S37. Plots of the Standard Uncertainty Values Corresponding to the Bond Lengths, Bond Angles and Interplanar Distances Referenced in Manuscript.

5. Spectral Charts of NMR and MS.

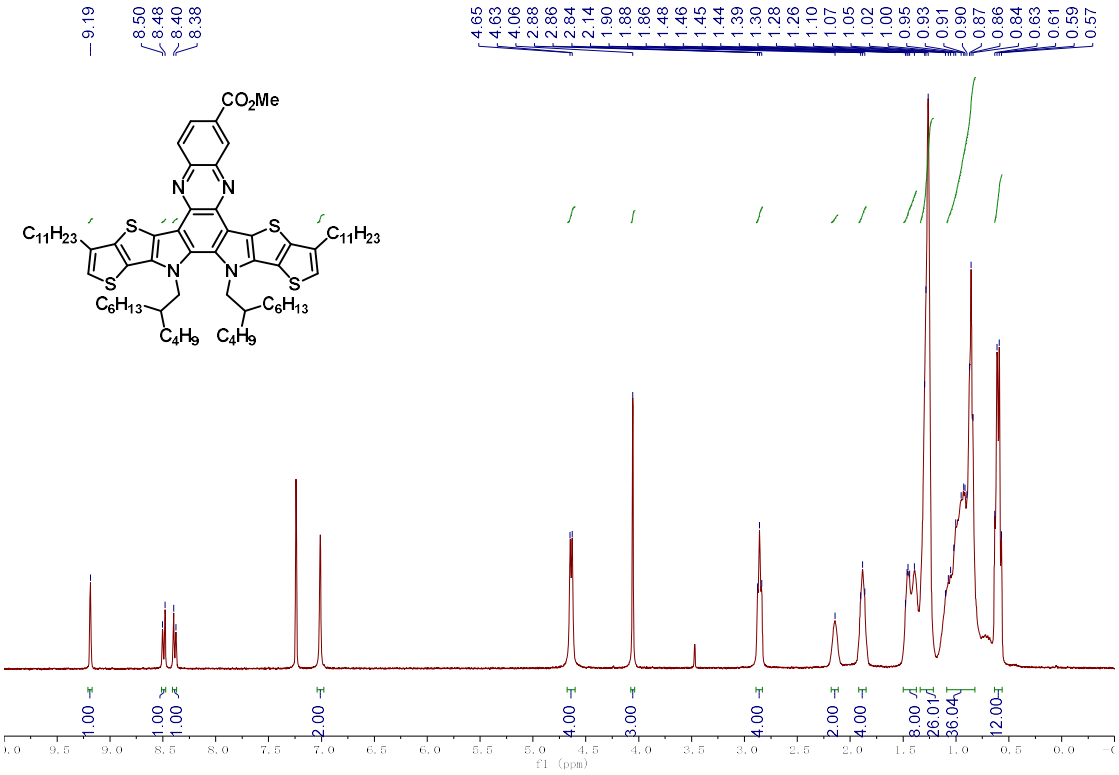

^{1}H NMR spectrum of **intermediate 2** in $CDCl_3$.

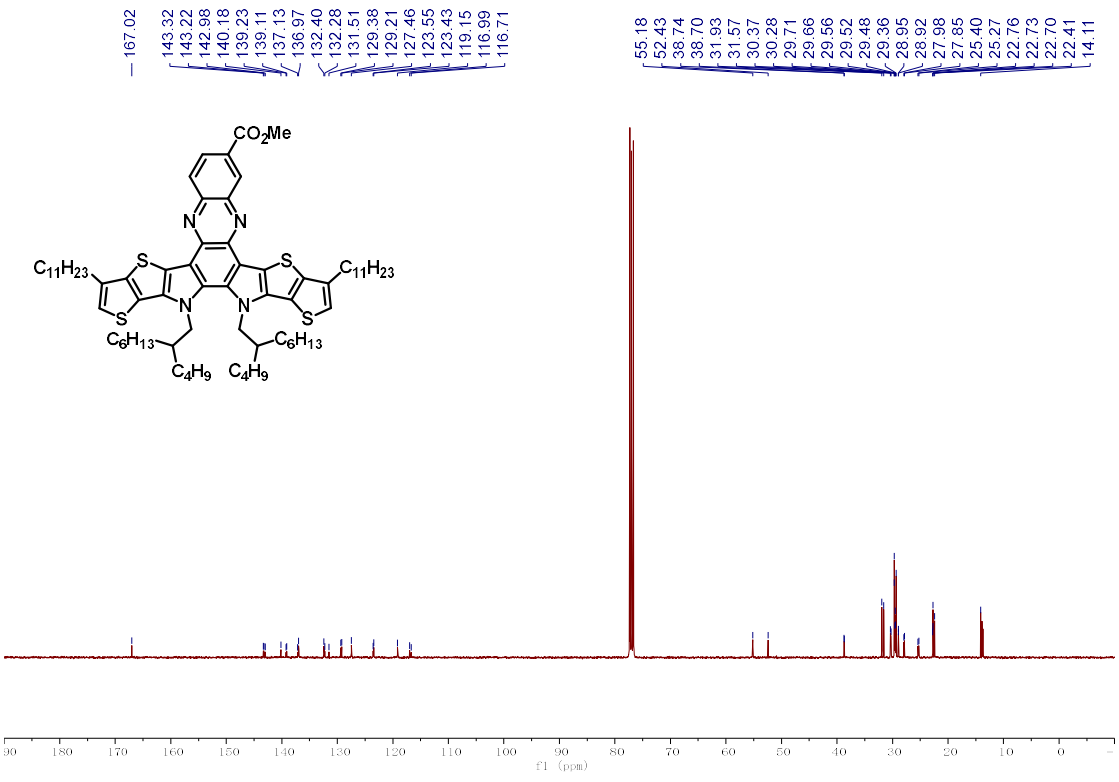

^{13}C NMR spectrum of **intermediate 2** in $CDCl_3$.

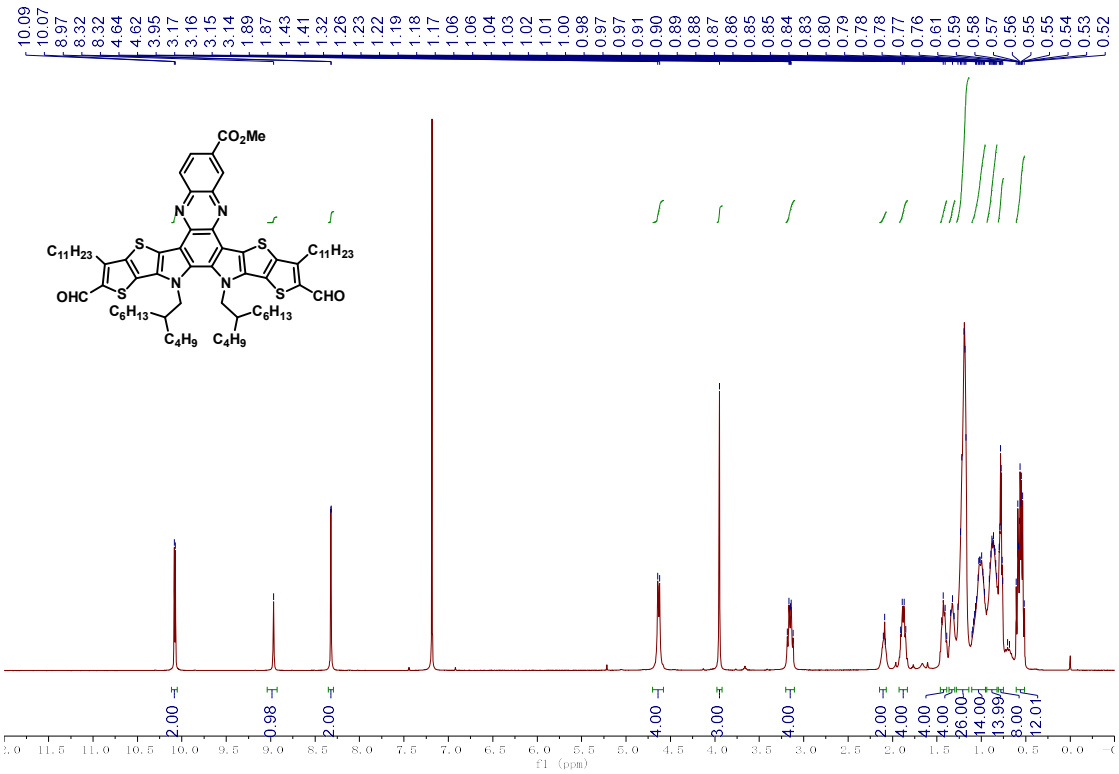

^{1}H NMR spectrum of **intermediate 3** in $CDCl_3$.

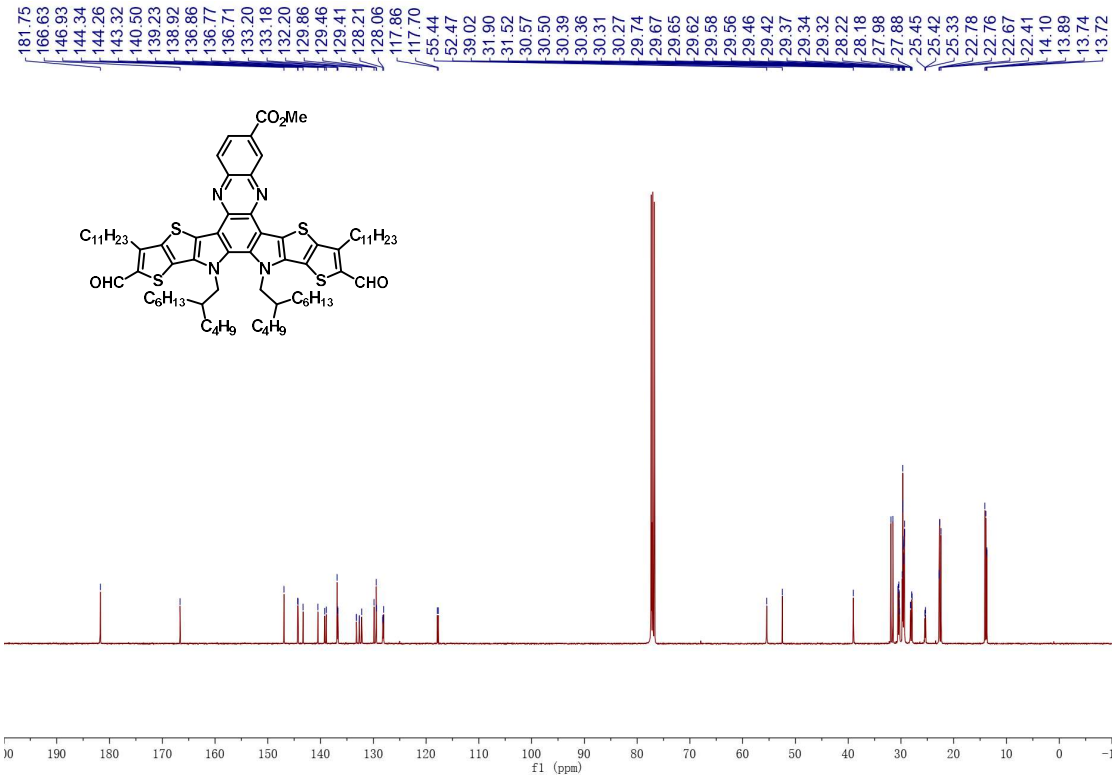

^{13}C NMR spectrum of **intermediate 3** in $CDCl_3$.

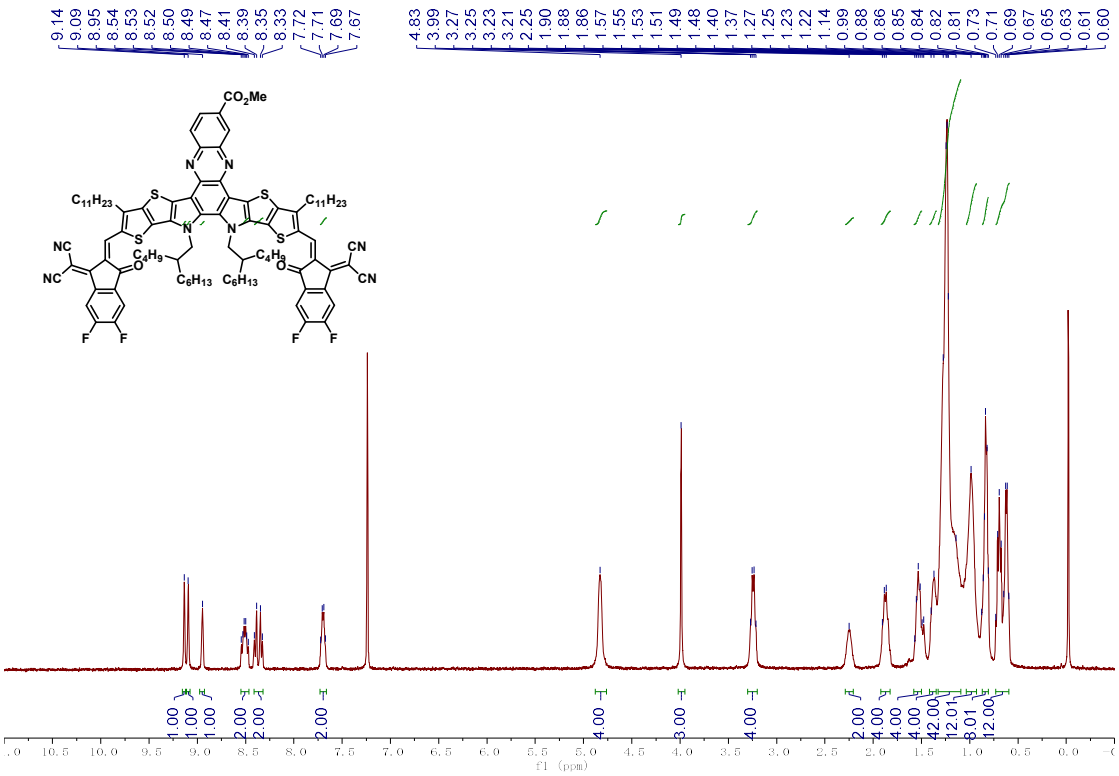

^{1}H NMR spectrum of **CHE-Me** in $CDCl_3$.

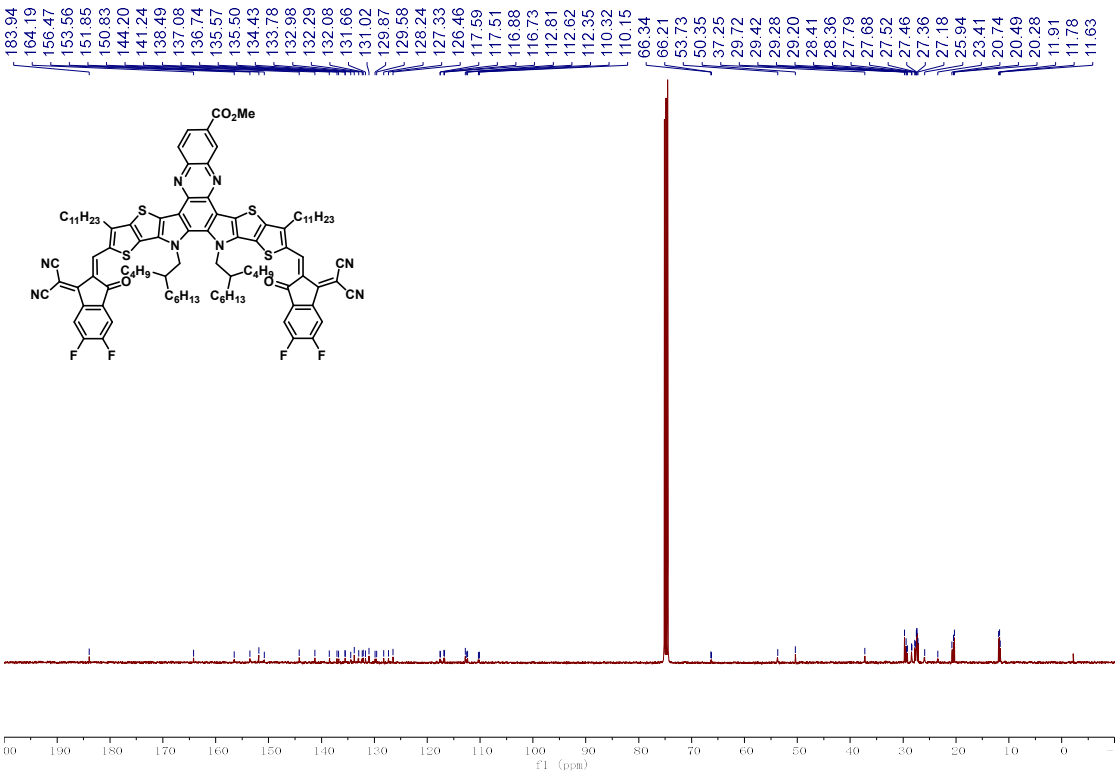

^{13}C NMR spectrum of **CHE-Me** in $CDCl_3$.

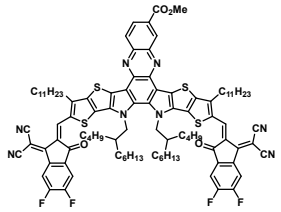

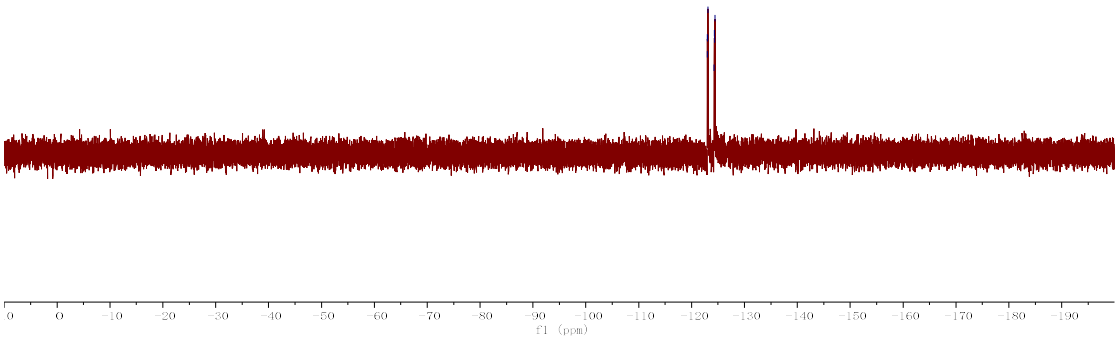

^{19}F NMR spectrum of **CHE-Me** in $CDCl_3$.

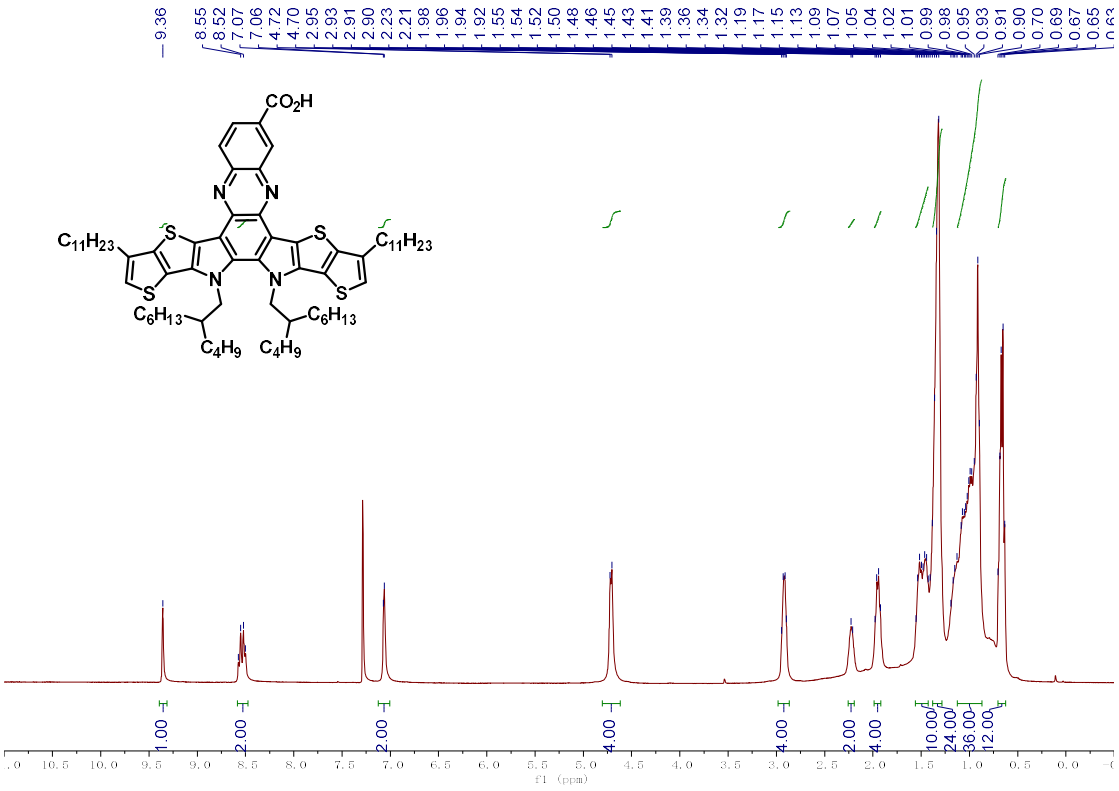

^{1}H NMR spectrum of **intermediate 4** in $CDCl_3$.

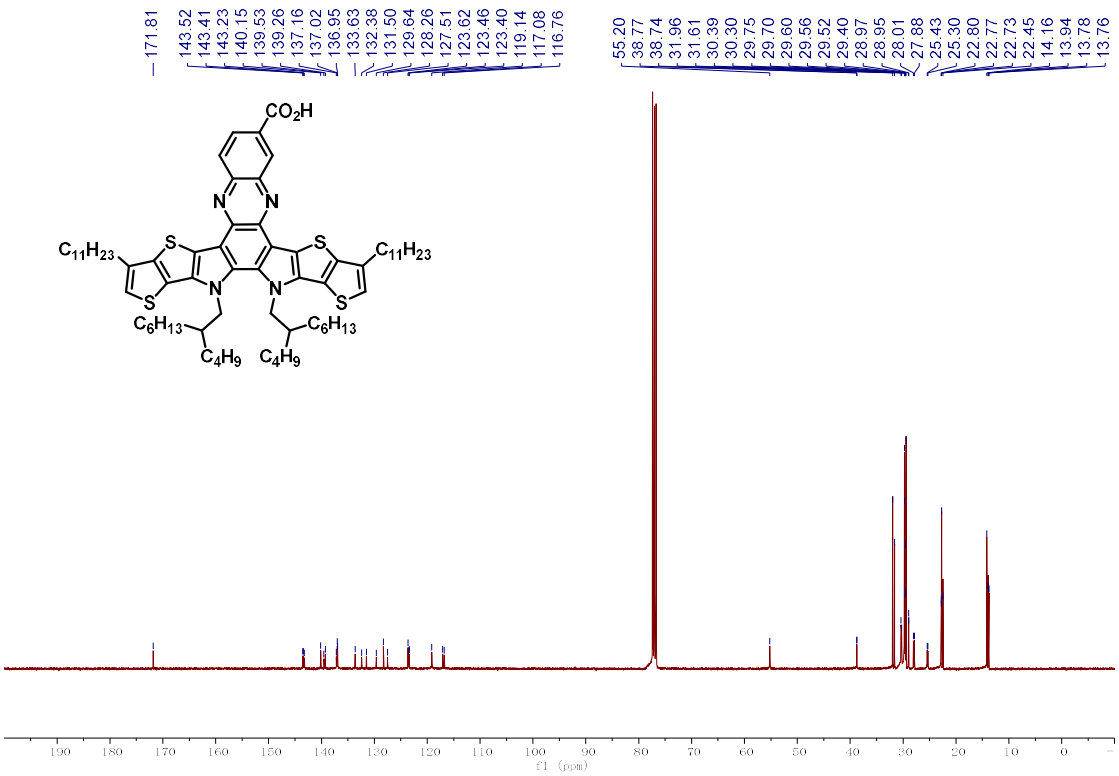

^{13} C NMR spectrum of **intermediate 4** in $CDCl_3$.

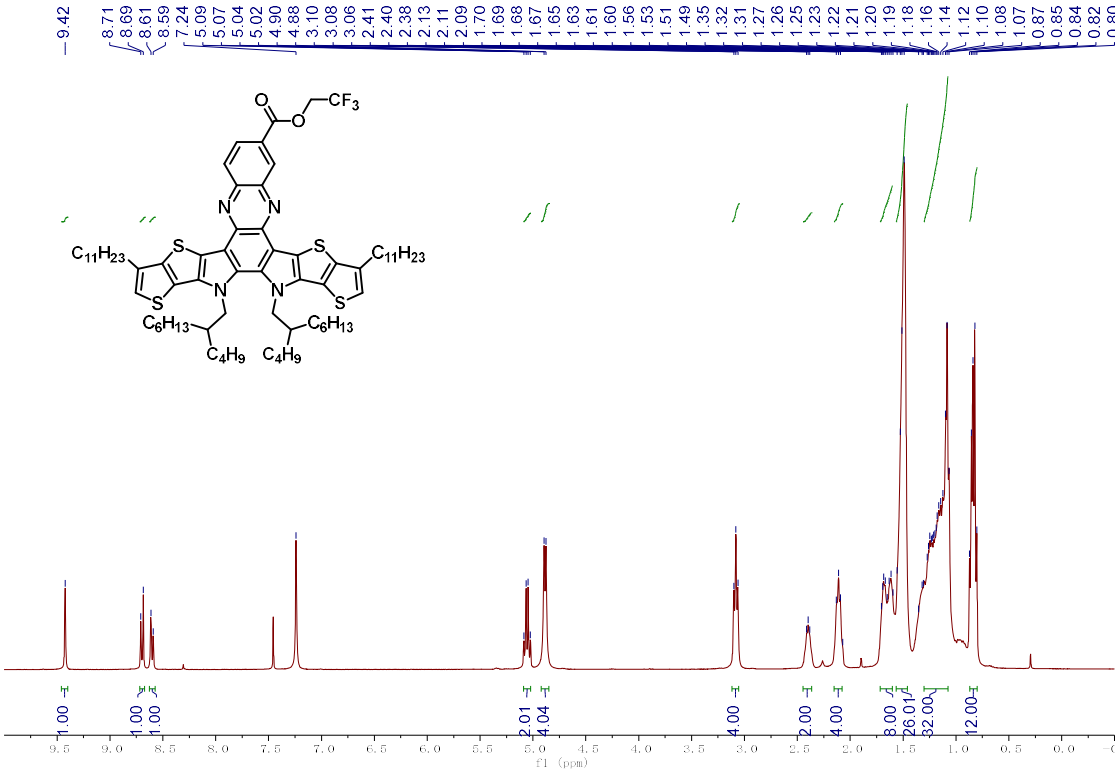

^{1}H NMR spectrum of **intermediate 5a** in $CDCl_3$.

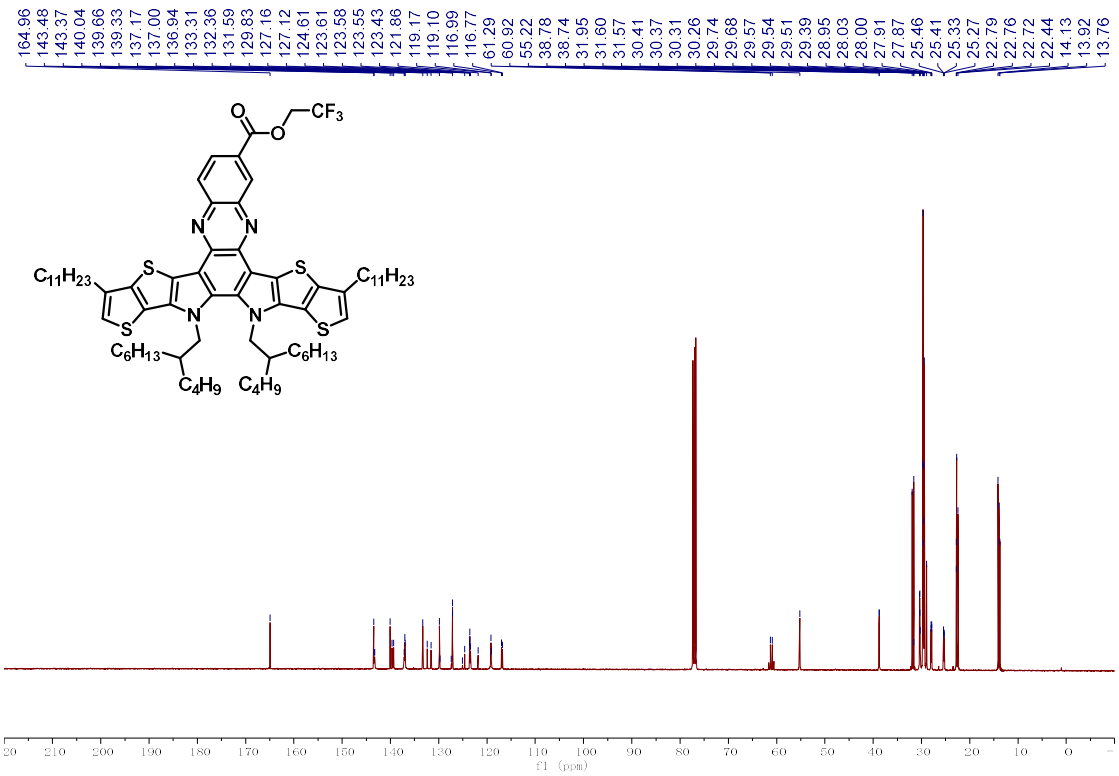

^{13}C NMR spectrum of **intermediate 5a** in $CDCl_3$.

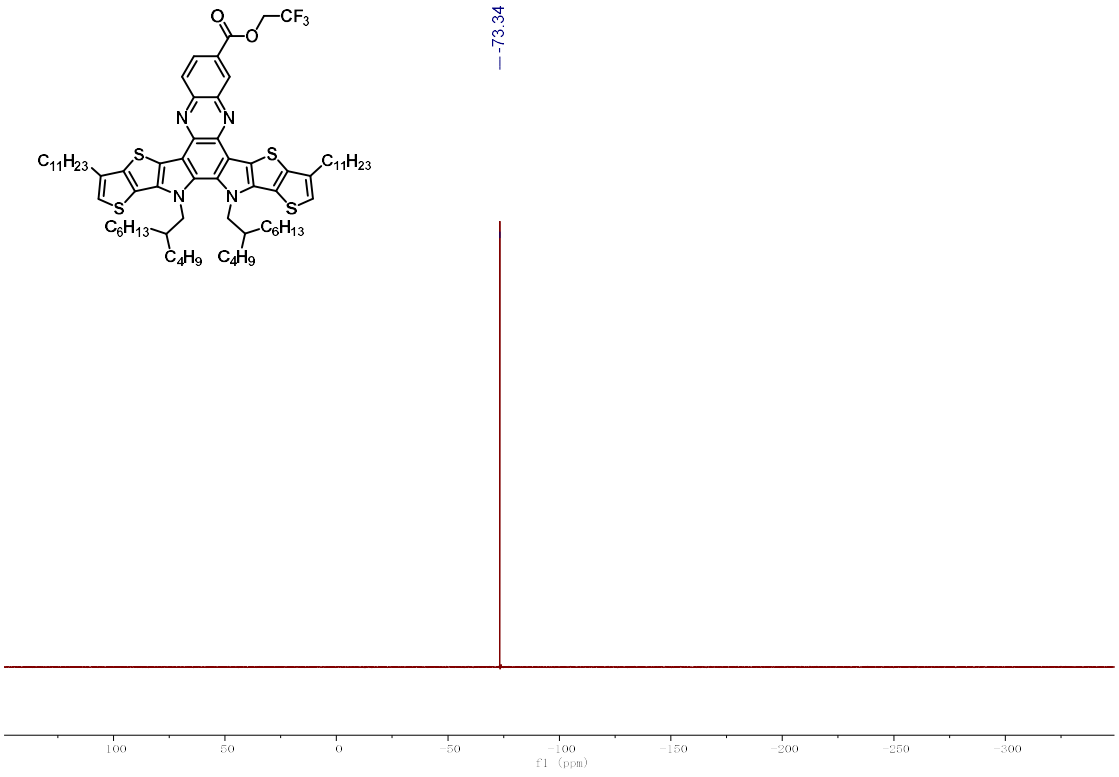

^{19}F NMR spectrum of **intermediate 5a** in $CDCl_3$.

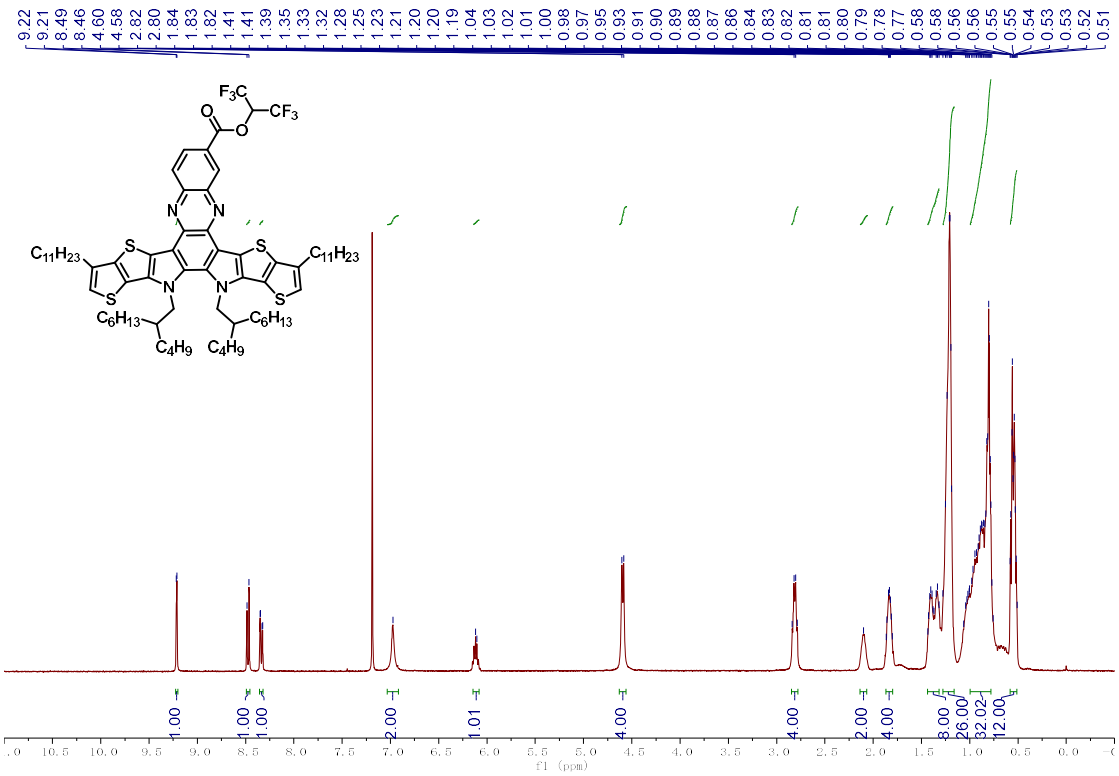

^{1}H NMR spectrum of **intermediate 5b** in $CDCl_3$.

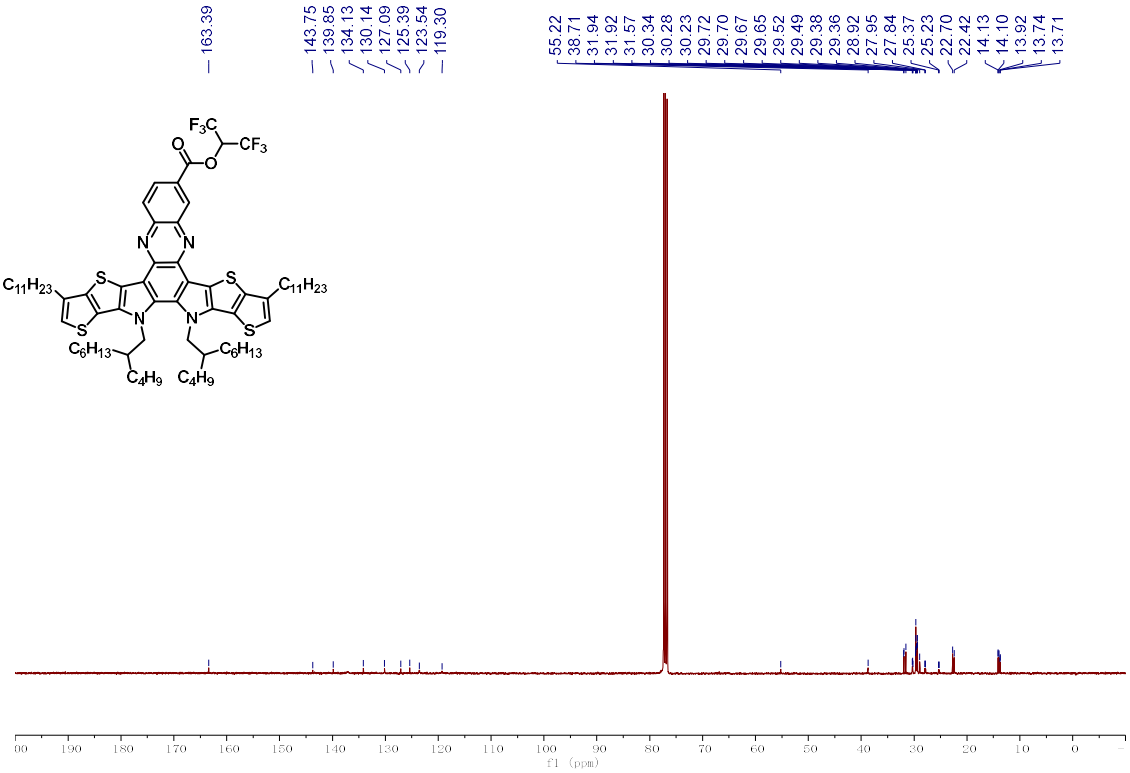

^{13}C NMR spectrum of **intermediate 5b** in $CDCl_3$.

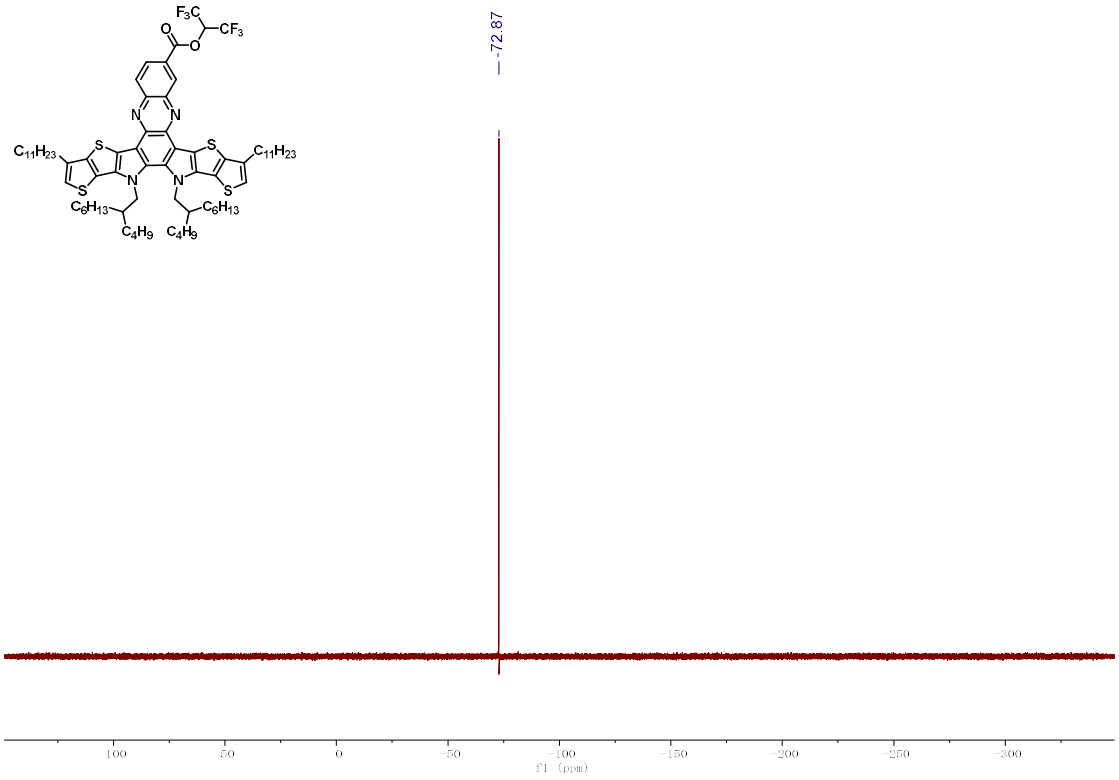

^{19}F NMR spectrum of **intermediate 5b** in $CDCl_3$.

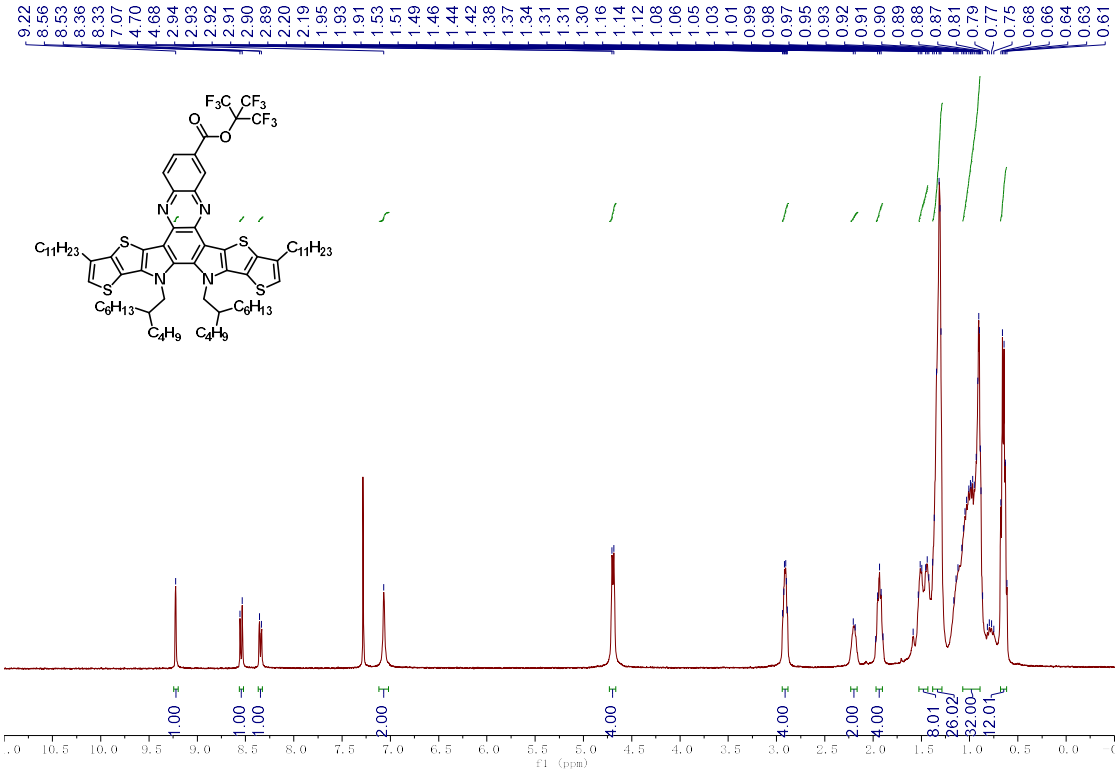

^{1}H NMR spectrum of **intermediate 5c** in $CDCl_3$.

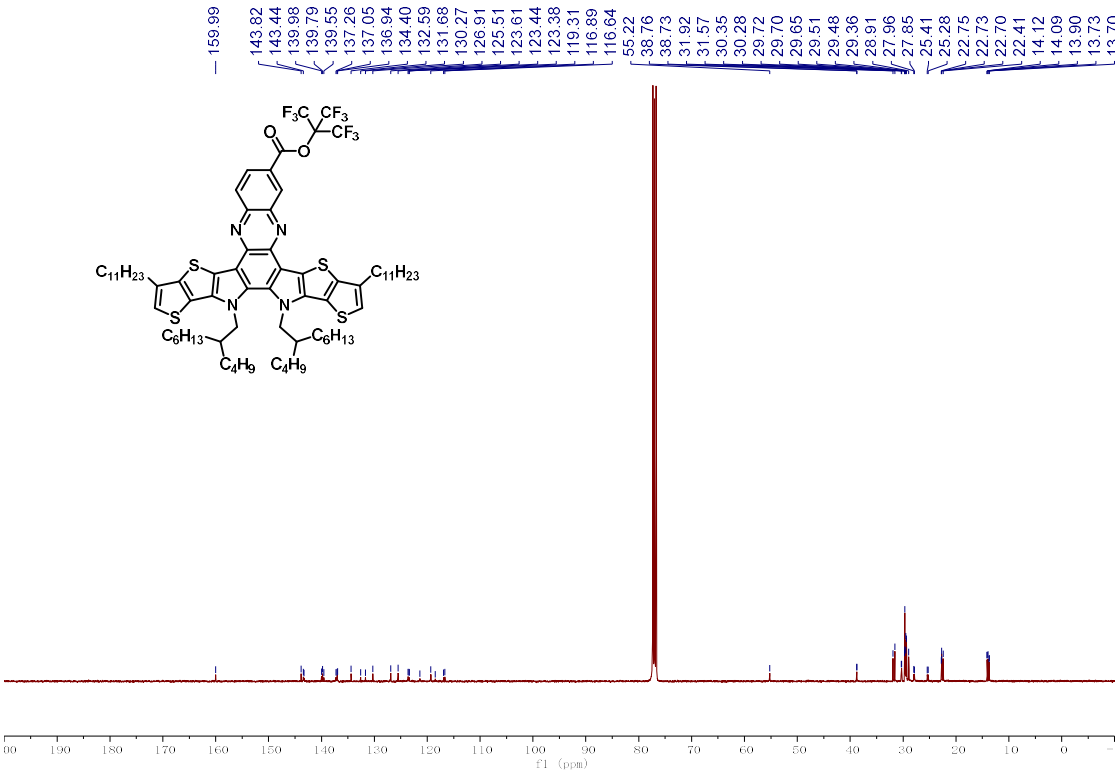

^{13}C NMR spectrum of **intermediate 5c** in $CDCl_3$.

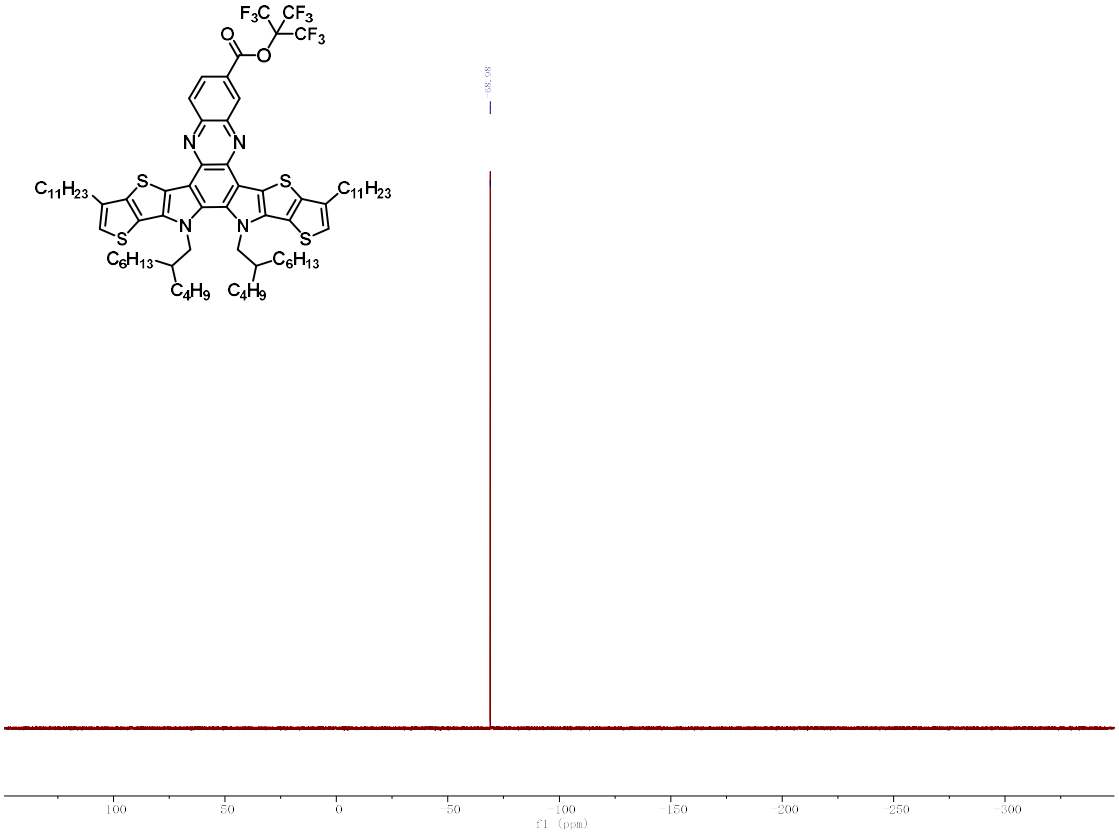

^{19}F NMR spectrum of **intermediate 5c** in $CDCl_3$.

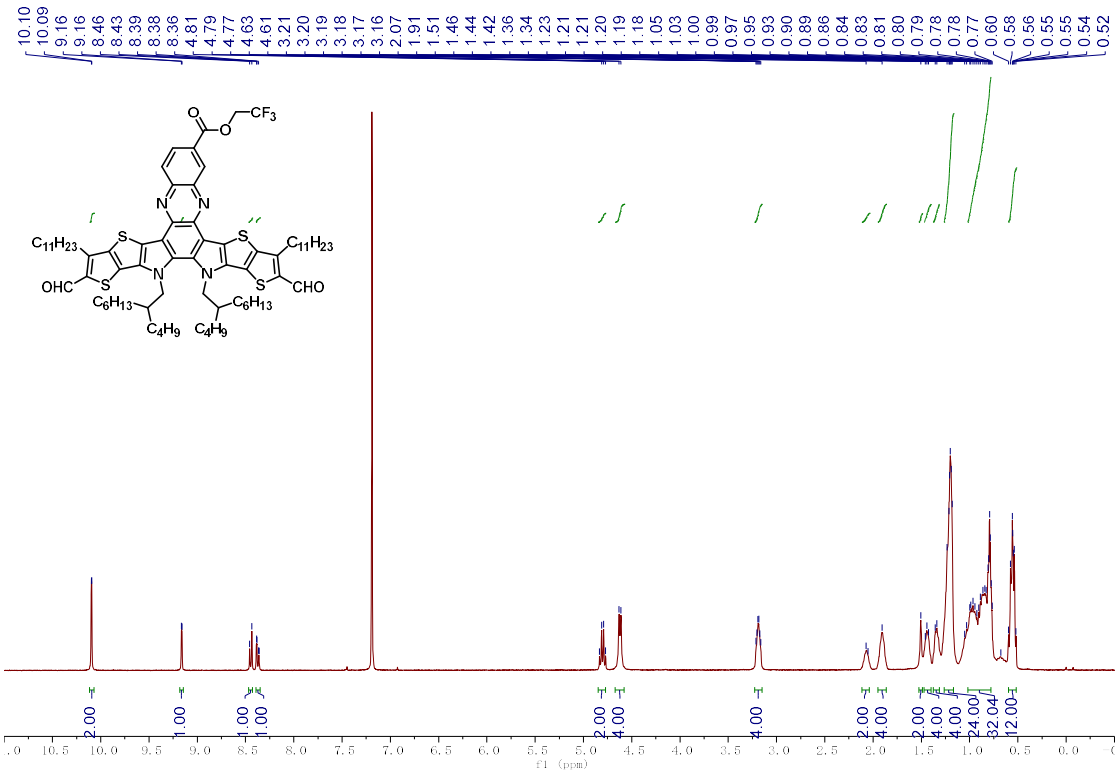

^{1}H NMR spectrum of **intermediate 6a** in $CDCl_3$.

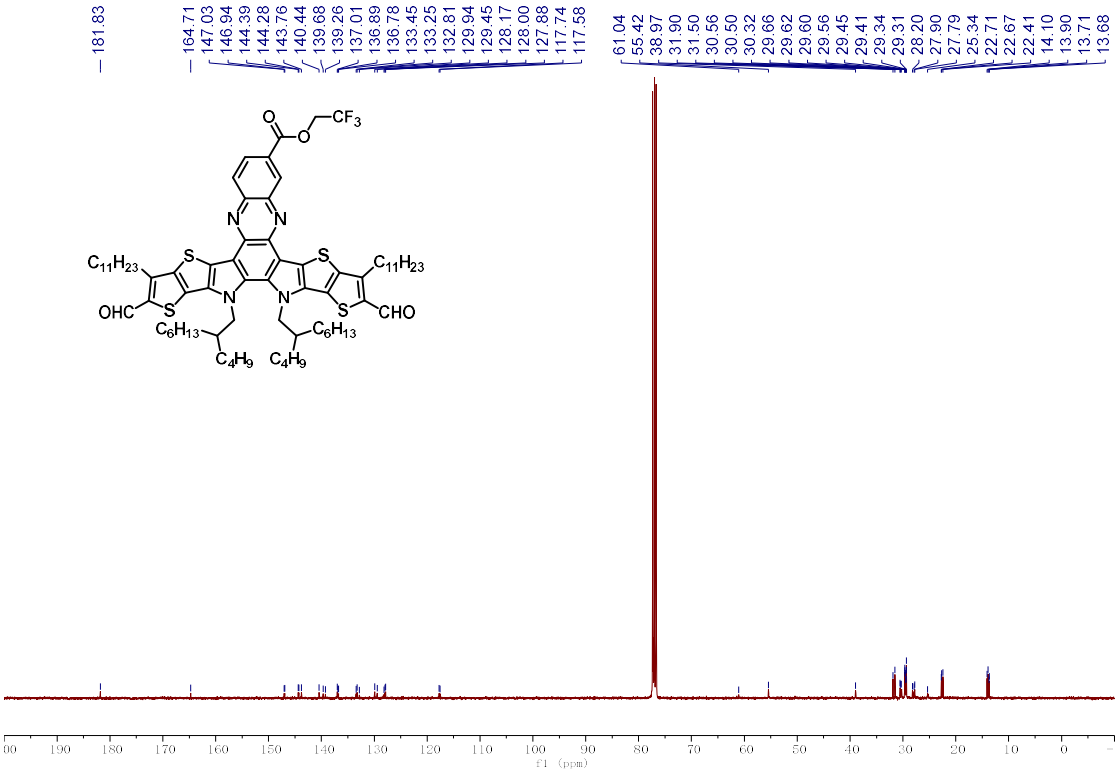

^{13}C NMR spectrum of **intermediate 6a** in $CDCl_3$.

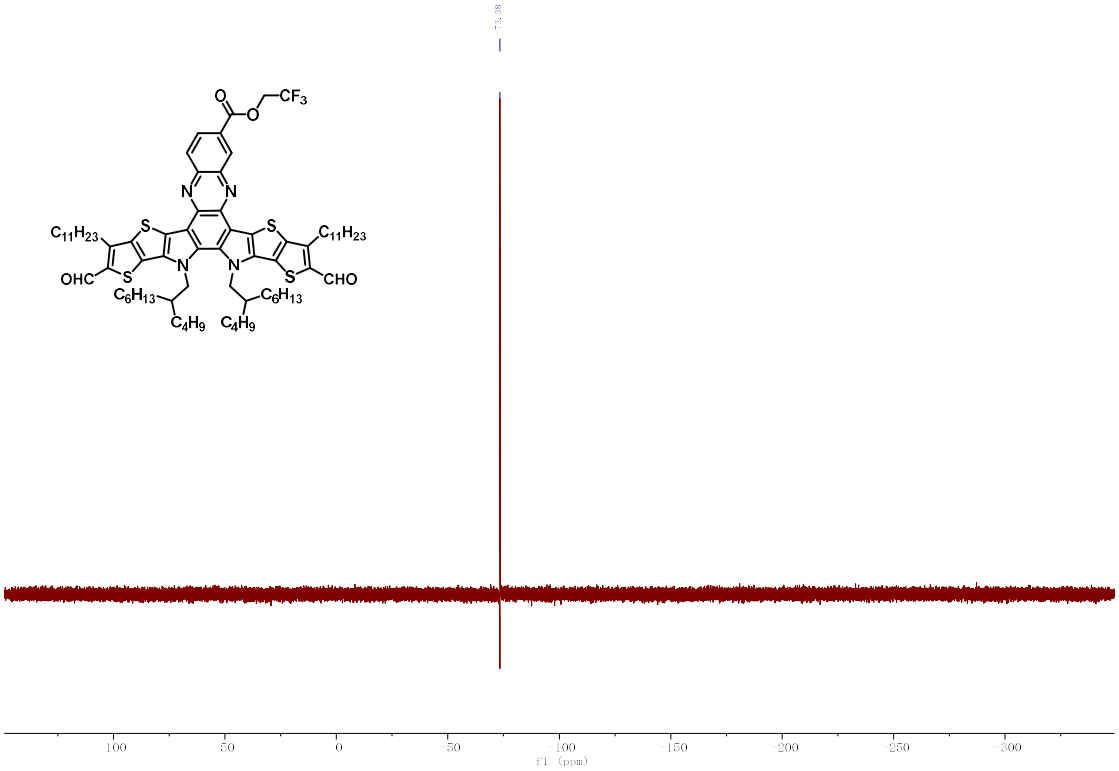

^{19}F NMR spectrum of **intermediate 6a** in $CDCl_3$.

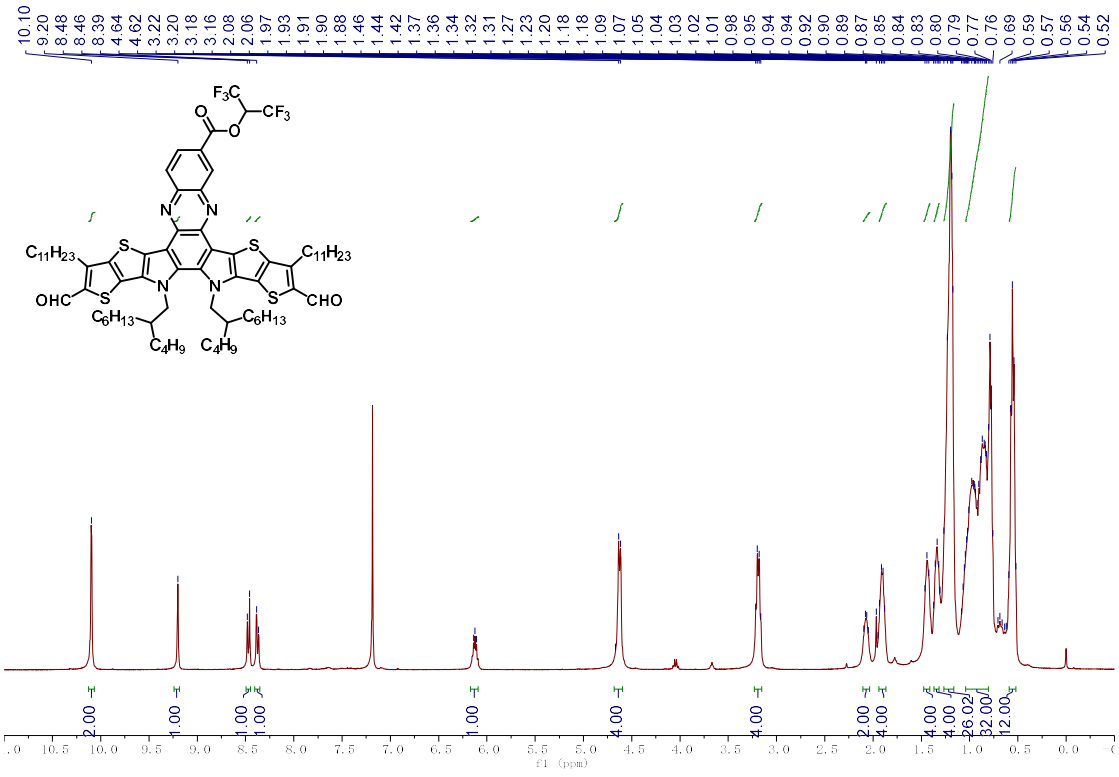

^{1}H NMR spectrum of **intermediate 6b** in $CDCl_3$.

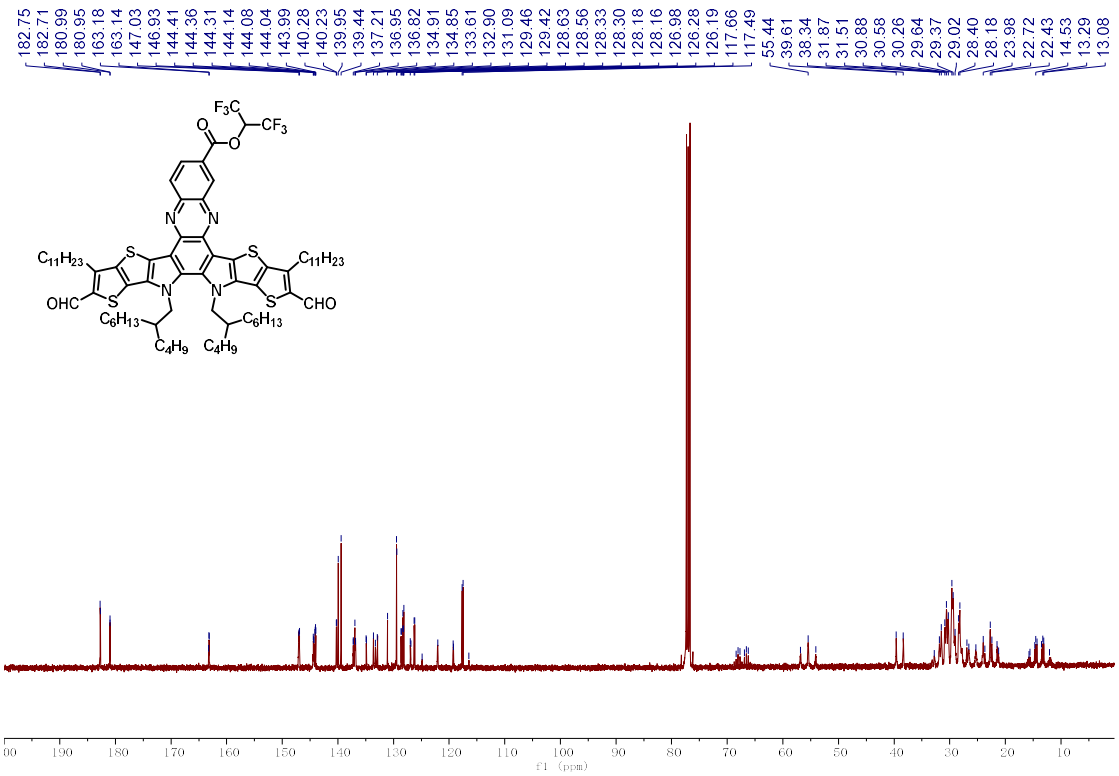

^{13}C NMR spectrum of **intermediate 6b** in $CDCl_3$.

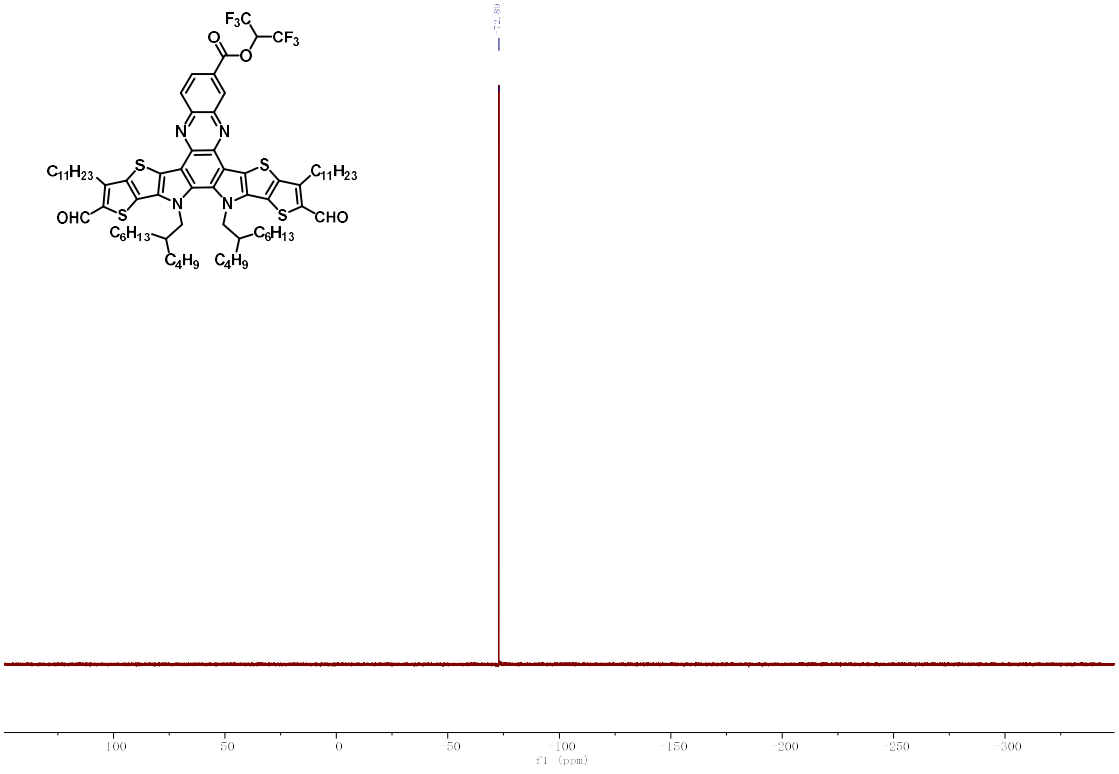

^{19}F NMR spectrum of **intermediate 6b** in $CDCl_3$.

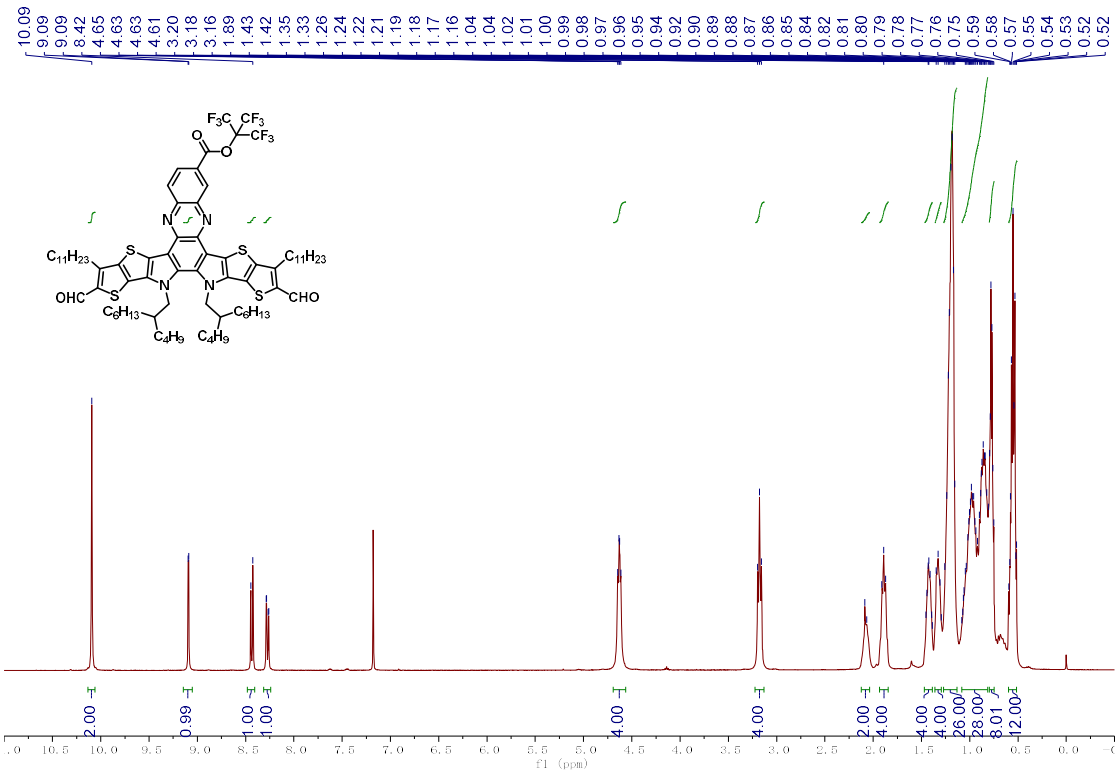

^{1}H NMR spectrum of **intermediate 6c** in $CDCl_3$.

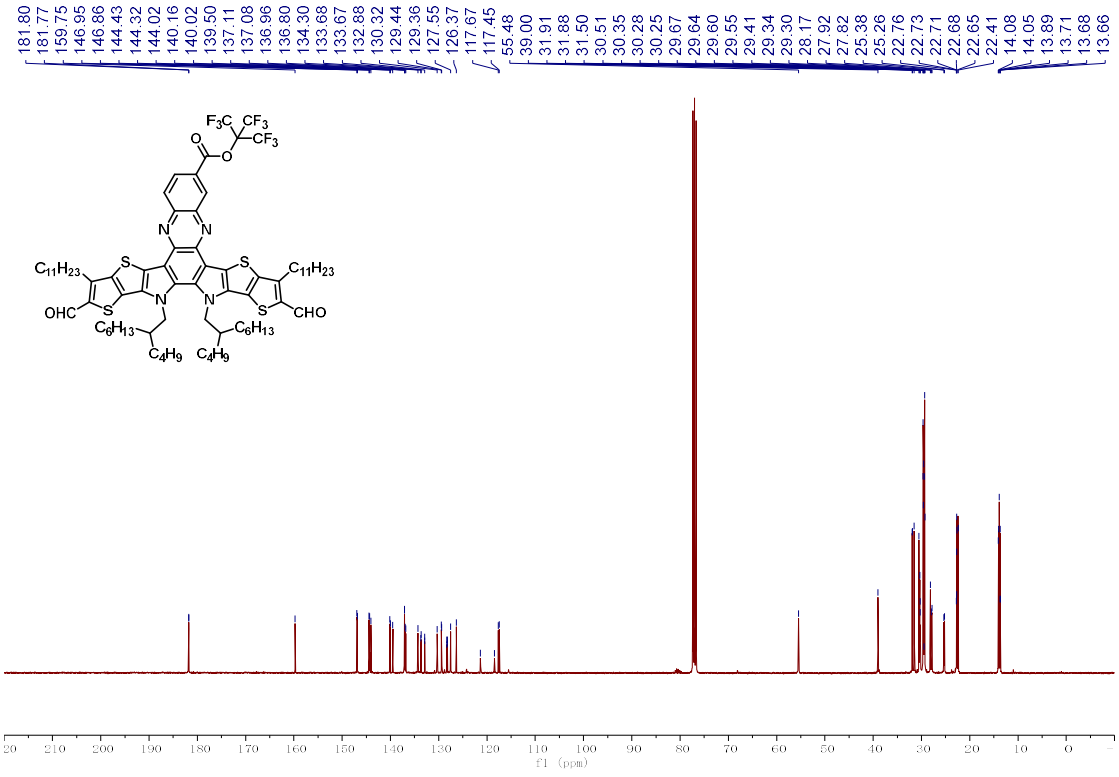

^{13}C NMR spectrum of **intermediate 6c** in $CDCl_3$.

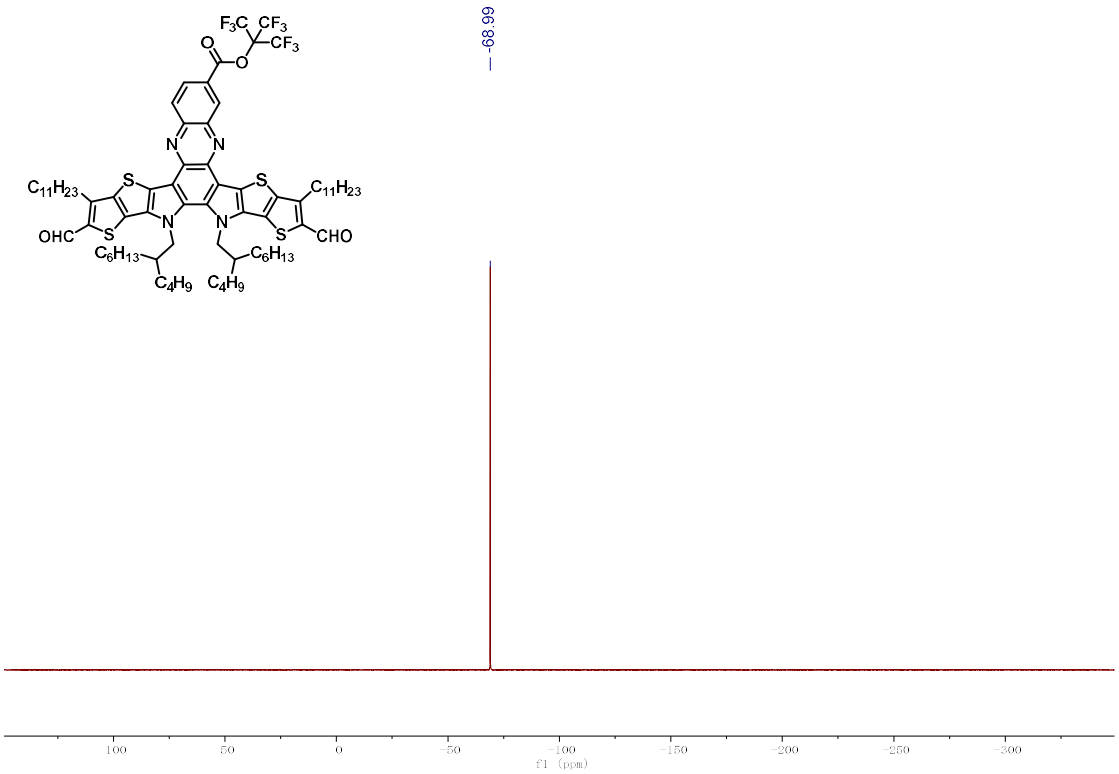

^{19}F NMR spectrum of **intermediate 6c** in $CDCl_3$.

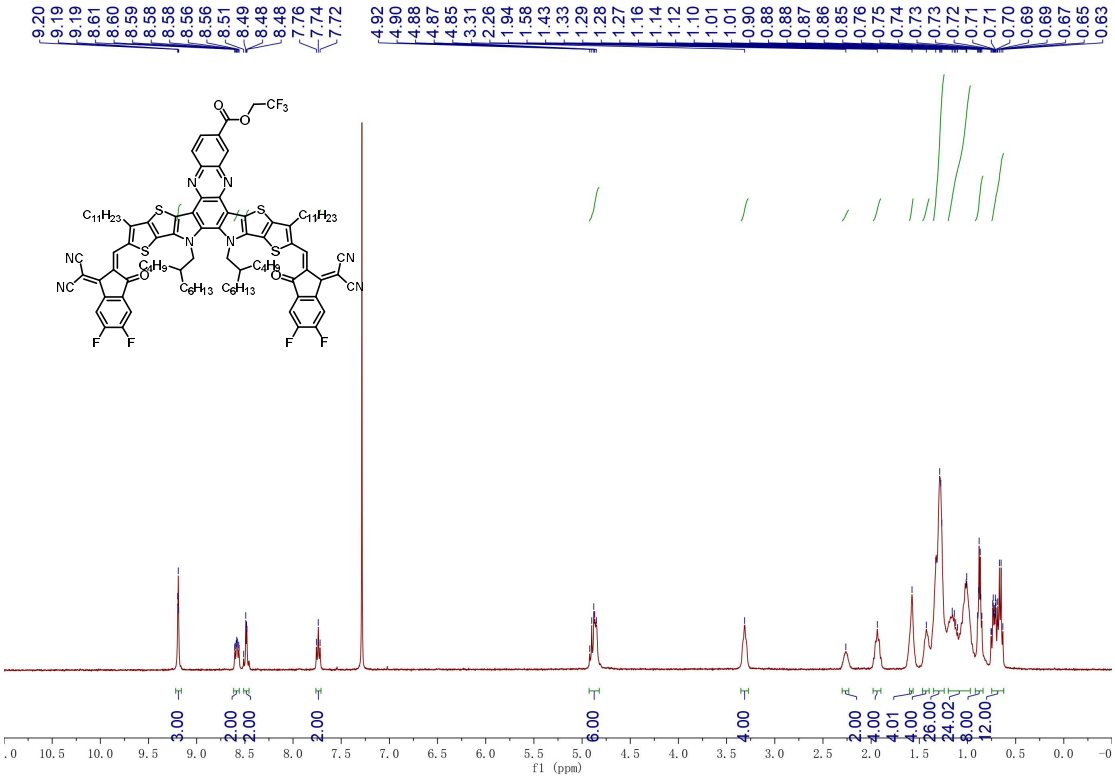

^{1}H NMR spectrum of **CHE-3F** in $CDCl_3$.

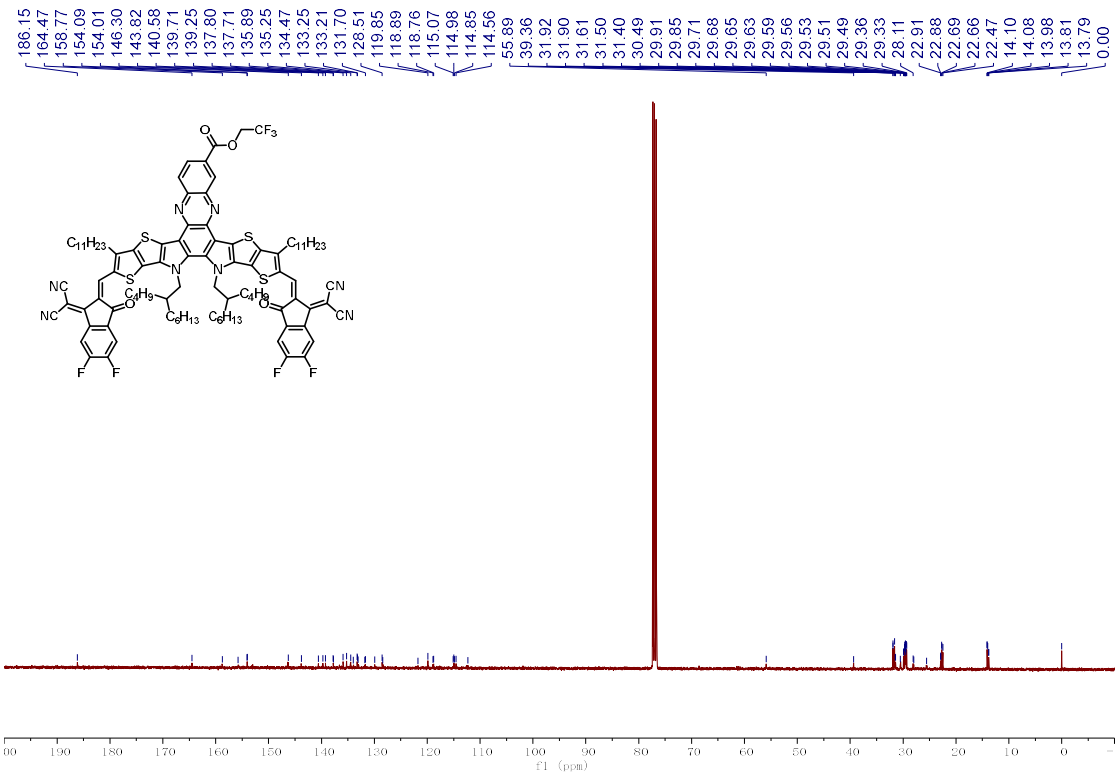

^{13}C NMR spectrum of **CHE-3F** in $CDCl_3$.

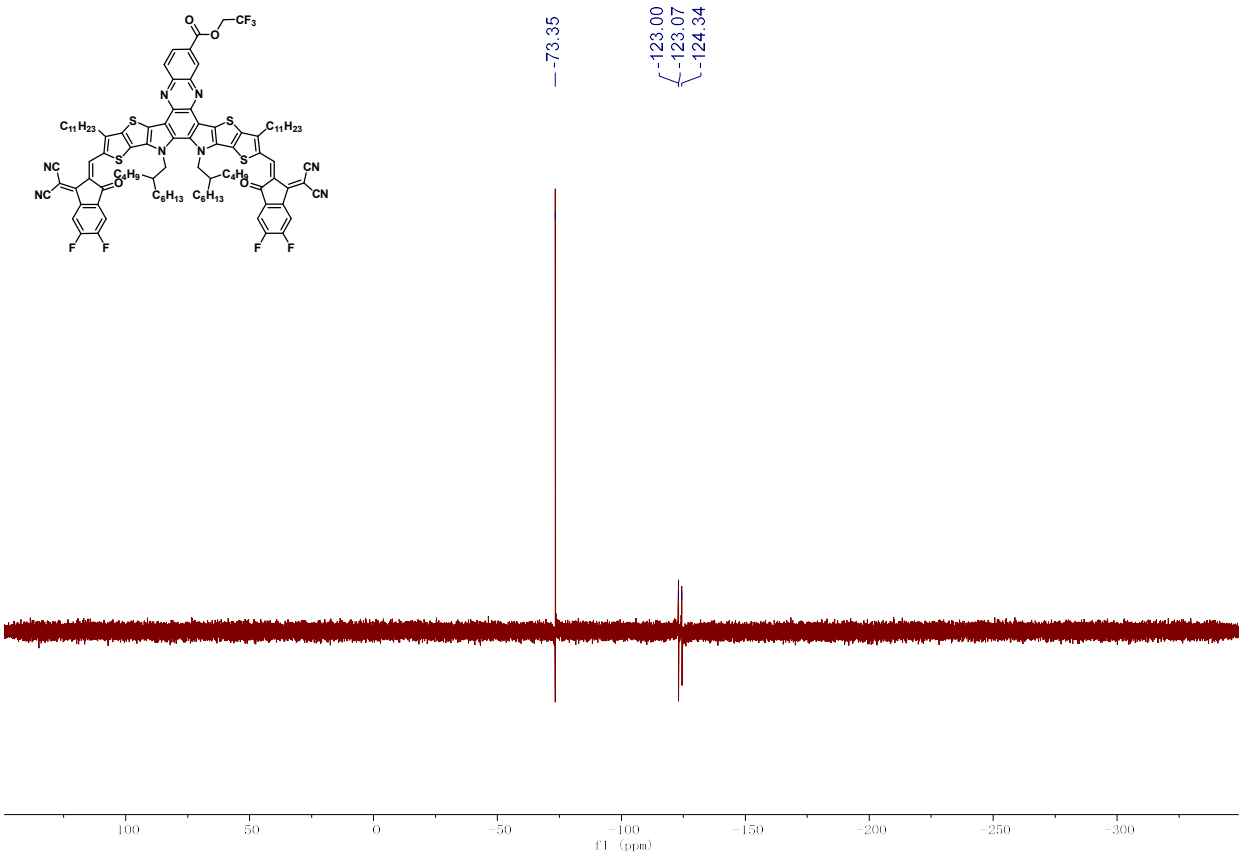

^{19}F NMR spectrum of **CHE-3F** in $CDCl_3$.

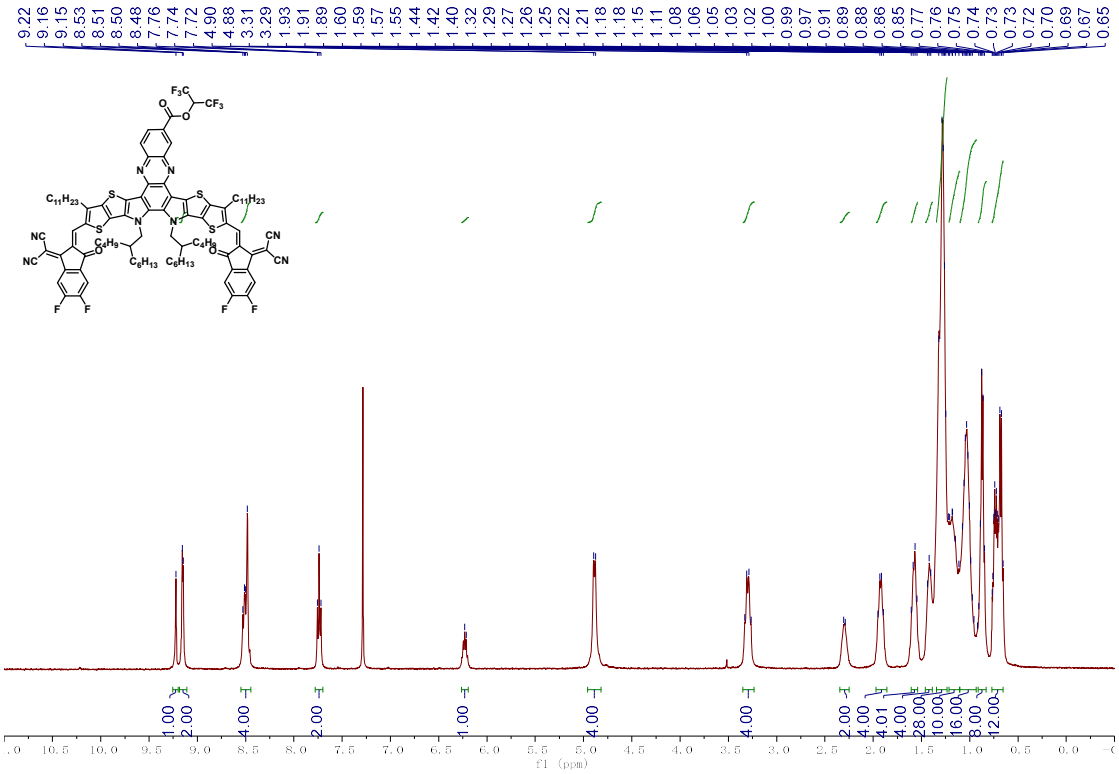

^{1}H NMR spectrum of **CHE-6F** in $CDCl_3$.

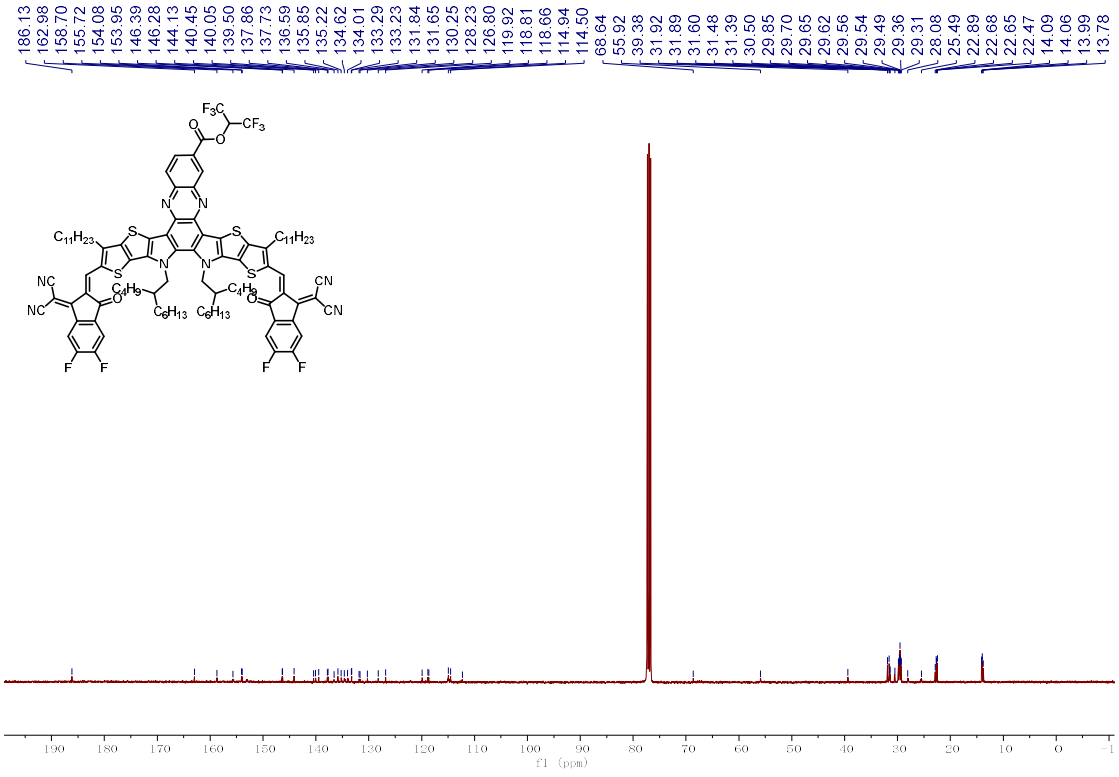

^{13}C NMR spectrum of **CHE-6F** in $CDCl_3$.

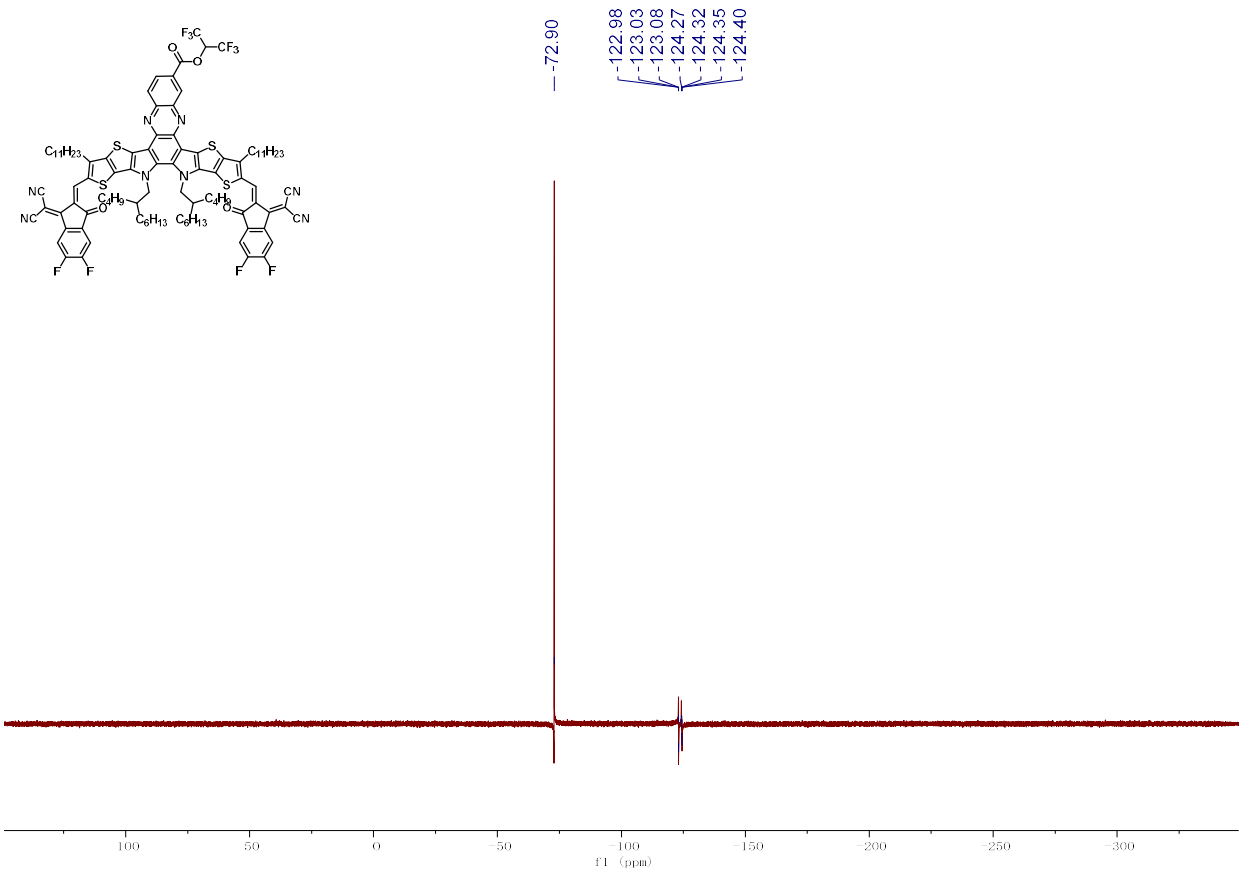

^{19}F NMR spectrum of **CHE-6F** in $CDCl_3$.

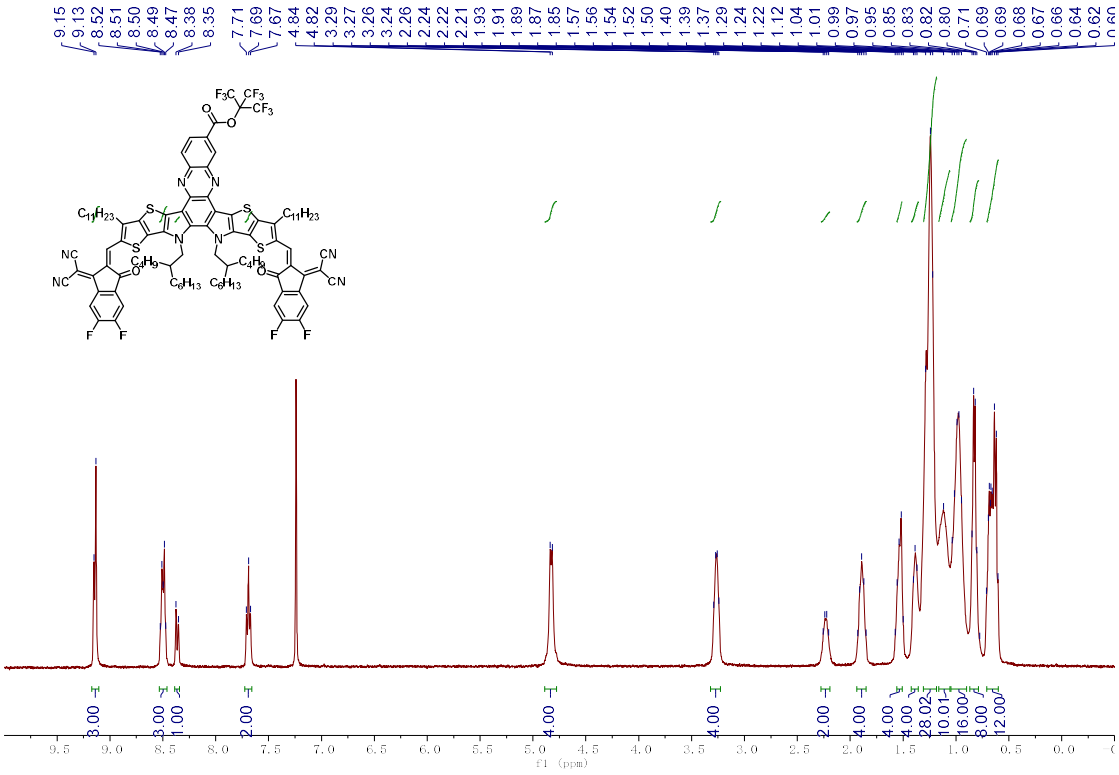

^{1}H NMR spectrum of **CHE-9F** in $CDCl_3$.

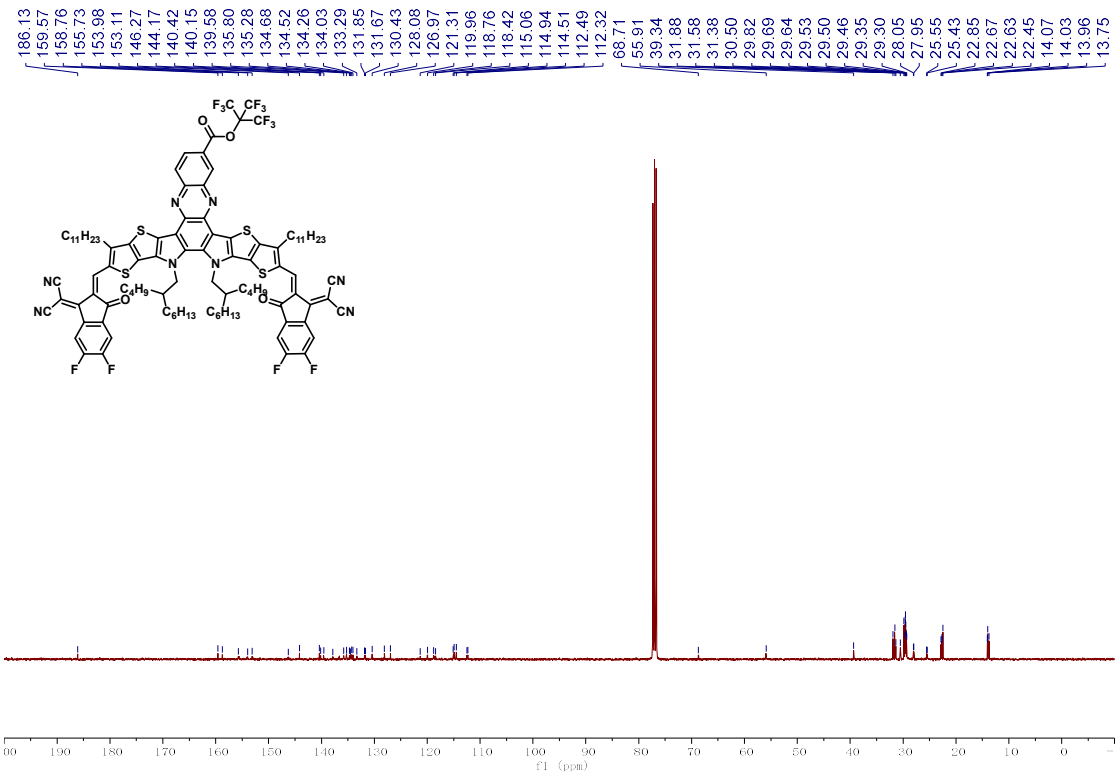

^{13}C NMR spectrum of **CHE-9F** in $CDCl_3$.

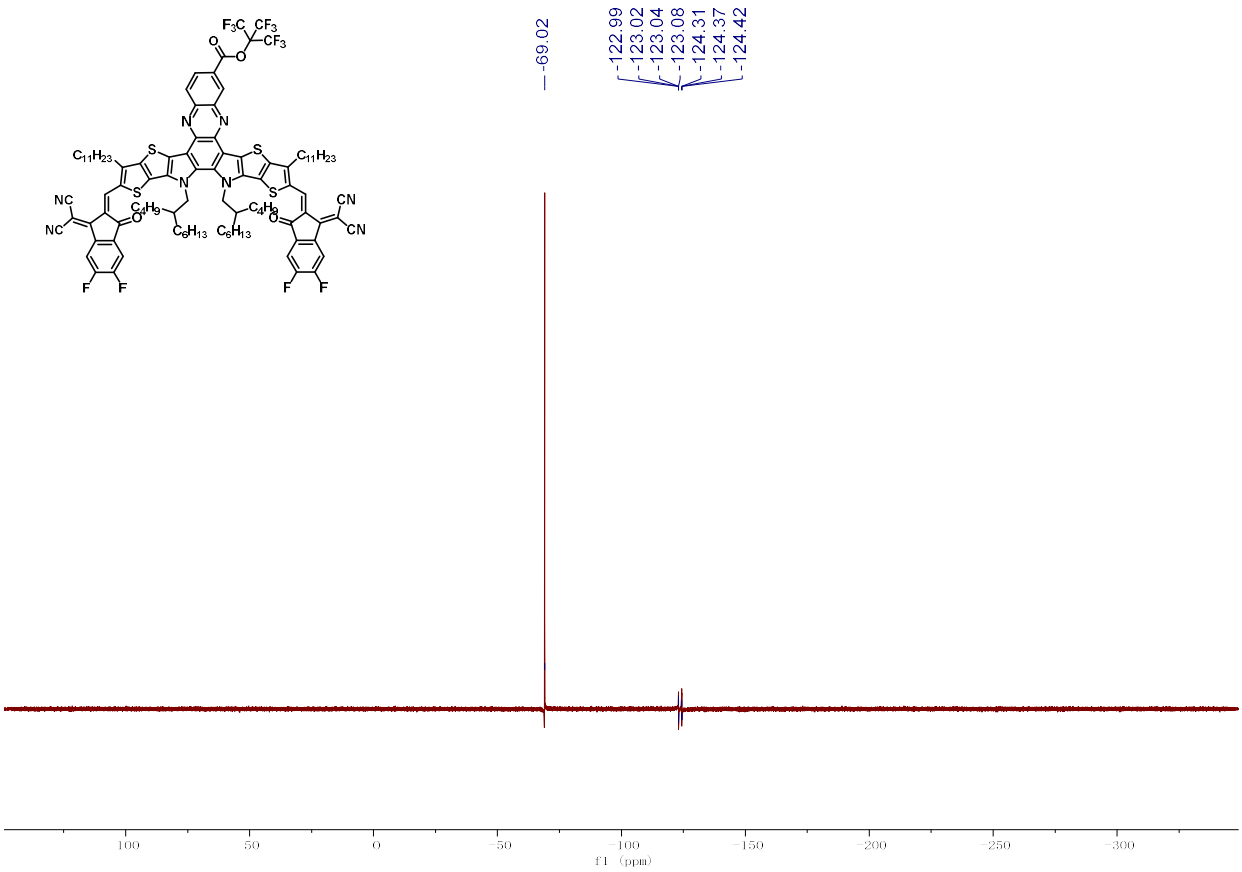

^{19}F NMR spectrum of **CHE-9F** in $CDCl_3$.

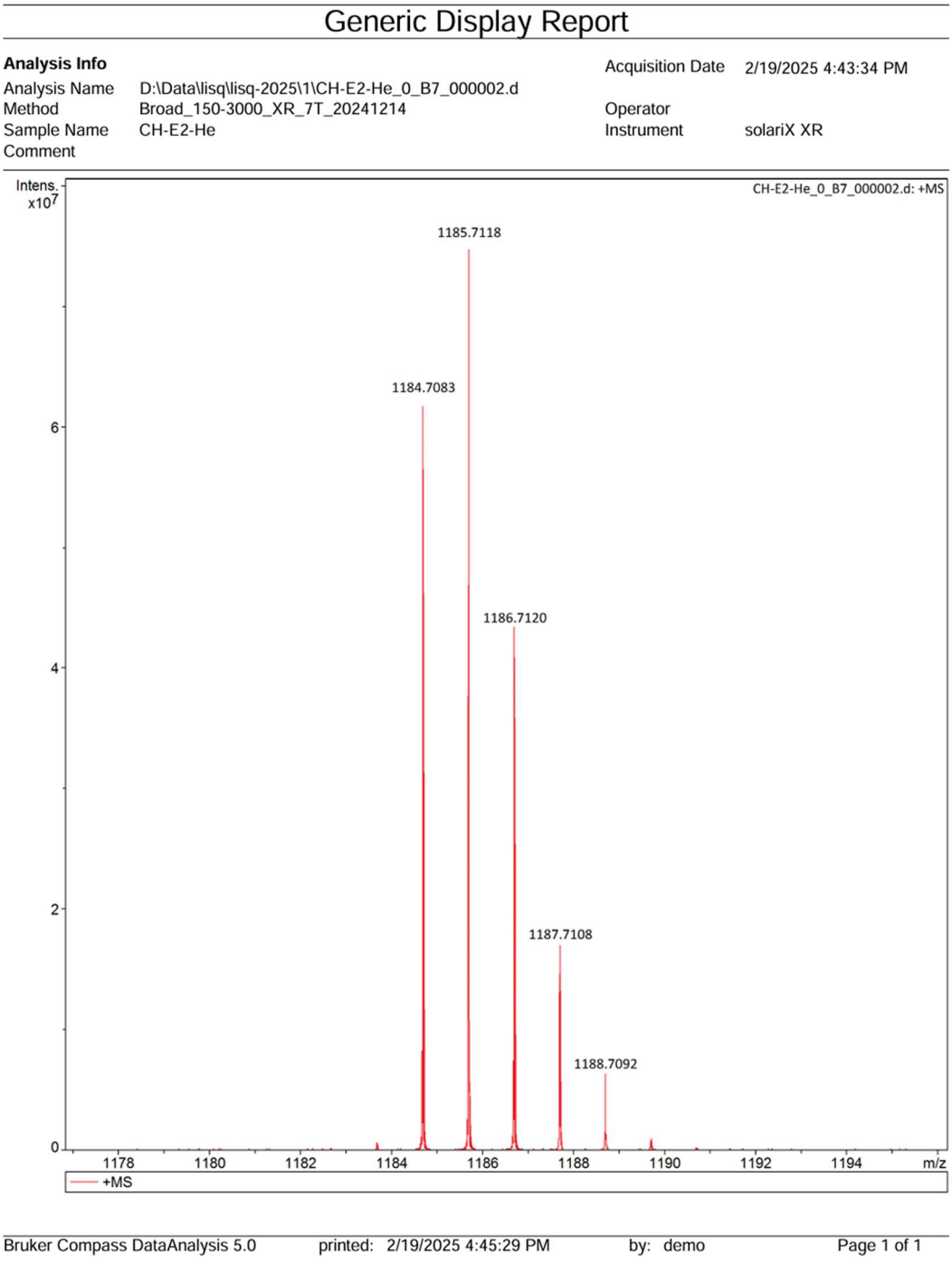

HRMS of **interment 2.**

Generic Display Report

Analysis Info

Analysis Name	D:\Data\lisq\lisq-2025\1\CH-E2-CHO_0_A24_000001.d	Acquisition Date	2/19/2025 4:33:26 PM
Method	Broad_150-3000_XR_7T_20241214	Operator	
Sample Name	CH-E2-CHO	Instrument	solariX XR
Comment			

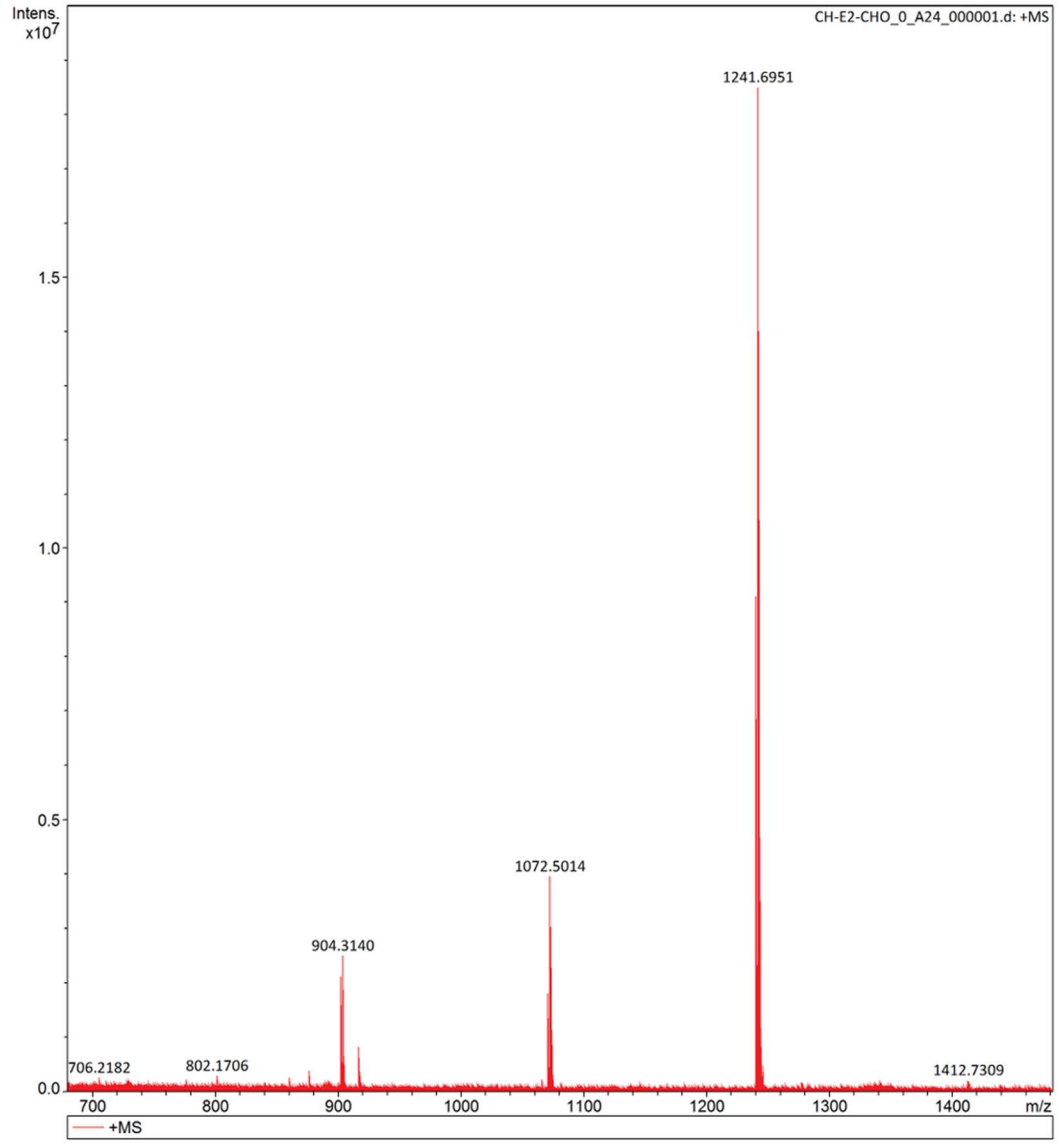

Bruker Compass DataAnalysis 5.0 printed: 2/19/2025 4:34:41 PM by: demo Page 1 of 1

HRMS of **interment 3.**

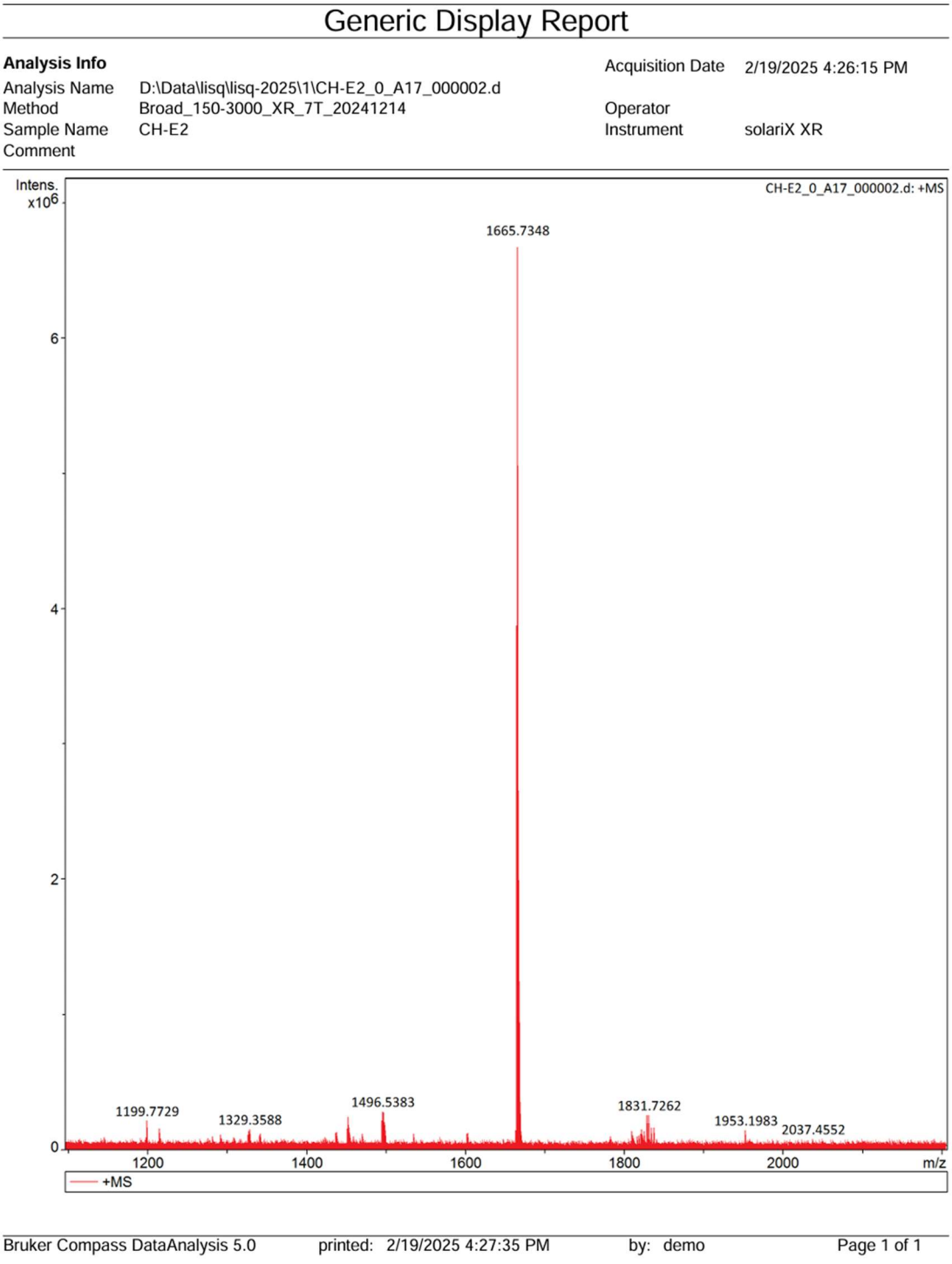
Generic Display Report
Analysis Info
Analysis Name D:\Data\lisq\lisq-2025\1\CH-E2_0_A17_000002.d
Method Broad_150-3000_XR_7T_20241214
Sample Name CH-E2
Comment
Acquisition Date 2/19/2025 4:26:15 PM
Operator
Instrument solariX XR
Intens.
x10^6
CH-E2_0_A17_000002.d: +MS
1665.7348
1199.7729
1329.3588
1496.5383
1831.7262
1953.1983
2037.4552
6
4
2
0
1200
1400
1600
1800
2000
m/z
+MS
Bruker Compass DataAnalysis 5.0
printed: 2/19/2025 4:27:35 PM
by: demo
Page 1 of 1

HRMS of **CHE-2.**

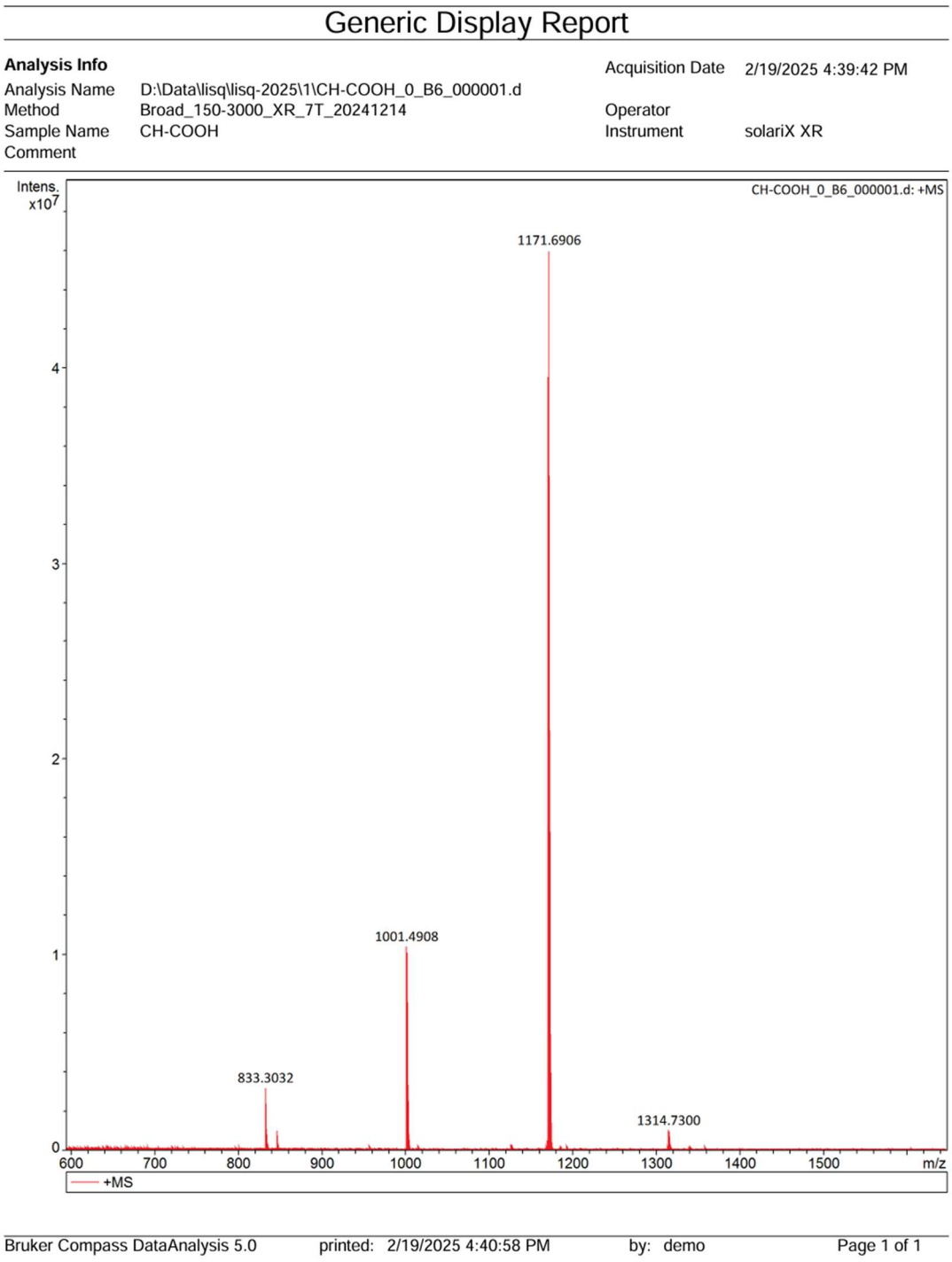

HRMS of **interment 4.**

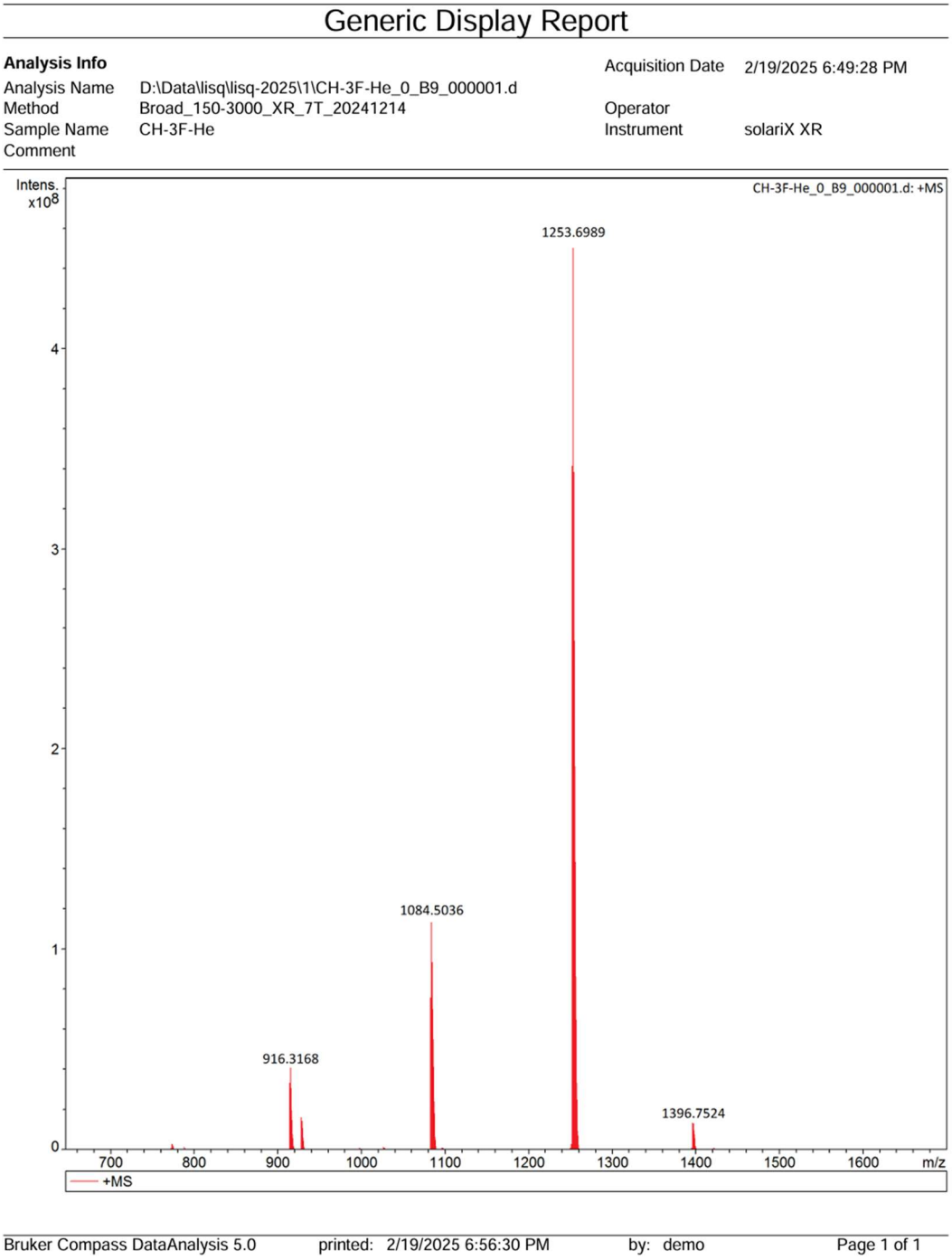

HRMS of **interment 5a.**

Generic Display Report

Analysis Info

Analysis Name	D:\Data\lisq\lisq-2025\1\CH-6F-He_0_B11_000001.d	Acquisition Date	2/19/2025 6:57:26 PM
Method	Broad_150-3000_XR_7T_20241214	Operator	
Sample Name	CH-6F-He	Instrument	solariX XR
Comment			

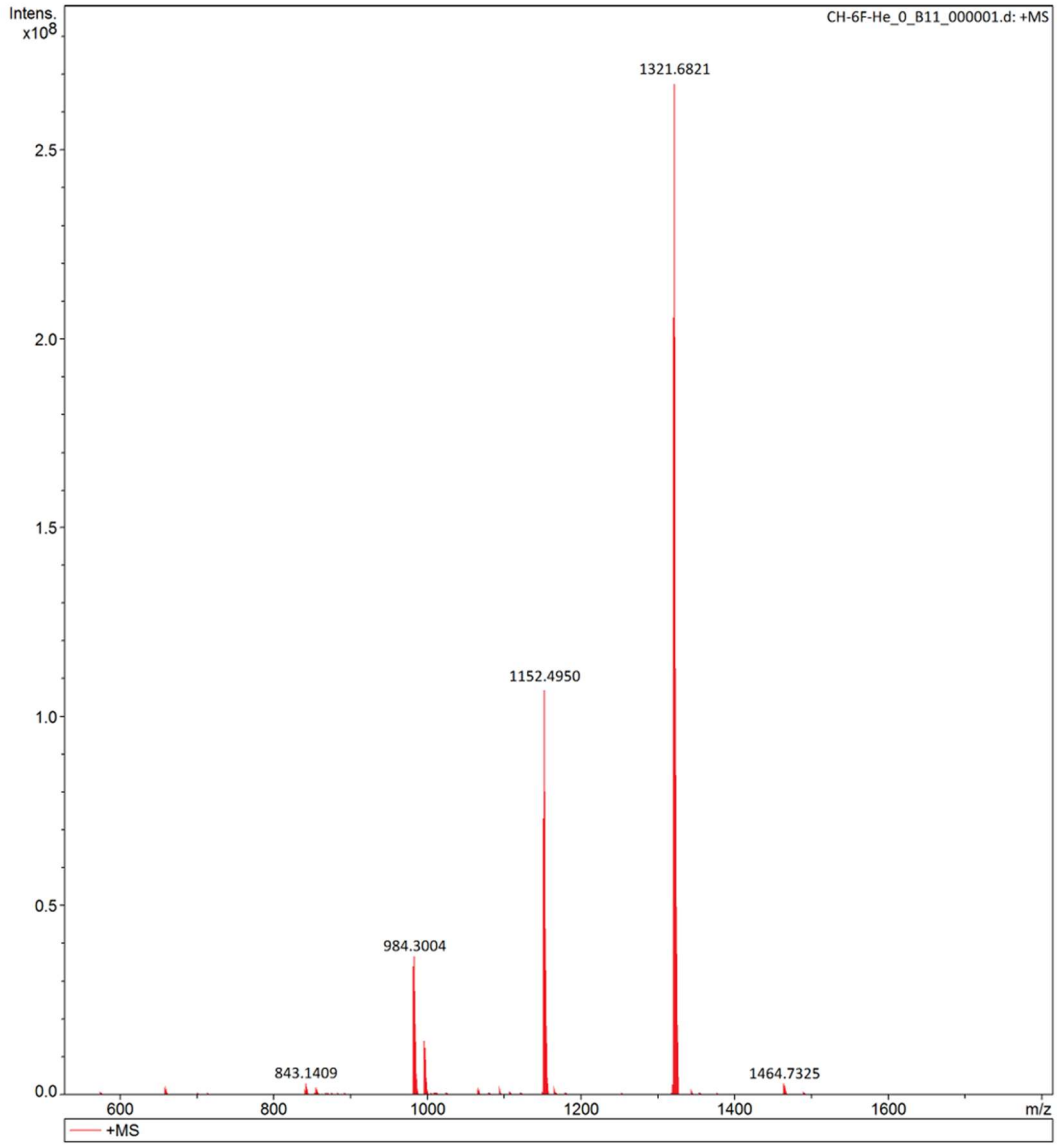

Bruker Compass DataAnalysis 5.0 printed: 2/19/2025 6:58:46 PM by: demo Page 1 of 1

HRMS of **interment 5b.**

Generic Display Report

Analysis Info

Analysis Name	D:\Data\lisq\lisq-2025\3\CHE-9F-He_0_B15_000001.d	Acquisition Date	3/26/2025 12:12:56 PM
Method	Broad_150-3000_XR_7T_20241214	Operator	
Sample Name	CHE-9F-He	Instrument	solariX XR
Comment			

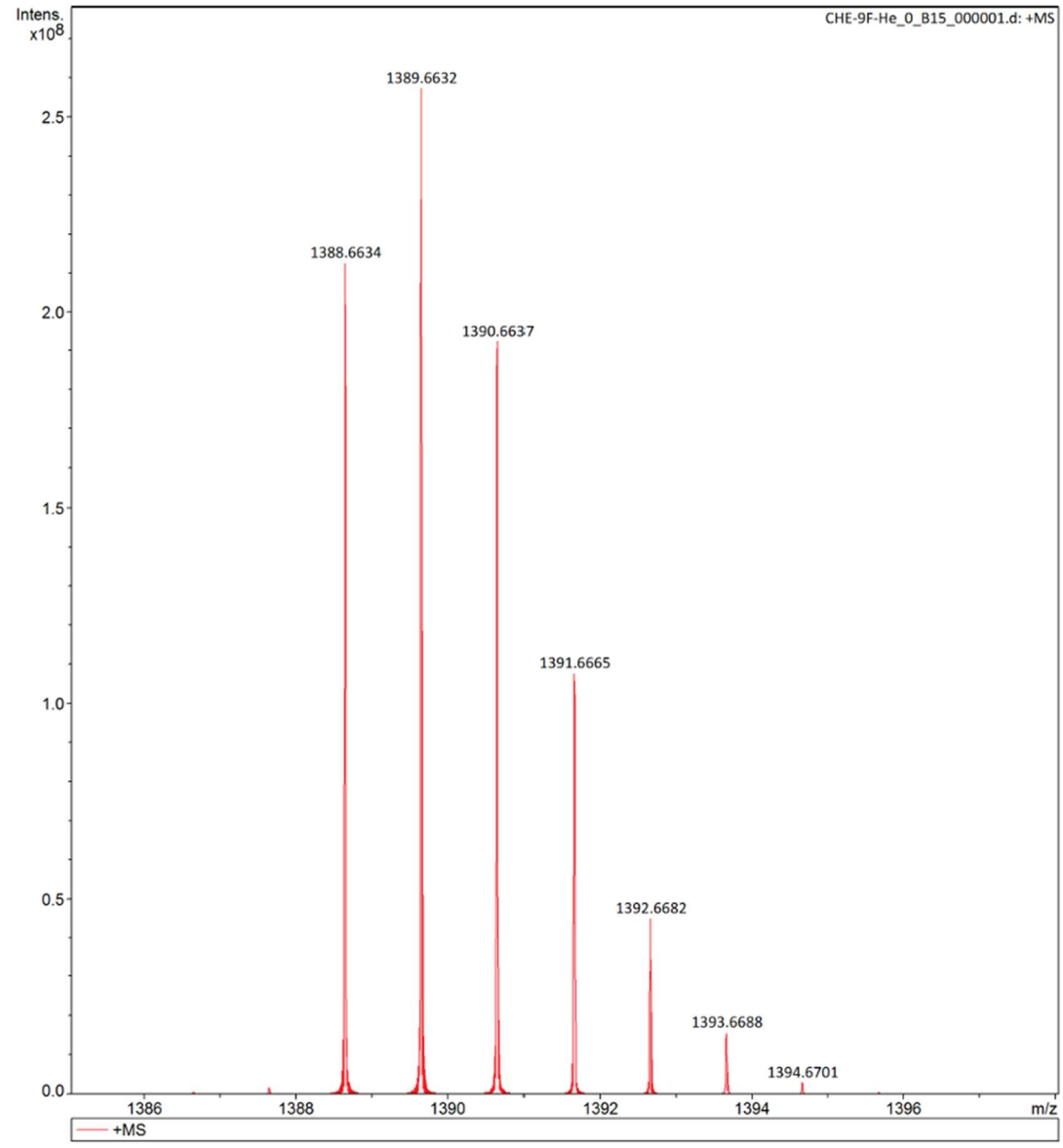

Bruker Compass DataAnalysis 5.0 printed: 3/26/2025 12:15:50 PM by: demo Page 1 of 1

HRMS of **interment 5c.**

Generic Display Report

Analysis Info

Analysis Name	D:\Data\lisq\lisq-2025\1\CH-3F-CHO_0_B1_000001.d	Acquisition Date	2/19/2025 4:35:27 PM
Method	Broad_150-3000_XR_7T_20241214	Operator	
Sample Name	CH-3F-CHO	Instrument	solariX XR
Comment			

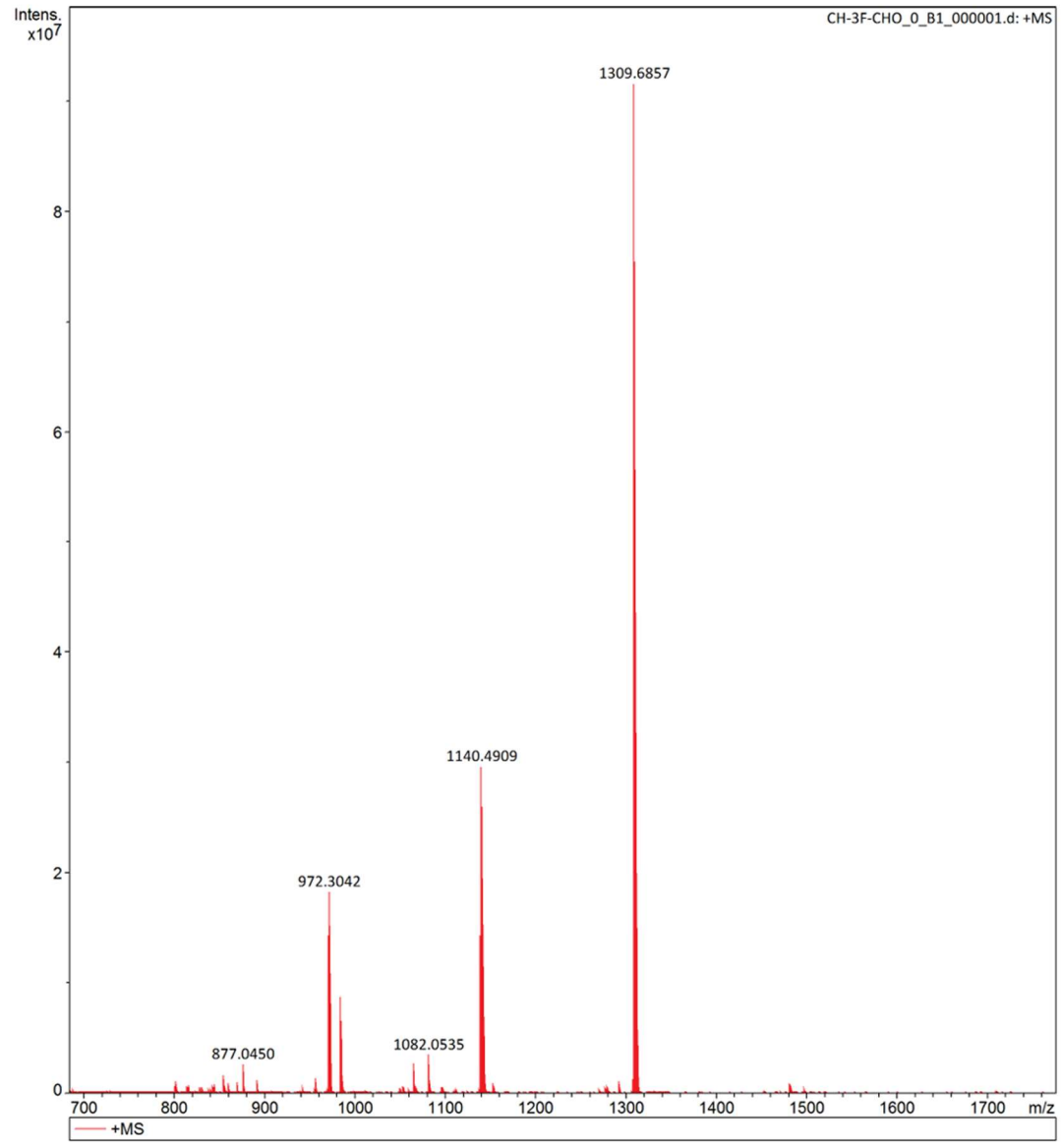

Bruker Compass DataAnalysis 5.0 printed: 2/19/2025 4:37:09 PM by: demo Page 1 of 1

HRMS of **interment 6a.**

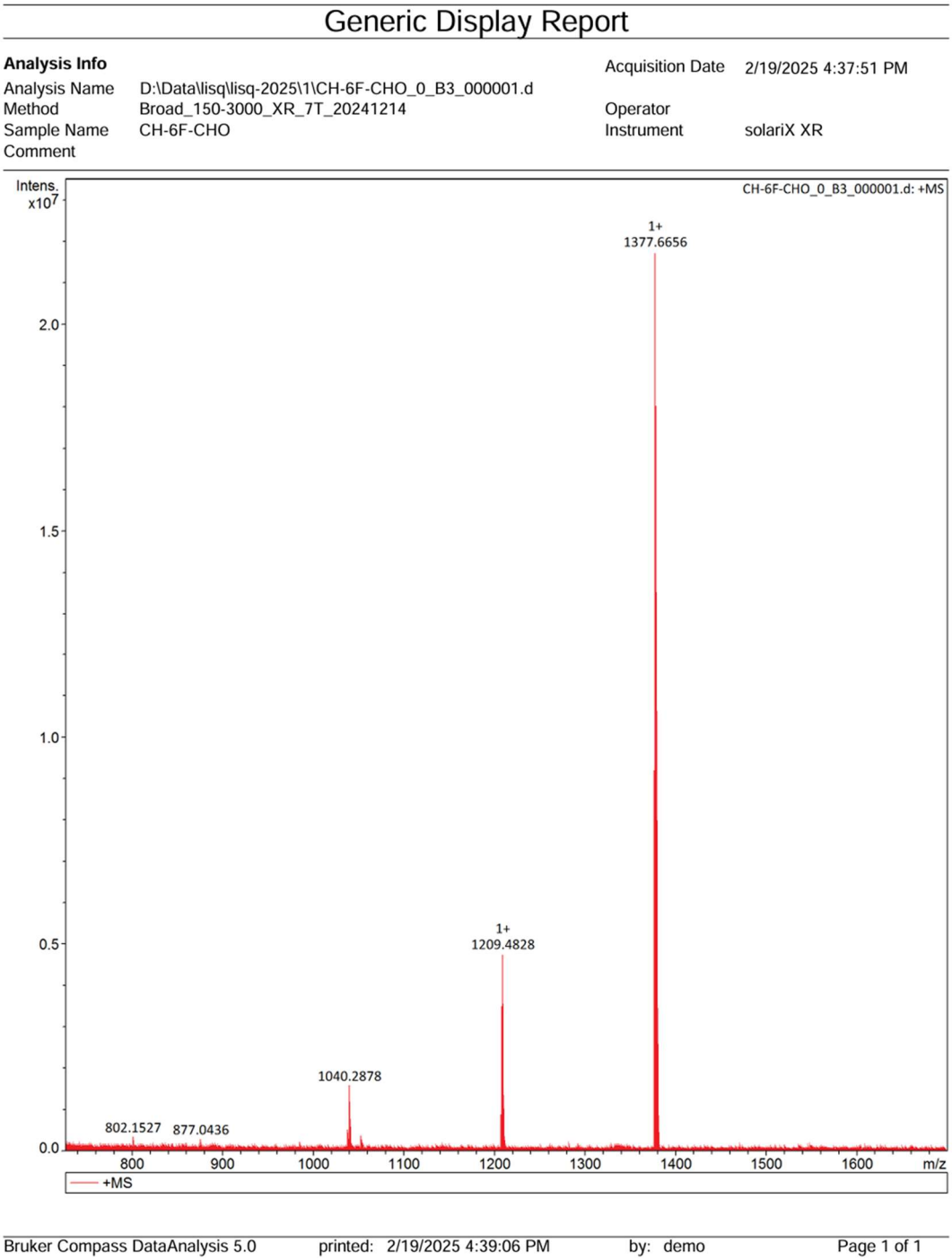

HRMS of **Intermediate 6b.**

Generic Display Report

Analysis Info

Analysis Name	D:\Data\lisq\lisq-2025\3\CHE-9F-CHO_0_B16_000001.d	Acquisition Date	3/26/2025 12:16:28 PM
Method	Broad_150-3000_XR_7T_20241214	Operator	
Sample Name	CHE-9F-CHO	Instrument	solariX XR
Comment			

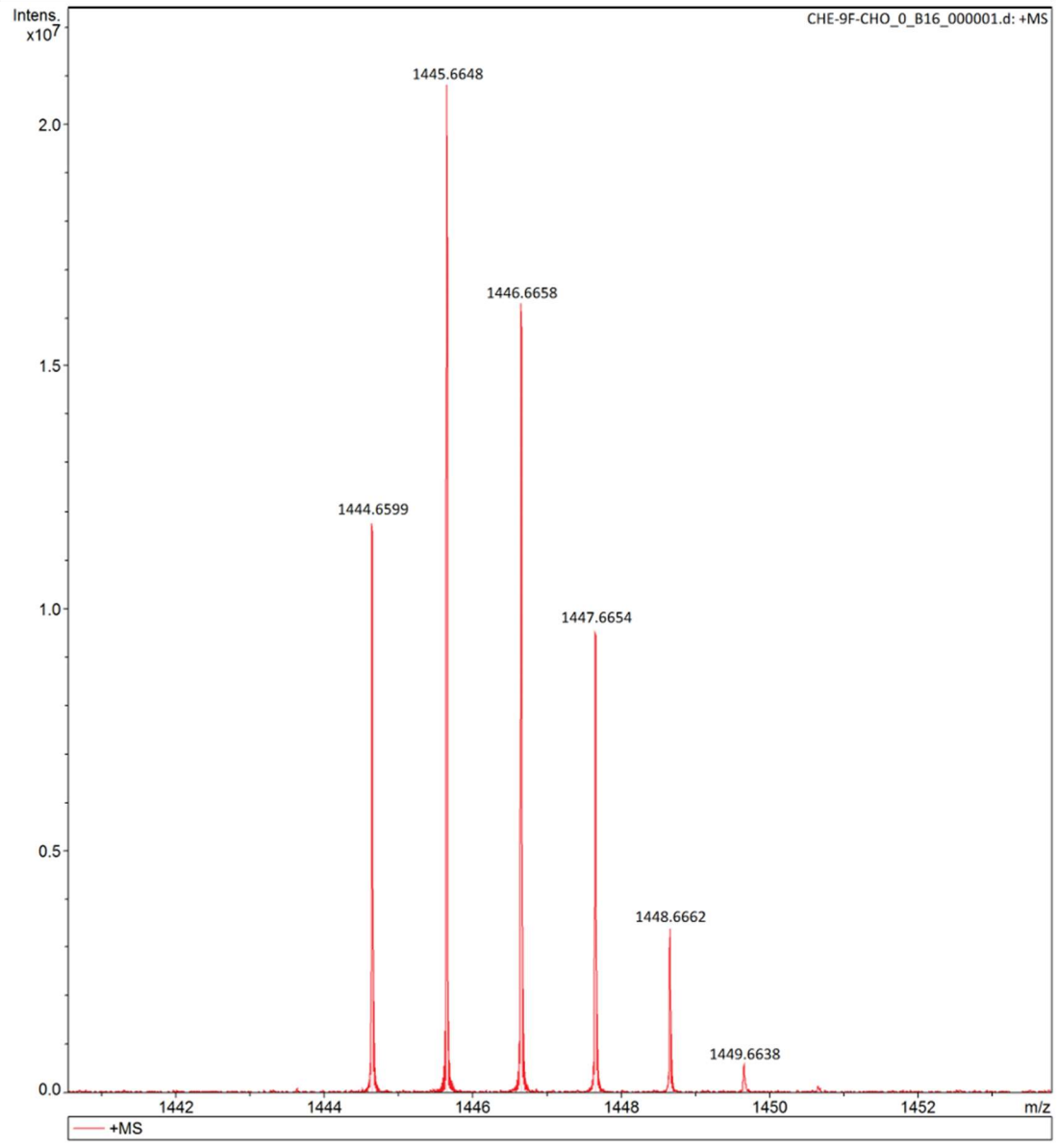

Bruker Compass DataAnalysis 5.0 printed: 3/26/2025 12:18:05 PM by: demo Page 1 of 1

HRMS of **Intermediate 6c.**

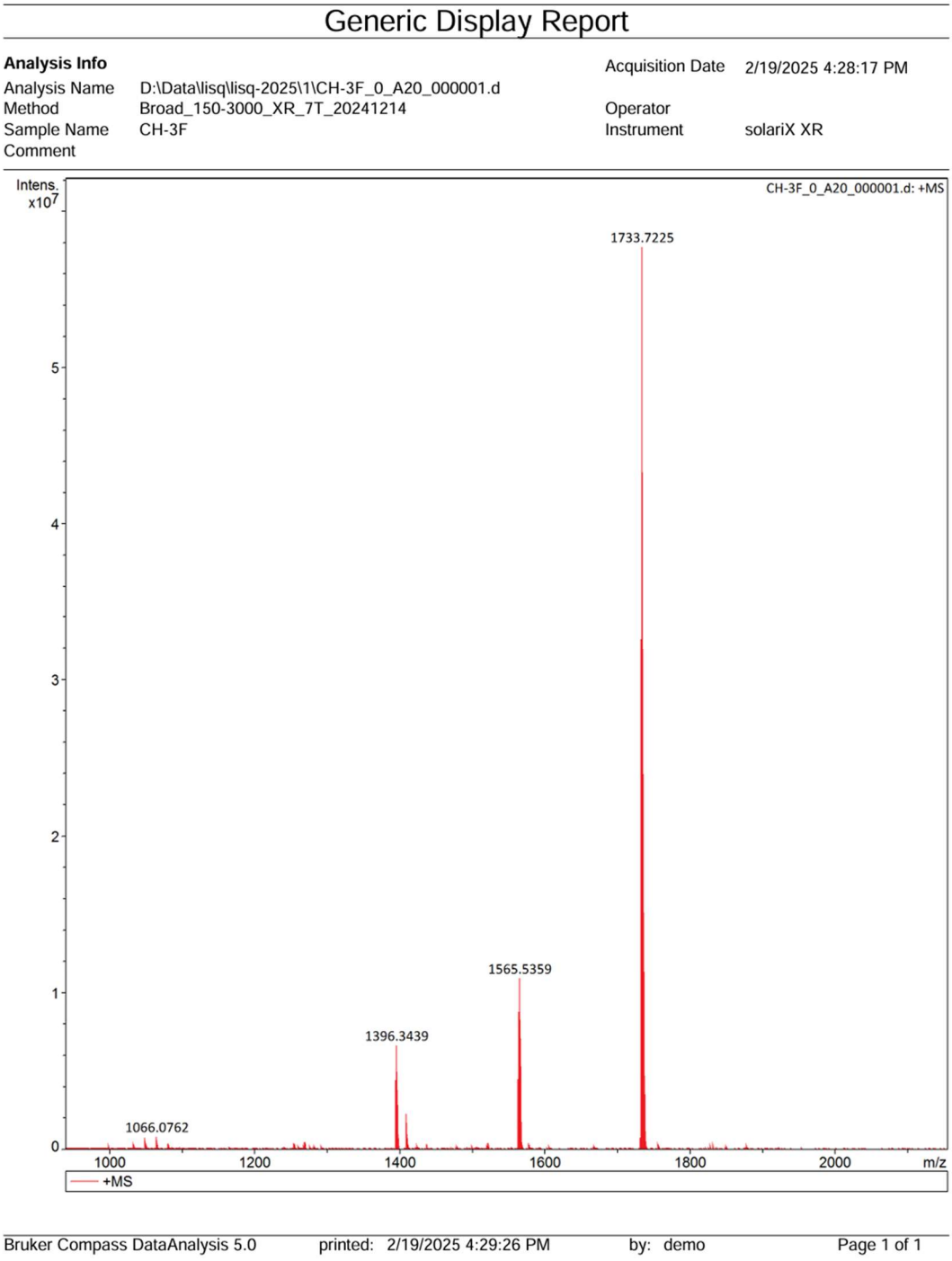

HRMS of **CHE-3F.**

Generic Display Report

Analysis Info

Analysis Name	D:\Data\lisq\lisq-2025\1\CH-6F_0_A22_000001.d	Acquisition Date	2/19/2025 4:30:03 PM
Method	Broad_150-3000_XR_7T_20241214	Operator	
Sample Name	CH-6F	Instrument	solariX XR
Comment			

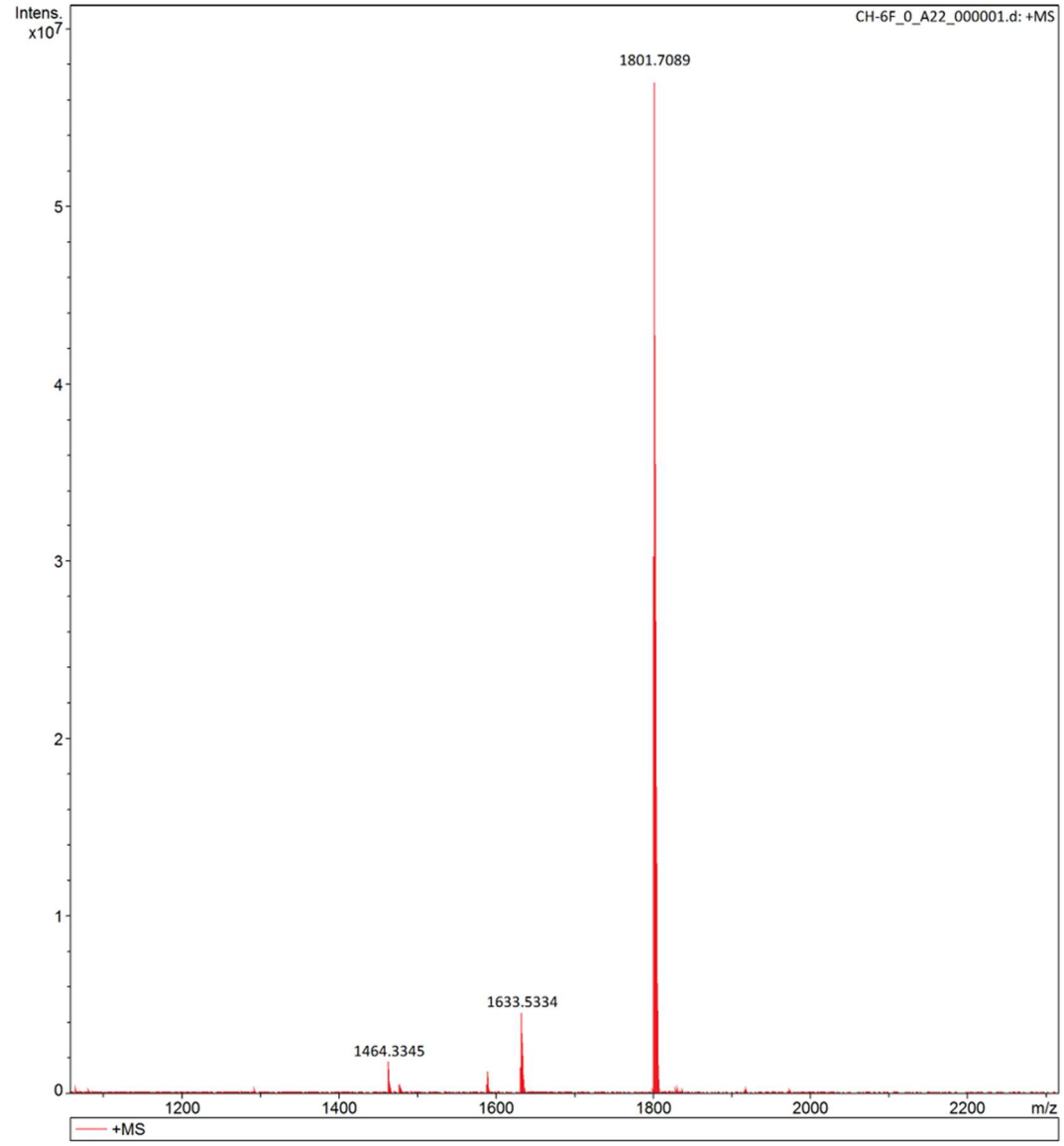

Bruker Compass DataAnalysis 5.0 printed: 2/19/2025 4:31:54 PM by: demo Page 1 of 1

HRMS of CHE-6F.

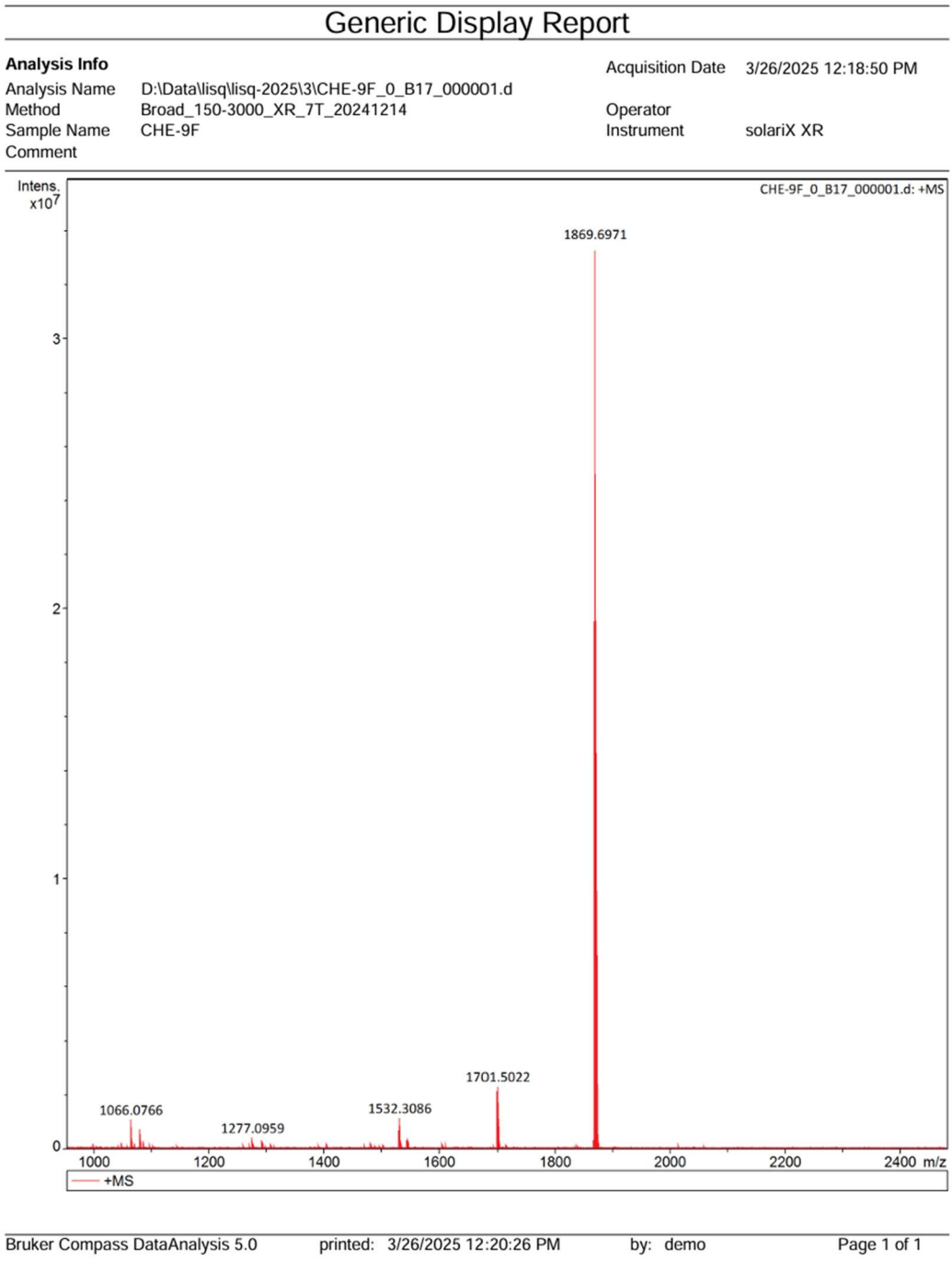

HRMS of CHE-9F.

6. Supplementary References.

[1] A. D. Becke, *J. Chem. Phys*. **1993**, 98, 5648-5652.

[2] P. C. Hariharan, J. A. Pople, *Mol. Phys*. **1974**, 27, 209-214.

[3] G. Frisch, J. Robb, M. C. Nakatsuji, M. Sonnenberg, J. B. F. Farkas, e. al., *Gaussian 16, Gaussian, Inc*. Wallingford, CT **2016**.